Politecnico di Torino

Master's Degree in Physics of Complex Systems


Politecnico
di Torino

Master's Thesis

# Critical behavior of two-dimensional disordered Potts model



Supervisors:
Alessandro Pelizzola
Marco Picco

Candidate:
Ivan Lecce

July 2024

# Contents

# Abstract

Phase transitions describe abrupt changes in the physical properties of systems and represent fundamental complex phenomena. While in the past, ideal models were used in order to obtain analytical results, in the last decades much attention has been directed towards more realistic representations. In fact, real materials are naturally characterized by defects and inhomogeneities which, even in small amounts, can have a strong influence on the features of second order phase transitions. Understanding the impact of disorder, or randomness, on critical statistical models is the main goal of this thesis. It represents the first step to describe more peculiar phenomena such as random lines of impurities.

In particular this work focuses on the disordered Potts model on a square lattice, which, as a generalization of the Ising model, is able to describe different and broader classes of phenomena and phase transitions. The disorder is treated using the replica method, while the study of criticality is carried out using renormalization group techniques in real space and conformal field theories. In addition, these approaches are used for two general disorder distributions which are able to capture possible short-and long-range interactions.

The two disorder critical points found confirm the existence of new universality classes, and their stability study is considered to represent the renormalization flow in the parametric space. The theoretical development is supported by numerical results using Monte Carlo methods with non-local updates, with a particular interest in the magnetization critical exponents. The study of the relevancy of the random fixed points is carried out numerically in several cases and provides additional evidence for the importance of disordered models.

# Introduction

Many-body problems are the paradigmatic example of *Complex System*, consisting of a large number of interacting elements whose phenomena cannot be easily derived or predicted[1]. Despite their complexity and the difficulties in solving and describing them, these systems characterize the world we live in, from the activity of biological molecules, to turbulent flows in liquids and glass materials[2], from climate[3] and vehicular traffic[4] to the economic sector of financial markets[5].

Modelling is a powerful tool that helps to reproduce features, but more importantly to predict and control them. The dynamics of many complex phenomena nowadays are still impossible to be solved analytically. Some approximation may lead to solutions that grasp some properties, but are not always able to capture in a satisfactory way both the microscopic and macroscopic characteristics. A collective effort from different fields has been required to finding ways for a further progress in this branch of physics [6] and has pushed research in several domains. The role of mathematics, in particular, stood out for its ability to describe physical phenomena and its potential to treat complex systems[7].

Amongst the possible complex phenomena studies, a great curiosity has been directed towards transition between states which are controlled by physical parameters like temperature or pressure. Whilst we may be familiar with the usual transition of water between the liquid form and the gas one when brought to the ebullition point, not all phase transitions include a change in the state of matter, although they are all characterized by an abrupt change in the physical features[8]. Magnets, for instance, at a given temperature, may loose or gain the property to attract or repel other magnets, commonly known as *ferromagnetic-paramagnetic phase transition*[9], although, there exists even more peculiar ones, like *superconductivity* [10] where the resistance of a material to electrical current drops to zero, or *super-fluidity*[11] in which there is a drop of the viscosity between particles of a fluid.

When these collective phenomena were first studied, it was important to find a scheme and a structure to deal with their complexity. It was the peculiarity of the *helium phase transition*[12] that led to a first mathematical development, using thermodynamical quantities to distinguish between broader types of phase transitions. The *Ehrenfest Classification* [12] is still used nowadays, and it makes use of the Gibbs free energy:

$$G = U - TS - pV \tag{1}$$

where U is the internal energy of the system, T the temperature, S the entropy, p the pressure and V the volume. *First order phase transitions* are defined as the ones in which the first derivative of the free energy, with respect to a thermodynamical control parameter, is discontinuous and *second order phase transition*, the one in which the second derivative of the free energy becomes discontinuous but not the first one. There exists *higher order* phase transition which are simply linked to higher order discontinuous derivatives of the free energy.

In the description of these phenomena it comes natural to define physical quantities which are able to characterize fully different phases, and these quantities are called *order parameters*[13]. Whilst in some cases it is easy and direct to define them, in some other there must be an ad-hoc study, for instance this is what happens for liquid crystals for the description of the nematic phase: in general symmetries or broken symmetries of systems become crucial for the definition of these quantities[14]. It is important to have an understanding of how they vary with respect to different external conditions and the way in which they do it. Since they are strictly linked to the free energy of the systems, it is useful to classify phase transitions based on their behaviour, and it is possible to rephrase in an equivalent way the previous classification based on the presence of jumps in their expressions or derivatives. To better understand this, a well-studied phase transition will be presented, the ferromagnetic-paramagnetic one of the *Ising model*[15]. The energy, or hamiltonian, is given by:

$$H_{Ising} = J \sum_{\langle ij \rangle} s_i s_j + h \sum_i s_i \tag{2}$$

where $s_i$ is the spin binary variable which describes the orientation of magnetic dipoles of a material and can take values:

$$s_i = \begin{cases} +1 \\ -1 \end{cases}$$

The indexes $i, j$ run over all the number of spins of the system, which can be chosen to be $N$. The sum is over nearest neighbours, defined as the group of spin closest to a given one, whilst $J > 0$ is an interaction term that allows to define the energy magnitude of the interaction between spins. Finally $h$ is an additional parameter that describes the possible presence of an external magnetic field. The order parameter which characterize the system, in this case, is the magnetization density, given by:

$$m = \frac{1}{N} \sum_{i=1}^{N} \langle s_i \rangle \tag{3}$$

It is possible in this way to differentiate mathematically the two known phases of the model. The paramagnetic phase is characterized by disorder, which gives a null average magnetization, all the spins can be seen as random variables with zero mean. The system in the ferromagnetic phase instead is characterized by some order, spins choose one of two possible configuration in which the average of the order parameter no longer remains null, but or negative or positive.

$$m = \begin{cases} 0 & paramagnetic \\ \pm \tilde{m} & ferromagnetic \end{cases}$$

This different behaviour is exactly what can be described as a change in the property of the systems, which is said to undergo a phase transition if the order parameter changes from one of its values into the other one.

The description of phase transition is mathematically related to the non analyticity of the partition function[16], whose general form, in the canonical ensemble, is:

$$\mathcal{Z} = \sum_{\{s\}} e^{-\beta H\{s\}} \tag{4}$$

with $\beta = \frac{1}{k_B T}$ the Boltzmann factor. The summation is performed over all the possible states of the spins, which in this case will be $2^N$. But since the summation is amongst a finite set, and the finite sum of exponential quantities does not cause singularities, the only way for these to appear is considering the thermodynamical limit

$$N, V \to \infty \; such \; that \; \frac{N}{V} \exists \; finite$$

so that the sum is amongst an infinite amount of states. Phase transition can therefore be of *I order* if the first derivative of the free energy $F = -k_B T log Z$ is discontinuous or *II order or continuous* if the first derivative is continuous but the second one is discontinuous. This is exactly equivalent to the previous classification, since the Helmholtz free energy is linked to the Gibbs one through a simple Legendre transformation, which entails:

$$F = G - pV \tag{5}$$

Therefore the singularities of $G$ and its derivatives are reflected in the singularities of $F$. If one considers the related *order parameter* for physical systems, it can be simply connected to the free energy as below:

$$m = -\frac{1}{N} \frac{\partial F}{\partial h}\bigg|_{T=T*}$$

so the classification of the phase transition can be done in terms of the order parameters and below it will be given an example.

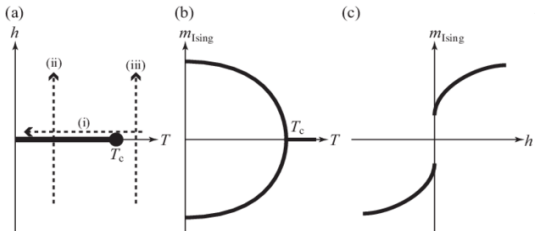


Figure 1: Phase diagram h-T of the Ising model for dimension $d \geq 2$. Different behaviours of the magnetizations with respect to the temperature and external field are shown[17].

In *Figure* 1 it is shown how the phase transition can occur in different ways depending on the choice of the external parameters $T$, and $h$. The general

phase diagram is given by the panel (a), where the critical line separating the two different phases is highlighted. Let's focus on line (i). At $h = 0$ for $T > T_c$, the system is in the paramagnetic phase, then at the critical temperature, it enters in the ferromagnetic phase, so below the critical temperature $T < T_c$ the magnetization density has a non null value. The exact value of the magnetization density can be seen in the second panel (b) where it is clear how the order parameter is characterized by a continuous behaviour. Although the derivative does not change continuously, this will describe a second order phase transition (consisting in a jump in the second derivative of the free energy). In the presence of an external magnetic field $h \neq 0$ we expect the system to be in its ferromagnetic phase and this is what happens for $T \neq T_c$. Line (iii) describes how moving from a negative external magnetic field to a positive one brings the system to change continuously, for $T > T_c$, its magnetization. The other case of interest can be explained following line (ii), again moving at a fixed temperature but smaller than the critical one $T < T_c$. As it can be seen in panel (c), the magnetization no longer changes in a continuous way, but, by varying the sign of $h$, a jump in $m$ appears.

Another interesting analysis which can be carried out is related to the study of the covariance of spins at different lattice points. This is called *correlation function*

$$G(|i-j|) = \langle s_i s_j \rangle - \langle s_i \rangle \langle s_j \rangle \tag{6}$$

and it gives information on how much two spins can influence each other at a given distance. This quantity has in general an exponential behaviour:

$$G(|i-j|) \propto e^{-\frac{|i-j|}{\xi}}$$

that allows to define a new quantity representative of the characteristic length decay of correlation, called *correlation length* $\xi$ [18]. For first-order phase transitions, at critical temperature, the correlation length $\xi$ remains finite at the critical temperature, whereas for second-order phase transitions, the power low behaviour of $\xi$ leads to its divergence at criticality. Whilst in physics it is fundamental to distinguish different scales of the systems (as for instance in hydrodynamics fluids can be considered as continuous media neglecting the discreetness of the particles) this cannot be longer done in the latter. As a result, all scales are strictly connected to each other and cannot be analyzed independently. Without the presence of a characteristic length the system acquires the property of being *scale-invariant* or *self-similar*[13]. The point at which this criticality occurs defines *critical phenomena*[13]; they have been widely studied in statistical mechanics due to their interesting properties. In particular critical systems which describe very different physical events, may share equivalent type of behaviour for their observables near criticality. This allows to introduce the concept of *universality*[13] which consists on systems who belongs to *classes* that share equivalent and universal properties despite their domain of applications and modeling. In general this simplify a lot the possibility to treat a problem at criticality since if a universality class is known, even hard-to-treat problems, with complex interaction, can be perfectly mapped in any other model

belonging to the same class. Therefore, in general, problems can be expressed in terms of a much simpler model which is able to capture all the physics of the phenomenon in an equivalent way.

The importance in statistical physics of the Ising model lies in these common behaviours for a great number of different phenomena, all of which can share equivalent phase transitions. Moreover, despite being a toy model its complexity can be increased by simple generalization. For instance, this led to the so-called Potts-model which hamiltonian is written below, in the absence of a magnetic field:

$$H_{Potts} = J \sum_{<ij>} \delta_{s_i,s_j} \tag{7}$$

where $J$, the interaction term, is still taken as in the Ising case ($J > 0$), this ensures the study of ferromagnetic behaviours only. The major difference in this case relies on the spins, in fact in general they can take values of $Q$ such that

$$s_i = \{1, 2, ..., Q\} \ \forall \ i \in \{1, ..., N\}$$

We will focus on a 2-dimensional lattice with only nearest neighbours interactions. However, we will begin to introduce additional details for a more in depth description of the model. In particular the interactions have been chosen taking into account periodic boundary conditions (PBCs), in such a way that all the spins will have the same number of neighbours $nn = 4 \ \forall \ i \in \{1, ...L^2\}$, where $L$ is the linear size of the lattice. The energy contributions due to the interactions are given only by spins in the same group of values and this is mathematically described by the presence of a Kronecker delta. It is easy to check that if the spins can have only two possibilities the model is perfectly equivalent to the previous Ising one (despite for a constant term which does not change the physical properties of the model but only causes an energy shift). While for $Q = 1$, it corresponds to Percolation model which usually refers to a class of models that describe geometric features of random media[19], and, for instance, can describe the possibility for a fluid in a porous medium to reach the core of the material or the spread of an epidemic. The Potts hamiltonian is represented for better visualization of the model in *Figure* 2.

The Potts model can undergo both type of phase transition depending on the number of possible values of the spins [20]:

$$\begin{cases} Q \leq 4 & II \ order \\ Q > 4 & I \ order \end{cases} \tag{8}$$

The order parameter for the Potts model must be generalized[21] due to the different values of the spins and cannot longer be taken as the normalized average of the spins. For this reason, two quantities must be introduced:

$$\begin{cases} N_i = \sum_{j=1}^{N} \delta_{s_j,i} \\ \rho_i = \frac{N_i}{N} \end{cases}$$

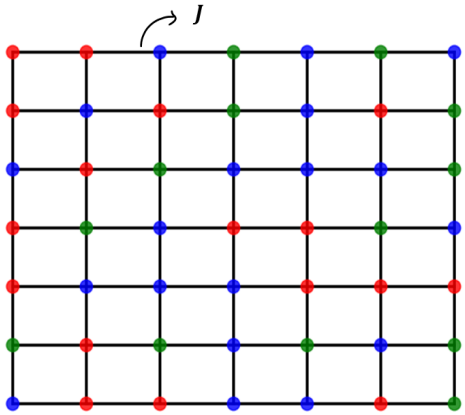


Figure 2: Graphical representation of the Potts model. Here the spins can take Q=3 values, which are shown as colours: green, blue and red. The interaction is taken between nearest neighbours and constant, shown through black straight lines. For simplicity the boundary conditions in this case have been taken as open ones.

where $i = 1, ..., Q$, $N_i$ represents the total number of spins with a given value, while $\rho_i$ represents its corresponding density. The magnetization will be defined as:

$$m = \frac{Q(max\{\rho_i\}) - 1}{Q - 1} \tag{9}$$

which corresponds to different possible ordered phases. In this thesis we will be interested only on the following values $Q \in \{1, 2, 3\}$ which coincide to the following critical models:

$$Q = \begin{cases} 1 & Percolation \\ 2 & Square\ Ising \\ 3 & 3 - Potts \end{cases} \tag{10}$$

In general, at criticality, there exists a simple relation to link the values of the spins, the critical temperature and the interaction magnitude, through the expression [22]:

$$\beta_c J = log(1 + \sqrt{Q}) \tag{11}$$

The Potts model has been largely studied in these above case, and its properties, physics, criticality and classes of universality are well known (for $Q \neq 1$). Further developments have been carried out with an additional generalization, trying to make the model less ideal and more realistic. In fact, until now, the interaction term has always been taken as homogeneous and constant, although real materials in nature are always characterized by *inhomogeneities* and *impurities*. There exists even some interesting and peculiar phenomena caused by

disorder, such as random lines of impurities [23]. The disorder can be taken into account in the model by rewriting the Hamiltonian as follows:

$$H^{dis}_{Potts} = \sum_{<ij>} J_{ij}\delta_{s_i,s_j} \tag{12}$$

where $J_{ij}$ is taken as a random variable. Without adding further complexity, we will focus once again only on ferromagnetic cases, therefore choosing $J_{ij} > 0$. The simplest way to implement this randomness, is to take the random variable between *two possible values*: $J_{ij} \in \{J_1, J_2\}$ [24]. There could be other options, such as three or more variables, although two are sufficient to describe disorder at this level, more complex implementations would not enrich the physical problem of interest, in fact we will see in the following section 2 that the relevant quantities which fix the problem are the cumulants of the disorder distribution. In *Figure* 3 it is shown how the previous representation is actually changed when the presence of defects in the lattice is considered.

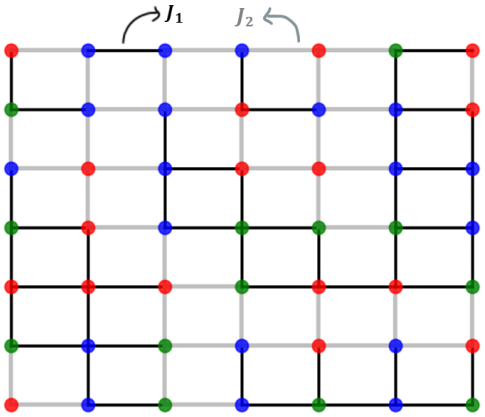


Figure 3: 3-states random Potts model on a square lattice. The interaction term is no longer constant but it is a random variable, then each bond is representative of an interaction between two spins with two possible different values, $J_1$ and $J_2$. For graphical representation they have been shown with a black straight line and a grey one.

This model, contains in its formulation the previous one since if we consider the interaction in terms of an additional random variable $\sigma_{ij}$:

$$J_{ij} = \frac{J_1 + J_2}{2} + \sigma_{ij}\frac{J_1 - J_2}{2}$$

it is simple to check that this construction allows the bimodal disorder:

$$J_{ij} = \begin{cases} J_1 & \sigma_{ij} = +1 \\ J_2 & \sigma_{ij} = -1 \end{cases} \tag{13}$$

With this, it is possible to see better how the disordered Potts model, sometimes called Random Bond Potts model, contains its *pure* formulation:

$$H^{dis}_{Potts} = \sum_{\langle ij \rangle} J_{ij}\delta_{s_i s_j} = \sum_{\langle ij \rangle} \left( \frac{J_1 + J_2}{2} + \sigma_{ij}\frac{J_1 - J_2}{2} \right) \delta_{s_i s_j}$$

$$H^{dis}_{Potts} = H_{Potts} + \sum_{\langle ij \rangle} \sigma_{ij}\frac{J_1 - J_2}{2}\delta_{s_i s_j} \tag{14}$$

To study this model, two additional parameters must be introduced, the first one will be the *disorder strength*

$$\Delta J = J_1 - J_2 \tag{15}$$

this is a measure of how far this generalized Random Potts model is from the previous classical, *pure*, one. In fact when the values of the interaction are equal $J_1 = J_2$ then we fall back in the previous case, and the quantity gives: $\Delta J = 0$. Sometimes, it will be useful even to consider an equivalent quantity, whose name will still be disorder strength, being just a different formulation of it:

$$r = \frac{J_1}{J_2} \tag{16}$$

Due to symmetry reasons, it can be chosen without any loss of generality $J_1 \geq J_2$. This will imply that $r \in [1, \infty)$; the pure model is recovered when the fraction is $r = 1$. The final additional parameter to be considered, is related to the correlation of the random variable and therefore of the bonds' interaction. If one takes two bonds $J_0$ and $J_d$, whose distance is denoted by $d$, as shown in *Figure* 4, their correlation can be defined as:

$$\langle J_0 J_d \rangle \propto |d|^{-a} \; for \; d >> 1 \tag{17}$$

The quantity $a$ will be called *correlation exponent*. Depending on the values of this quantity, there could be two different possible phenomena to describe. When $a \geq 2$, in a 2 dimensional system, the power low distribution has a fast decay and will be referred to *Short-Range* disorder whilst in the case of $a < 2$ this does not occur and it will correspond to the so-called *Long-Range disorder*[23].

This disorder that we are aiming to describe may influence a lot the macroscopic behaviours; sometimes randomness can shift the critical temperature up to destroying completely the presence of phase transitions, or it may lead to new physical behaviours[23][25]. A first important step to understand this, is characterizing the disorder in terms of the dynamical behaviour of the impurities. For the treatment of interest, in fact, it will be focused only on *quenched disorder*, meaning that the impurities are considered as parameters frozen in time[26]. This will allow to consider the probability distribution of the interactions as a function of a set of parameters that will not change in time. Considering the

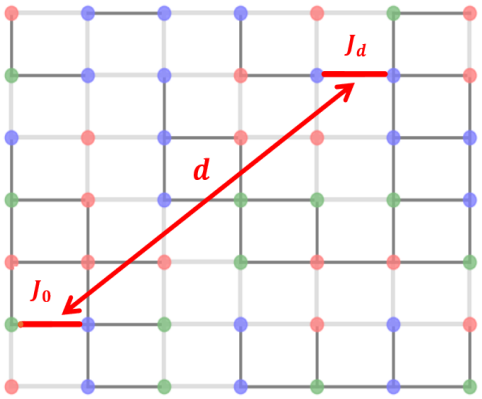


Figure 4: Representation of two bonds at a far distance $d$ to characterize the correlation between interactions

variable $\sigma$, the generic partition function will result in the parametric dependence of these degrees of freedom such that:

$$Z(\{\sigma\}) = \sum_{\{s\}} e^{-\beta H(\{s\},\{\sigma\})}$$

where it has been written explicitly the dependence of the previous Hamiltonian (14) with respect to the configuration of spins $\{s\}$ and disorder $\{\sigma\}$. The corresponding free energy will be:

$$F(\{\sigma\}) = -\frac{1}{\beta} log Z(\{\sigma\})$$

Each possible configuration of the disorder will be described by a probability distribution $P(\{\sigma\})$ such that the free energy in the thermodynamical limit must be equal to the free energy averaged over these degrees of freedom

$$\overline{F} = \sum_{\sigma} F(\{\sigma\}) P(\{\sigma\})$$

therefore:

$$\overline{F} = \overline{-\frac{1}{\beta} log Z(\{\sigma\})} \tag{18}$$

This quantity is called *quenched average free energy*. Moreover, since the free energy satisfy the self-average property, averages over the disorder are equivalent to their typical value [27]:

$$F_{typ} = \overline{F} \ for \ N, V \to \infty$$

so that all the relevant quantities can be derived from the computation of this quantity $\overline{F}$ and this is what will be done in this work.

When introducing these defects, in this framework, it comes natural asking: are the critical properties of the model affected by the disorder? If so, there still exists a critical behaviour or does it disappear? If there is still a phase transition what are the differences with the well known ones of the pure model? This thesis, structured in three different parts, aims at providing answers to the above questions with a particular interest in recognizing the presence of different universality classes and their domain of existence by both analytical and numerical techniques.

In the first part statistical physics tools and methods will be presented, starting from a general introduction to Renormalization Group (RG) in real space. The replica trick for the analytical treatment of disorder will be reported as well as the tool of Conformal Field Theory (CFT) and the perturbative approach. Additionally an insight on numerical techniques is given with a focus on the theoretical foundations of Monte Carlo methods and some of the most relevant algorithms which will be later used.

In the second section the techniques previously presented will be applied to the Short-Range Potts model. A dynamical equation of the parameter of the model will be obtained through RG up to 2-loop-order revising some of the computations made by Dotsenko, Picco and Pujol from a paper published in 1995 [28]. The fixed points will be computed to find the class of universality corresponding to the SR case. The stability of these critical phenomena will be carried out by means of nonlinear dynamical equations and the corresponding phase and bifurcation diagrams will be reported. A numerical investigation of the existence of these two universality classes will be presented, focusing on the computation of the magnetization critical exponents for a direct comparison with the analytical computation in the case of the 3-Potts model. Furthermore, a numerical perturbative approach will be implemented for a precise description of the renormalization flow near the critical pure point in order to obtain numerically its corresponding renormalization disorder eigenvalue.

In the last section it will be studied in an analogous way the Long-Range disordered Potts model, where a different disordered class of universality will be found with respect to the previous one. RG computation will be carried out up to 1-loop-order based on recent computations of Chippari, Picco and Santachiara on a paper published in 2023[29]. Fixed points will be studied in depth providing stability conditions by analytical and graphical means. Once again, numerical result will be presented, this time for 1,2,3-Potts models, through the perturbative technique developed before and providing disorder eigenvalues for each case, comparing the results with the theoretical predictions. This numerical method and the corresponding outcomes, in agreement with analytical computations, will represent the main, and novel, results of this work.

In the end of the thesis, general conclusions will be given, with a final recap of the methods used, the goals reached, some open questions left and possible additional scenario to gain a better understanding of the physics of this disordered model.

# 1 Analytical and Computational Tools [1]

## 1.1 Renormalization Group in real space [30]

### 1.1.1 General Framework

The whole idea of renormalization group relies on expressing a problem, modifying the scale, in terms of a simpler one if possible, which keeps unchanged the physical properties of the system. This can be done by exploiting the property of critical systems to be scale-invariant. Having an equivalent rescaled model requires parameters to be varied, and this creates the so called *renormalization group flow* in phase-space of the parameters involved in model. A mathematical example of a transformation of a system can be seen through the *coarse-graining procedure*, the focus will be from now on to work only in the real space, although, momentum space methods are widely used. Considering for instance a square Ising model described by the lattice parameter $a$ one can think to rewrite the Hamiltonian by grouping spins by nine ($3 \cdot 3$). They can be put together into a larger spin following a given rule (either the simple sum of the spins, or majority rule for instance), in such a way that the lattice rescales by a factor 3. This transformation leaves unchanged the property of the system and therefore the partition function at criticality. In this framework one can consider a more generic transformation indicated by $\mathcal{R}$ which acts on the parameters of the model $\{K\}$ in such a way to produce a new set of parameters following the expression:

$$\{K'\} = \mathcal{R}(\{K\})$$

For instance given a generic Ising model (2) the set of parameters is:

$$\{K\} = \{J, h\}$$

and a possible transformation could be considering the coarse grain mentioned before, in which 9 spins can be grouped together as in *Figure* 5.

Due to the equality of the partition function before and after the above transformation for the self-invariant property:

$$Z = \sum_{\{s\}} e^{-H(\{s\})} = \sum_{\{s'\}} e^{-H'(\{s'\})} = Z' \tag{19}$$

The Boltzmann factor has been absorbed in the Hamiltonian definition and for here the set $\{s'\}$ refers to the new variable coming from the coarse-graining procedure of grouping spins. The transformation can then be iterated till it reaches a fixed, point, this means that an additional transformation $\mathcal{R}$ will leave the parameters unchanged. Mathematically it can be expressed as:

$$\{K^*\} = \mathcal{R}(\{K^*\})$$

[1] In this first part of the thesis, at the beginning of sections or subsection, there will be reported references of textbooks or lecture notes and papers which have been used to provide the introduction to these well-known topics

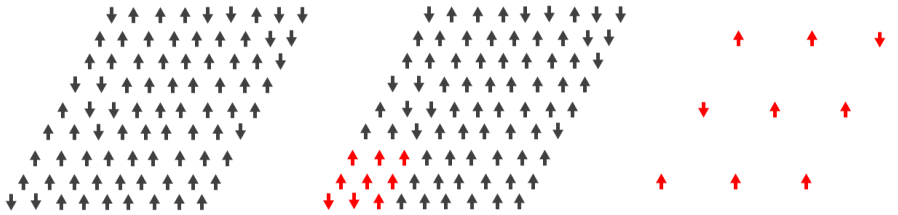

Figure 5: Example of transformation $\mathcal{R}$ on a square Ising model. each set of 9 spins, as in the central panel, are grouped together to form spins on a square lattice with three times the previous size

The equations describing the flow of parameters can be linearized in the vicinity of the fixed point through Taylor expansion:

$$K'_a \sim K^*_a + \sum_b \left.\frac{\partial K'_a}{\partial K_b}\right|_{K=K^*} (K_b - K^*_b) \tag{20}$$

where we can take the Jacobian entries $T_{ab} = \left.\frac{\partial K'_a}{\partial K_b}\right|_{K=K^*}$. Considering the set of left eigenvectors $\{e\}$ it can be written the corresponding secular equations:

$$\sum_a e^i_a T_{ab} = \lambda^i e^i_b$$

where $\{\lambda\}$ are the set of corresponding eigenvalues.

Generally the Jacobian is not symmetric, therefore there is no reason to assume that the right eigenvector are equivalent to the left eigenvectors so what follows will be considered for this specific set. One can introduce the *scaling variables*

$$u_i = \sum_a e^i_a (K_a - K^*_a)$$

which are linear deviation of the parameters at the fixed points. They transform in a multiplicative way through renormalization:

$$u'_i = \sum_{a,b} e^i_a T_{ab} (K_b - K^*_b) = \sum_b \lambda^i e^i_b (K_b - K^*_b) = \lambda^i u_i \tag{21}$$

One can now define the fundamental quantities quantities: $\lambda^i = b^{y_i}$ where $y_i$ are the *renormalization group eigenvalues* and $b$ is the rescaling of the lattice size $a' = ba$. Three different cases can be distinguished:

1. $y_i > 0$
   relevant eigenvalue, the iterations of the transformation bring away from the fixed point

2. $y_i < 0$
   this defines an irrelevant eigenvalues, successive iteration will lead the parameter to smaller values

3. $y_i = 0$
   called marginal case, the behaviour cannot be known without further information.

### 1.1.2 Scaling of the free energy and critical exponents

It can now be taken into account the free energy which, in the general case, will depend on the parameters of the model:

$$f(\{K\}) = \frac{1}{N} log(Z(\{K\}))$$

Now applying the renormalization equations, due to (19) a new term appears which is constant and related to the coupling, it will be denoted $g(\{K\})$ such that

$$e^{-Nf(\{K\})} = e^{-Ng(\{K\})-N'f(\{K'\})}$$

where $N' = b^{-d}N$ which gives the fundamental relation:

$$f(\{K\}) = -g(\{K\}) + b^{-d}f(\{K'\}) \tag{22}$$

which represents an inhomogenous transformation. However, since we are interested just in the singular behaviour of the free energy, we can simply consider the homogeneous relation dropping the additional term $g$ giving the relation:

$$f_s(\{K\}) = b^{-d}f_s(\{K'\}) \tag{23}$$

For the following part we focus on the computation of critical exponents considering the simple example of the Ising model, in which the number of physical parameters it depends on is equal to two. This corresponds to consider two relevant terms in the Hamiltonian, a thermal one (therefore related to the temperature) and one related to the external magnetic field. They will be denoted as $u_t, u_h$ with corresponding eigenvalues $y_t$ and $y_h$. The equation of the free energy becomes:

$$f_s(u_t, u_h) = b^{-d}f_s(u'_t, u'_h) = b^{-d}f_s(b^{y_t}u_t, b^{y_h}u_h)$$

Iterating now the renormalization, for instance rescaling $n$ times the size of the system, we get the recursive relation:

$$f_s(u_t, u_h) = b^{-nd}f_s(b^{ny_t}u_t, b^{ny_d}u_h) \tag{24}$$

Since $u_t$ and $u_h$ are both relevant variables, meaning that the eigenvalues are positive, the free energy will depend on increasing quantities. Therefore, to avoid problems in the equation, we stop at a given iteration in such a way that

$$|b^{ny_t}| = u_{t0}$$

where $u_{t0}$ is arbitrarily chosen but it is fixed to be sufficiently small to ensure the linear approximation's (20) validity.

This allows to perform the following change of variable:

$$b^n = \left| \frac{u_{t0}}{u_t} \right|$$

$$f_s(u_t, u_h) = \left| \frac{u_t}{u_{t0}} \right|^{\frac{d}{y_t}} f_s\left( \pm u_{t0}, \left| \frac{u_t}{u_{t0}} \right|^{\frac{-y_h}{y_t}} u_h \right)$$

Finally this expression can be rewritten in terms of the original reduced variable $t, h$:

$$f_s(t, h) = \left| \frac{t}{t_0} \right|^{\frac{d}{y_t}} \Phi\left( \left| \frac{t}{t_0} \right|^{\frac{-y_h}{y_t}} \frac{h}{h_0} \right)$$

The dependence on the left hand side of the equation, for $t_0$, is not present therefore it cannot be present on the right hand side either. The function defined $\Phi$ is called *scaling function* and from this expression one can compute all the critical exponents. The critical exponent related to the specific heat is given, for instance, by the following computation:

$$\left. \frac{\partial^2 f}{\partial t^2} \right|_{h=0}$$

which will be developped before. We start from the computation of the first derivative:

$$\frac{\partial f}{\partial t} = \left| \frac{t}{t_0} \right|^{\frac{d}{y_t}-1} \frac{d}{y_t t_0} \Phi\left( \left| \frac{t}{t_0} \right|^{\frac{-y_h}{y_t}} \frac{h}{h_0} \right) + \left| \frac{t}{t_0} \right|^{\frac{d}{y_t}} \Phi'\left( \left| \frac{t}{t_0} \right|^{\frac{-y_h}{y_t}} \frac{h}{h_0} \right) \left| \frac{t}{t_0} \right|^{\frac{-y_h}{y_t}-1} \frac{-y_h}{y_t t_0} \frac{h}{h_0}$$

Now it can be computed the second derivative, since this will be given by the contribution of fours terms, the only quantity which we will be interested is the non-null one when we set to zero the magnetic field. The only resulting term will be:

$$\left. \frac{\partial^2 f}{\partial t^2} \right|_{h=0} = \left| \frac{t}{t_0} \right|^{\frac{d}{y_t}-2} \frac{d}{y_t t_0^2} \left( \frac{d}{y_t} - 1 \right) \propto |t|^{\frac{d}{y_t}-2}$$

such that the specific heat exponent is:

$$\alpha = 2 - \frac{d}{y_t}$$

In a completely analogous way one can get through simple derivation of the free energy the following relations (with some additional manipulation for the computation of $\delta$):

$$\left. \frac{\partial f}{\partial h} \right|_{h=0} \propto (-t)^{\frac{d-y_h}{y_t}}$$

$$\left. \frac{\partial^2 f}{\partial h^2} \right|_{h=0} \propto |t|^{\frac{d-2y_h}{y_t}}$$

$$\left.\frac{\partial f}{\partial h}\right|_{t=0} \propto h^{\frac{d}{y_h}-1}$$

which gives the following scaling exponents:

$$\beta = \frac{d-y_h}{y_t},\ \gamma = \frac{d-2y_h}{y_t},\ \delta = \frac{d}{y_h} - 1$$

In general there are not all independent, but there exist different scaling relations which link them:

$$\begin{aligned} \alpha + 2\beta + \gamma = 2 \quad & Rushbrooke \\ \beta + \gamma = \beta\delta \quad & Griffiths \\ 2 - \alpha = d\nu \quad & hyperscaling \end{aligned} \tag{25}$$

### 1.1.3 Scaling of the correlation length

An additional important analysis is related to the critical exponent of the correlation length, which is the quantity already introduced, but defined in more details below:

$$G(r_1 - r_2, H) = \langle s(r_1)s(r_2)\rangle_H - \langle s(r_1)\rangle_H \langle s(r_2)\rangle_H$$

where $H$ is taken as the hamiltonian without external field term. The presence of this additional magnetic field parameter however, can be added in the Hamiltonian to link directly $G$ to the partition function:

$$G(r_1 - r_2, H) = \left.\frac{\partial^2 lnZ}{\partial h'(r_1')\partial h'(r_2')}\right|_{h=0}$$

One now can apply the renormalization procedure, and since the field changes as follows: $h'(r') = b^{y_h}h(r)$, due to (19) it must be true:

$$\frac{\partial^2 lnZ'}{\partial h'(r_1')\partial h(r_2')} = \frac{\partial^2 lnZ}{\partial h(r_1)\partial h(r_2)}$$

The first expression is the renormalized correlation length, which can be written in terms of the first lattice length through the rescaling $b$ :

$$G\left(\frac{r_1 - r_2}{b}, H'\right) = \frac{\partial^2 lnZ'}{\partial h'(r_1')\partial h(r_2')}$$

Now, it is possible to link through some rescaling arguments the correlation function of the original lattice:

$$G\left(\frac{r_1 - r_2}{b}, H'\right) = b^{2(d-y_h)}G(r_1 - r_2, H)$$

This can be expressed in terms of the parameters and setting the field to zero

$$G(r,t) = b^{-2(d-y_t)}G\left(\frac{r}{b}, b_t^y t_0\right)$$

Repeating the same procedure that led to (24), renormalizing n times, stopping sufficiently close to a point in which the linear expansion is still valid, we will obtain a scaling function which will depend on a critical exponent such that:

$$\nu = \frac{1}{y_t} \tag{26}$$

### 1.1.4 Scaling operator and scaling dimensions

When in these statistical models the continuous limit is taken, the theories become equivalent to quantum field theories, therefore one can speak about fields as operators through. One can then write, given a set of operators, a univocal equivalence to a linear combination of the scaling fields:

$$\sum_i u_i \phi_i = \sum_a (K_a - K_a^*) S_a$$

and it is possible to show that as $|r_1 - r_2| \to \infty$ it is possible to relate the renormalization group eigenvalue of a scaling variable to the behaviour of the fixed point of the two point correlation function of the operator considered such that:

$$\langle \phi(r_1)\phi(r_2) \rangle \propto |r_1 - r_2|^{-2h_i} \tag{27}$$

the quantity $h_i$ is called *scaling dimension* of the scaling operator and this relation can be explain taking the continuous limit of this quantity;

$$\sum_i \sum_r u_i \phi_i \to \sum_i u_i \int \phi_i(r) \frac{d^d r}{a^d}$$

where $a$ here is the lattice size that under renormalization becomes $a' = ba$. If under renormalization we must ensure the partition function to be invariant we must require that:

$$\phi_i(r) \to b^{h_i} \phi_i(r)$$

This transformation allows in general to compute how the N-point correlation function behaves, and it can be shown below:

$$\langle \phi(r_1)\phi(r_2)...\phi_N(r_N) \rangle \propto R^{-x_1 - x_2 - ... - x_N} \left\langle \phi\left(\frac{r_1}{R}\right)\phi\left(\frac{r_2}{R}\right)...\phi\left(\frac{r_N}{R}\right) \right\rangle \tag{28}$$

## 1.2 Random systems and disorder treatment [30]

### 1.2.1 Replica Method

The quenched free energy (18) requires the computation of the average over the logarithm of the partition function which is hard to treat. In disordered systems there exist a way to overcome this, called *replica trick* and which consists on the following equality:

$$logZ = \lim_{n\to 0} \frac{Z^n - 1}{n} \tag{29}$$

This allows to rewrite the quenched average in the following way:

$$\overline{F} = -\frac{1}{\beta} \lim_{n\to 0} \frac{\overline{Z^n} - 1}{n} \tag{30}$$

The series expansion of the quantity involved is called *replicated partition function*, which can be seen as $n$ identical copies of the initial system, therefore each of them will be identified by their own states and configurations.

One can therefore write:

$$Z^n(\{\sigma\}) = \sum_{\{s_a\}} e^{-\sum_a H(\{s_a\},\{\sigma\})}$$

where $a$ is the index of the replica such that $a \in \{1, ..., n\}$. The corresponding averaged quantity is:

$$\overline{Z^n} = \sum_{\{\sigma\}} \sum_{\{s_a\}} P(\{\sigma\}) e^{-\sum_a H(\{s_a\},\{\sigma\})}$$

and the two sums can be exchanged giving

$$\overline{Z^n} = \sum_{\{s_a\}} \sum_{\{\sigma\}} P(\{\sigma\}) e^{-\sum_a H(\{s_a\},\{\sigma\})}$$

This quantity can be treated, and can lead to possible solutions of the problems of interest by later requiring the limit of vanishing replicas $n \to 0$. An example of this disordered calculation is given below.

### 1.2.2 Harris criterion

Let's consider the following Hamiltonian:

$$H = H^* + \sum_i \sigma_i \epsilon(i)$$

where $\epsilon$ represent the local energy density and $i$ is one of the $N$ vertex of the square lattice with a systems size of $L$, such that it runs in $\{1, ..., L^2\}$. The quenched average partition function becomes:

$$\overline{Z^n} = \sum_{\{s_a\}} \sum_{\{\sigma\}} P(\{\sigma\}) e^{-\sum_a H_a^* - \sum_a \sum_i \sigma_i \epsilon_a(i)}$$

where $a$ takes into account the replica of the systems. The idea now is to apply a cumulant expansion, more in detail:

$$\overline{Z^n} = \sum_{\{s_a\}} e^{-\sum_a H_a^*} \sum_{\{\sigma\}} P(\{\sigma\}) e^{-\sum_a \sum_i \sigma_i \epsilon_a(i)}$$

$$\overline{Z^n} = \sum_{\{s_a\}} e^{-\sum_a H_a^*} e^{-\overline{\sigma} \sum_a \sum_i \epsilon_a(i) + \frac{1}{2} \sum_{a,b} \sum_{i,j} (\overline{\sigma(i)\sigma(j)} - \overline{\sigma}^2) \epsilon_a(i) \epsilon_b(j)} + \mathcal{O}(\epsilon^3) \quad (31)$$

where additional higher order terms have been neglected. The relevance of the operator $\epsilon\epsilon$ that couples different replica, therefore for $a \neq b$ can be computed through the scaling of its two point percolation function:

$$< \sum_{a \neq b} \epsilon_a(i) \epsilon_b(i) \sum_{c \neq d} \epsilon_c(j) \epsilon_d(j) > \sim \frac{1}{|i-j|^{4h_\epsilon}}$$

given $h_\epsilon = d - y_\epsilon$ the local energy field dimension and $y_\epsilon$ the renormalization eigenvalue. In particular we recall that due to (26):

$$d - y_\epsilon = d - \frac{1}{\nu}$$

Therefore the perturbation due to randomness, given by $\epsilon\epsilon$, whose dimension is related by a factor two with the one of the operator $\epsilon$, gives

$$y = d - h_{\epsilon\epsilon} = d - 2h_\epsilon = \frac{2}{\nu} - d$$

which is irrelevant for $y < 0$ and equivalent to the condition:

$$d\nu > 2$$

Due to the hyperscaling relation (25) this previous result can be simply encoded in the condition of the critical exponent of the specific heat to give the so-called *Harris criterion* for the relevancy of the disorder:

$$\alpha < 0$$

Even though the randomness is irrelevant shift to the critical temperature (to lower values) occurs, meanwhile when the operators become relevant a new fixed point must be found. Although all of this is consistent if and only if the disorder is uncorrelated. When this condition does not hold anymore, there exist a generalization called, *Extended Harris criterion* or *Weinrib-Halperin* conjecture [23], which has been relevant in the disorder studies. In fact it generalise the previous result by taking the same expression of the correlated disorder given by equation (17) and states that the disorder is irrelevant if for $a < d$

$$\alpha < 2 - 2\frac{d}{a}$$

while for $d > a$ we find the previous condition. Moreover they provided, through heuristic arguments, a relation for correlation exponent:

$$\nu = \frac{2}{a} \quad (32)$$

## 1.3 Conformal Field theory and Perturbative RG

### 1.3.1 Conformal Field Theory [31]

An important tool that can be exploited for the study of critical models is the one of conformal field theories. To briefly introduce it, we need to understand its connection with the type of analysis we would like to carry out throughout the thesis. CFT is strictly related to quantum field theories. But then the question would be how statistical mechanics and QFT are linked to each other. There are different way to connect and construct from classical Hamiltonian effective field theories, but the similarities go beyond direct formal transformations from the one to the other. Despite their differences, the ways some problems are tackled are analogous: for instance the computation of averages in statistical mechanics makes use of the partition function and it can be compared to the computation of averages of path integrals in QFT with a given action[32]. Conformal field theory is a core element of QFT since it is a quantum field theory that is invariant under a *conformal group*. The most general way to define CFT, is considering the set of transformation for spacetime that leaves angles unchanged. The most simple transformation that follows this is a scale one. Taken for instance an equilateral triangle with given length $l$ for instance, the transformation $l' = \lambda l$ applied to each segment will rescale it to another equilateral triangle, in which angles are unchanged. In general conformal transformation are quite general and when applied to a given space, they correspond to the change of its metric. Although, if we think to systems that are characterized by scale invariant, they will necessarily have the property to be invariant under scale transformation, by definition. But then any theory with a scale-invariance will be conformally-invariant. Since all critical phenomena, due to the divergence of the correlation length are characterized by this property, they will necessarily be related to conformal theories. Some of the computations presented, for instance, were already main results of CFT, in fact the scaling behaviours of observables, which are governed by the set of critical exponents, are strictly connected to the relevant operators of CFTs. Even the renormalization procedure seen is well connected to CFT. When we have described in the equations of parameters, after rescaling the system, the presence of fixed point whose stability controls the renormalization group flow, a generic point in the phase diagram can actually be seen as a QFT described by some given coupling set. Since fixed points are actually conformal field theories, any QFT can actually be seen as their perturbation, and this is exactly the idea to apply the pertrubative RG technique presented below.

### 1.3.2 Perturbative Renormlization group [30]

If a system has two fixed points that are close to each other for instance, a perturbative analysis can be applied from a known fixed point to reach the other one; this is useful to deduce possible new universality classes by analyzing the renormalization group flow. The main idea relies on the description of an Hamiltonian as the sum of two contributions similarly to what has been done

previously with the random Potts model:

$$\tilde{H} = H^* + H_p$$

where $H^*$ represent the hamiltonian at the known fixed point, meanwhile $H_p$ represents a perturbation. In the following, it will be taken of the general from:

$$H_p = \sum_i g_i \sum_r a^{h_i} \phi_i(r)$$

with $g_i$ the set of perturbation coefficients or parameters, each associated to a generic field $\phi_i$. Since it is necessary to calculate the exponential of this hamiltonian for the computation of the partition function, the expressions that appear must be adimensional. The quantity $a^{h_i}$ takes into account the field dimensionality $[\phi_i] = L^{-h_i}$ such that adimensionality is ensured:

$$Z = \sum_{states} e^{-H^* - \sum_i g_i \sum_r a^{h_i} \phi_i(r)}$$

In critical phenomena, the divergence of the correlation length allows to replace the summation over discreet lattice points, due to $a << \xi$, with a continuous limit:

$$\sum_r \to \frac{1}{a^d} \int d^d r$$

therefore one is able to write:

$$\tilde{H} = H^* + \sum_i g_i \frac{1}{a^{d-h_i}} \int d^d r \phi_i(r)$$

and performing an expansion of the partition function in terms of the coupling one can obtain:

$$\begin{aligned} Z = Z^* \Bigg[ 1 - \sum_i g_i \frac{1}{a^{d-h_i}} \int d^d r \langle \phi_i(r) \rangle \\ + \frac{1}{2} \sum_{i,j} g_i g_j \frac{1}{a^{2d-h_i-h_j}} \int d^d r_1 \int d^d r_2 \langle \phi_i(r_1) \phi_j(r_2) \rangle + \\ - \frac{1}{3!} \sum_{i,j,k} g_i g_j g_k \frac{1}{a^{3d-h_i-h_j-h_k}} \int d^d r_1 \int d^d r_2 \cdot \\ \cdot \int d^d r_3 \langle \phi_i(r_1) \phi_j(r_2) \phi_j(r_3) \rangle + o(g_i g_j g_k g_l) \Bigg] \end{aligned} \tag{33}$$

which represents the first starting point to obtain the renormalization group equations. The renormalization transformation is performed now through a

rescaling of the system: $a \to ba$ where b it is chosen as an infinitesimal displacement: $b = 1+\delta l,\ \delta l << 1$. Exploiting the property of (19) it is possible to write the new rescaled partition function. Focusing on the first term:

$$\sum_i g_i \frac{1}{a^{d-h_i}(1+\delta l)^{d-h_i}} \int_{|r>a(1+\delta l)|} d^d r \langle \phi_i(r) \rangle$$

which implies

$$g_i \to g_i(1+\delta l)^{d-h_i} \sim g_i + g_i(d-h_i)\delta l \tag{34}$$

The second term gives a less intuitive result, first of all it is important to split the integral in two contributions exploiting the additive property of integrals:

$$\int_{|r_1-r_2|>a(1+\delta l)} = \int_{|r_1-r_2|>a} - \int_{a<|r_1-r_2|<a(1+\delta l)}$$

while the first term give the simple original contribution, the second one produces an effective change.

To understand the correct way to proceed it must be introduce the concept of product operator expansion (OPE). Given the correlation function expression

$$\langle \phi_i(r_1)\phi_j(r_2)\Phi \rangle$$

where it has been denoted the arbitrary product of all other operators with the notation $\Phi = \Pi_l \phi_l(r_l)$, it is wanted to study the behaviour in the case in which $|r_1 - r_l| << |r_1 - r_l|$ with $l > 2$, and in this limit it is possible to write

$$\langle \phi_i(r_1)\phi_j(r_2)\Phi \rangle = \sum_k C_{ijk}(r1-r2) \left\langle \phi_k\left(\frac{r_1+r_2}{2}\right)\Phi \right\rangle \tag{35}$$

Moreover the operators product $\Phi$, that appears on both sides, is independent from $\phi$ products, and can be simplified.

$$\langle \phi_i(r_1)\phi_j(r_2) \rangle = \sum_k C_{ijk}(r_1-r_2) \left\langle \phi_k\left(\frac{r_1+r_2}{2}\right) \right\rangle \tag{36}$$

Due to the scaling argument of the coefficients it must hold the relation:

$$C_{ijk}(r_1-r_2) = \frac{c_{ijk}}{|r_1-r_2|^{h_i+h_j-h_k}} \tag{37}$$

This expansion allows to compute the previous integral:

$$\frac{1}{2}\sum_{i,j} g_i g_j \frac{1}{a^{2d-h_i-h_j}} \int_{a<|r1-r2|<a(1+\delta l)} d^d r_1 d^d r_2 \langle \phi_i(r_1)\phi_j(r_2) \rangle =$$

$$= \frac{1}{2}\sum_{i,j} g_i g_j \frac{a^{h_i+h_j-h_k}}{a^{2d-h_i-h_j}} \sum_k C_{ijk}(r_1-r_2) \int_{a<|r_1-r_2|<a(1+\delta l)} d^d r_1 d^d r_2 \left\langle \phi_k\left(\frac{r_1+r_2}{2}\right) \right\rangle$$

$$= \frac{1}{2}\sum_{i,j} g_i g_j \frac{a^{h_i+h_j-h_k}}{a^{2d-h_i-h_j}} \sum_k c_{ijk} \int_{a<|r_1-r_2|<a(1+\delta l)} d^d r_1 d^d r_2 \frac{1}{|r_1-r_2|^{h_i+h_j-h_k}}$$

If one consider that the integration produces a factor $S_d a^d \delta l$ where $S_d$ is the area of the hyper-sphere of unit radius in d dimensions, one has the following rescaling:

$$g_k \to g_k - \frac{1}{2} S_d \sum_{ij} g_i g_j \delta l \tag{38}$$

and putting together (34), (38) the overall contribution is:

$$\frac{dg_k}{dl} = (d - x_k) g_k - \frac{1}{2} S_d \sum_{ij} g_i g_j + o(g_i g_j g_l)$$

therefore, considering the known relation one obtains the general expression:

$$\frac{dg_k}{dl} = y_k g_k - \frac{1}{2} S_d \sum_{ij} g_i g_j + o(g_i g_j g_l) \tag{39}$$

at the first loop-order. The second loop order has an increasing complexity, and will be treated in more details in the specific case of the Potts model in section 2.1.3. This concludes a brief introduction to the techniques which will be used for the analytical computations of the thesis and that require the renormalization method, but more will be said in each specific case considered.

## 1.4 MonteCarlo methods

### 1.4.1 Towards a stochastic development for simulations [33]

In physics the importance of the formalism used to treat problems has always been a core element to comprehend systems physical features. Newton's mechanics, which posed the basis for the equation of motion in classical physics, were found not to be appropriate to tackle certain phenomena, and this pushed the search for new ways to describe and solve problems.

Fundamental branches of physics like relativity and quantum mechanics were developed following this need to shift from the common prospective trying to find a language who could suit the problems which wanted to be treated. But not all new descriptions were born just from this need, sometimes even a simple change of point of view on problems already known and solved would have pushed new methods. This is what happened for instance for analytic mechanics developped by Lagrange and Hamilton, they rethought classical mechanics in terms of new and equivalent equation of motions, solving already known problems in different manners and generalizing them.

Statistical physics represents another paradigmatic example of necessary language transformation, and due the relevancy on the subject which will be treated it will be understood more in details its impact. If one tries to describe N Avogadro number of particle of a perfect gas confined in a cubic box, the possibility of solving Newton's equation to know the trajectories and the velocities at each time steps, not only is not feasible but it lacks consistency in order to know macroscopic quantities which remains unaffected by precise microscopic representation.

The importance of statistical mechanics formalism comes from the impossibility to treat physical systems with large degrees of freedom in classical physics, adopting a non-deterministic approach based on probability distribution and measures which results sufficient to define quantities through means of averages and which are able to be compared with experimental results.

An example which highlights the main difference with this formalism comes from the computation of the energy of the above mentions confined gas: Newton's equations would require the solution of $2N_A$ differential equations and given a general energy function made up by kinetic terms and generic interaction between particles, the wanted quantity would then been computed as follows

$$E = \frac{1}{t_0}\int_0^{t_0} dt E(t) = \frac{1}{t_0}\int_0^{t_0} dt\left(\sum_i^N \frac{p_i^2(t)}{2m} + V(\vec{x}(t))\right)$$

where $p_i$ is the momentum of the particle and $V$ a generic potential. But with the introduction of the canonical formalism, the same quantity can be written through Boltzmann's measure:

$$E = \langle H\rangle = \frac{\int d\vec{p}\, d\vec{x}\; He^{-\beta H}}{\int d\vec{p}\, d\vec{x}\; e^{-\beta H}} = \frac{1}{\mathcal{Z}_{Canonical}}\int d\vec{p}\, d\vec{x}\; He^{-\beta H}$$

And this computation, for certain interactions, is perfectly feasible through factorization and integrals, without requiring to solve a proportional Avogadro number of differential equations.

Using this description, a generic observable for a system which is characterized by discreet configurations $C_{1,...,\mathcal{N}}$ can be computed as follows:

$$\langle \mathcal{O} \rangle = \frac{\sum_i^{\mathcal{N}} \mathcal{O}(C_i) e^{-\beta H}}{\sum_i^{\mathcal{N}} e^{-\beta H}} = \frac{\sum_i^{\mathcal{N}} \mathcal{O}(C_i) e^{-\beta H}}{\mathcal{Z}}$$

Whilst this is feasible for some types of hamiltonian and some type of observable, this formalism is still not sufficient for numerical implementation, since the partition function would still require a sum over all possible configuration, and if one takes the example of the Ising model (2), this results on all the possible up-down configurations which are exponential in the number of spins, and makes the system numerically intractable.

This led to the use of a different description of the physical systems, and the one adopted is related to go from a probabilistic dynamics to a stochastic one. This has been crucial for the development of the most used techniques in numerical simulation: Monte Carlo methods. Before going in depth with the latter it will be introduced the basis of this stochastic language to briefly show the shift in the description and the main characteristics.

### 1.4.2 Markov Chains and Markov Monte Carlo [34]

When a systems is characterized by some degrees of freedom which allow for a dynamic to happen amongst different possible configuration, knowing in which one the system will be at a certain time, given where it was at all time before from the initial one, can be done in terms of conditional probability. In this section it will be focused on a interval of time which is discreet, where for simplicity the time step in taken as a unit, whilst the configurations runs form $C_1, ..., C_{\mathcal{N}}$ and the mentioned probability can be written as follows:

$$P(x_t = C_{i_t} | x_{t-1} = C_{i_{t-1}}, ..., x_{t=0} = C_{i_0})$$

But for some processes this probability has a one step-memory, so what happens at a given time is fully characterize by what happens at the time before:

$$P(x_t = C_{i_t} | x_{t-1} = C_{i_{t-1}}, ..., x_{t=0} = C_{i_0}) = P(x_t = C_{i_t} | x_{t-1} = C_{i_{t-1}}) = P_{i_t, i_{t-1}}$$

This property, called *markovianity*, defines processes called *Markov chains*. It can be defined for a single step a matrix that describes the transition probabilities form a configuration to the next one. Its dimension is related to the number of configuration and it will in general be of the type: $P \in \mathcal{R}^{\mathcal{N},\mathcal{N}}$ characterized by the following features:

- all entries are non negative; $P_{ij} \geq 0$
- $\sum_j^{\mathcal{N}} P_{ij} = 1$

The last property comes from the fact that when a system is on a given configuration, since the probability is normalized, the sum of the probabilities of all the possible configuration must be one. A matrix with this property is called a *stochastic matrix*. If the initial condition is that the process starts from a given configuration $C_{\tilde{i_0}}$ then, the vector of probabilities of being on a given configuration at a given time will be entailed by a delta Kronecker:

$$\pi_{t=0} = (0, ..., 0, 1, 0, ..., 0)$$

being $\pi^i_{t=0} = \delta_{i,\tilde{i_0}}$ Then the probability at the next step will evolve through the stochastic matrix as follows:

$$\pi^T_{t=1} = \pi^T_{t=0}\ P$$

it is important to understand how the probability vector can be written if an interval of time is considered, to do so it can be used the Chapman-Kolmogorov equation that reads:

$$P^{(n)}_{ij} = (P \cdot P \cdot P \cdot ... \cdot P) = (P^n_{ij})$$

such that:

$$\pi^T_{t=n} = \pi^T_{t=0}\ P^n$$

Therefore the evolution is completely determined by the stochastic matrix, as well as the transition probabilities from one configuration to another. We focus now on the description of systems which are characterized by stationary, therefore the systems who are able to fulfill the condition:

$$P \cdot P_{eq} = P_{eq} \rightarrow,\ P_{eq} = \lim_{n\to\infty} P$$

for which this limit exists and it is well defined. From this it follows that the probability vector on a given configuration does no longer change in time:

$$\lim_{n\to\infty} (\pi^n)^T = \pi^T_{eq} \rightarrow \pi^T_{eq} = \pi^T_{eq} P_{eq}$$

This asymptotic behaviour has been proved to hold for Ergodic Markov chains which are characterized by a probability stochastic matrix whose entries are, at all time steps, positive. We will focus just on systems which are characterized by this property. Therefore, using the Chapman Kolmogorov equation and what mentioned above it can be written the relation:

$$\pi^{t+1}_j - \pi^t_j = \sum_{i\neq j} P_{ij}\pi^T_i - P_{ji}\pi^T_j$$

But if the system reach stationary then;

$$0 = \sum_{i\neq j} P_{ij}\pi^T_i - P_{ji}\pi^T_j$$

And moreover, if we are not just interest on systems which reach stationary but even the equilibrium condition, then it is possible to write the so-called *detailed balance condition* for which the above expression is fulfilled for each value of the sum:

$$P_{ij}\pi_i^T - P_{ji}\pi_j^T = 0$$
$$P_{ij}\pi_i^T = P_{ji}\pi_j^T \tag{40}$$

The above brief treatment for this formalism is sufficient to introduce the Monte Carlo methods.

Taking into account the mentioned Ising case (2) in which observables must be computed taking into account all possible configurations of spins, which are indeed exponential, one can think to restrict the space of configuration into a much smaller one in which terms with a low Boltzmann weight can be disregarded. In doing so, for instance, one could think to take $\tilde{C} \in \{C_1, ..., C_{\mathcal{N}}\}$ which elements can be denoted as $\tilde{C} \in C_{i_1}, ..., C_{i_T}$ with $T << \mathcal{N}$ such that the canonical average will be written as:

$$\langle A \rangle_{Canonical} \simeq \frac{1}{T}\sum_{j=1}^{T} A(C_{i_j}) \tag{41}$$

Then in this way, choosing the correct sequences of configuration transforms into choosing the stochastic matrix $P$ which generates, as the equilibrium distribution probability, the vector whose entries exactly corresponds to:

$$p_i = \frac{e^{-\beta H(C_i)}}{Z}$$

Taking entries which satisfy the detailed balance condition (40) it can be written

$$\frac{P_{ij}}{P_{ji}} = \frac{\pi_j}{\pi_i} = \frac{e^{-\beta H(C_j)}}{e^{-\beta H(C_i)}} = e^{\beta(H(C_i) - H(C_j)} \tag{42}$$

The main problem can be modified and addressed in finding a way to extract configurations $C_i, ..., C_{i_T}$ exploiting the ratio of elements of the equilibrium distribution vector. The computation of the partition function is avoided in this way, disregarding the possibility of implementing an algorithm which would be exponential in time linked to it.

### 1.4.3 Local updates: Metropolis-Hastings Algorithm [33],[34]

Amongst the possible update algorithms, *local ones* were the first invented and implemented, in particular the *Metropolis-Hastings algorithm* which is one of the most versatile and exploited. It consist on generate the correct configurations changing one spin at a time. In particular it considers the matrix entries

$$P_{ij} = P(C_j \to C_i) = \begin{cases} 1 & if\ E_{new} < E_{old} \\ e^{-\beta(E_{new} - E_{old})} & otherwise \end{cases} \tag{43}$$

which can be rewritten in a more compact way as follows:

$$P_{ij} = min\{1, e^{-\beta \Delta H}\}$$

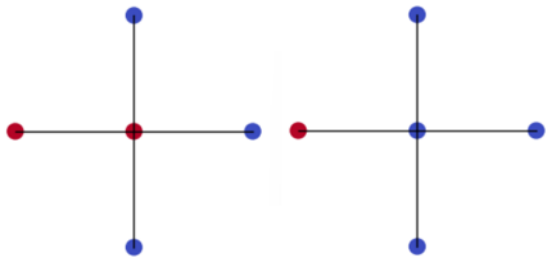

Figure 6: Example of local update in the Metropolis Hastings algorithm on 2d square Ising. A spin $s_i$ is flipped, since the energy of the new configuration is smaller than the original one

Therefore the algorithms select randomly a spin position, and tries to flip it, the energy of the previous configuration is computed as well as the one of the new configuration, than this new configuration is accepted in the way above shown (43). In particular, another random variable is extracted and, if this random value is smaller than $P_{ij}$, then the new configuration is accepted, otherwise, another spin is taken to repeat the process. One consider then a MonteCarlo sweep as the number of iterations of this algorithms that on average updates all number of degrees of freedom of the lattice size (all the spins). In this way the dynamics over time has been changed into a dynamics over MonteCarlo sweeps, from which now averages can be computed in a treatable time. The first MonteCarlo sweeps are always related to the dynamics to equilibrium, so those configurations which are necessary to reach the equilibrium condition of the system. Whenever simulations are performed, the first thing is setting MonteCarlo sweeps so that the system thermalizes. After that, MonteCarlo sweeps can be used for averages of the quantities of interest (like energy, magnetization and so on). The sweeps are necessary at this point to guarantee unbiased thermal averages, meaning that the quantities which are averaged must be uncorrelated measurements, this guarantee numerical averages to be the correct physical quantities corresponding to the ones that we want to measure.

### 1.4.4 Critical slowing down [34]

Local update algorithms have an easy and straightforward implementation, although, they have a major drawback. When one tries to simulate the systems close to the critical temperature, in presence of a second order phase transition, the correlation length diverges, and this has some main effects on correlation

time. If one consider the auto-correlation function defined as follows:

$$A(k) = \frac{\langle \mathcal{O}_i \mathcal{O}_{i+k} \rangle - \langle \mathcal{O}_i \rangle \langle \mathcal{O}_{i+k} \rangle}{\langle \mathcal{O}_i^2 \rangle - \langle \mathcal{O}_i \rangle^2}$$

for large time separation it decays exponentially as follows:

$$A(k) \to a e^{-\frac{k}{\tau_{\mathcal{O}}}}$$

which defines the exponential autocorrelation time. Close to a critical point, in an infinite volume, it follows a power law behaviour as follows:

$$\tau_{\mathcal{O}} \propto \xi^z \tag{44}$$

where $z$ is an additional critical exponent, called *dynamical critical exponent*. Since the correlation length diverges at the critical point, the same happens for the autocorrelation time, which leads to a phenomenon called *critical slowing down*.

As numerical simulation are characterize by finite size, the correlation length must scale at the critical point with respect to the lattice size:

$$\tau_{\mathcal{O}} \propto L^z \tag{45}$$

and for local updates, which change one spin at a time, the value of this critical exponent is quite large, and almost equal to $z \simeq 2$. This is the main reason of implementing *non-local updates*, they are a way to reduce the effect of this phenomenon, to avoid high correlation and therefore higher computation time to obtain quantities close to a phase transition.

### 1.4.5 Non Local updates: Swendsen-Wang and Wolff Algorithms [34]

To try and deal with the problem of critical slowing down one needs new expressions of the partition function which can be obtained with the *Fortuin-Kasteleyn* (FK) representation. An equivalent construction can be done with Potts model[35], without any loss of generality we will still work on the Ising model (2).

One exploits the fact that Boltzmann measure, in the absence of the field term, in the Ising model, can be made up only of two possible contribution, coming from $\sigma_i \sigma_j = \{-1, 1\}$ so it is possible to rewrite everything defining a new parameter:

$$Z = \sum_{\{s\}} e^{-\beta J \sum_{\langle ij \rangle} s_i s_j} = \sum_{\{s\}} \prod_{\langle ij \rangle} e^{\beta J} [e^{-2\beta J} + (1 - e^{-2\beta J}) \delta_{s_i, s_j}] =$$

$$= \sum_{\{s\}} \prod_{\langle ij \rangle} e^{\beta J} [(1-p) + p \delta_{s_i, s_j}]$$

where

$$p = 1 - e^{-2\beta J}$$

And at this point one can introduce a new variable, which allows to map the model of spins into a geometrical one, which is characterize only by the lattice and bonds which are present (activated) or not, as follows:

$$Z = \sum_{\{s\}} \sum_{\{b_{ij}\}} \prod_{\langle ij \rangle} e^{\beta J}[(1-p)\delta_{b_{ij},0} + p\delta_{s_i,s_j}\delta_{b_{ij},1}] \tag{46}$$

Here the variable $b_{ij}$ allows to create this additional geometrical lattice and one can sum over the spins configurations and remain only with a configuration of the bonds, this allows to map everything into a geometrical lattice, therefore a percolation model.

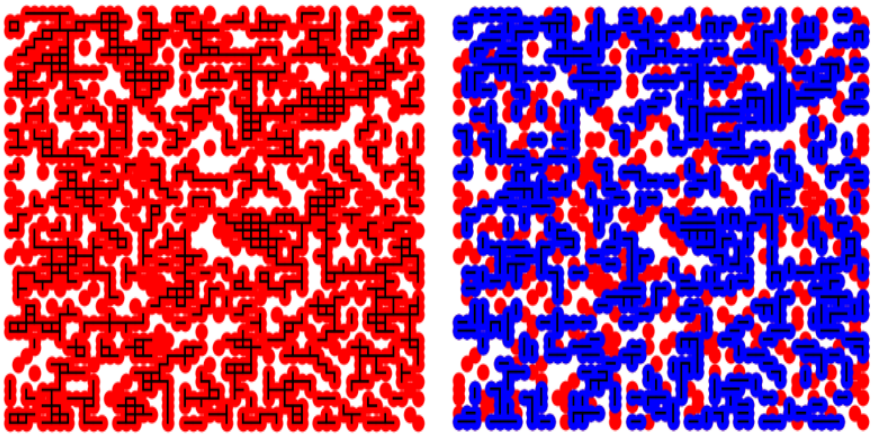

Figure 7: Non local update following Swendsen-Wang algorithm. It is taken 3-state Potts model, considering only all the cluster of red spins for better visualization to be updated

The first step of this algorithms is the *Swendsen-Wang Cluster* related to what was mentioned above, with the formation of this geometrical cluster, then one defines a new update which is made by two step. If two spins are aligned the cluster variable is $b_{ij} = 1$ with probability $p = 1 - e^{-2\beta J}$ otherwise is set to zero, the same happens if the two spins are different from each other. Therefore from a geometrical cluster one goes into a stochastic cluster, whose dimension is in general much smaller. Then the update consist in flipping all stochastic clusters formed as in *Figure* 7. In this case a Monte-Carlo sweep tends to update all spins in a single way. Only when $\beta$ tends to infinity, the probability tends to 1 so the geometrical cluster coincide with the stochastic one.

Another important algorithm used is the *Wolff Cluster* which is actually a variant of the previous one, since in this case one does not try to update all spins at once, rather it peaks a spin and the cluster it belongs to to build the stochastic cluster and simply flip it in an update procedure. One must take care in the comparison of the two methods especially to evaluate the auto-correlation functions, in fact an additional care must be given in the definition of a sweep. In the Wolff algorithm the average cluster size is given by $\langle |C| \rangle$, therefore to update in average all spins one has to perform $\frac{V}{\langle |C| \rangle}$ iterations. In general this variant is more efficient since in average larger cluster are flipped. The value of the critical exponent of slowing down changes significantly, here it is shows a table with the result for 2d Ising [36] [37] [38]:

| Algorithm | z |
|---|---|
| Metropolis | 2.1667(5) |
| Swendsen-Wang | 0.35(1) |
| Wolff cluster | 0.26(2) |

Table 1: Exponent for the critical slowing down phenomenon through different algorithms

For this reason, non-local algorithms are much more suitable for the calculation of averages at criticality. These will be later used in the Numerical section of the thesis: 2.3, 3.3

# 2 Short-range disordered Potts model

In this section we will restrict to the treatment of the short-range disorder. With the aim to describe the system at criticality, the discreet Potts Hamiltonian previously introduced (12) will be considered in its continuous version. Two operators must be taken into account for this end, the *density energy field* and *disorder field* defined as follows:

$$\delta_{s_i,s_j} \to \epsilon(x)$$

$$\sigma_i \to \sigma(x)$$

Moreover, in the framework of conformal field theory, discreet hamiltonians $H$ are taken as continuous action terms $S$. This change of vocabulary will be used from now on.

Equation (14) allows to distinguish two terms in the action, respectively the perturbation and the pure one. The critical action for the pure model will be denoted as $S^0$ whilst its perturbation:

$$S^{Pert} = \int d^2x \sigma(x)\epsilon(x)$$

So the final form of the action for the disordered Potts model will be:

$$S^{Potts} = S^0 + S^{Pert} = S^0 + \int d^2x \sigma(x)\epsilon(x) \tag{47}$$

with the corresponding partition function

$$\mathcal{Z}(\{\sigma\}) = Tr_s\{e^{-S^0 - \int \sigma(x)\epsilon(x)d^2x}\}$$

where the trace $Tr$ represents a summation over all possible states of the system. The quenched disorder, as mentioned in section 1.2.1 appears as a parameter for the partition function and it will not represent additional degrees of freedom to sum over. In the same way, this parametric dependence will be present in the free energy function such that the quenched one $\overline{F(\{\sigma\})}$ is:

$$\overline{F} = Tr_\sigma P(\sigma)F(\{\sigma\})$$

The short-range character of the disorder will be highlighted by the property of independence between the disorder at different points of the space, namely (for $x \neq y$):

$$\overline{\sigma(x)\sigma(y)} = 0$$

This behaviour is well described by a Gaussian probability distribution $P(\{\sigma\})$. It will be here shown the connection with the algebraic decay introduced before at equation (17). With simple scaling argument, performing the Fourier Transform of the correlation in the dimension of interest $d = 2$ of the quantity: $|x-y|^{-a}$ the cumulants of this distribution can be classified [23]. Due to

universality consequences, all microscopic details of the distribution will be lost during the renormalization procedure, and the first and the second cumulant will be sufficient to characterize the whole critical properties. Therefore the algebraic decay for $a \geq 2$ is effectively equivalent to the implementation of the Gaussian disorder, having all higher order cumulant (from the third) null. The probability distribution will be fully characterized by:

$$\begin{cases} \overline{\sigma(x)} = 0 \\ \overline{\sigma(x)\sigma(y)} = 2g_{SR}^0 \delta(x-y) \end{cases} \tag{48}$$

The consequences of this equation are fundamental:

*we are aiming at describing the behaviour of the disorder in a Potts model in a general framework, in fact, despite all possible distributions, the behaviour studied in the following section will be exactly equivalent for all of those distributions who share the same mean and variance of (48), with higher order cumulants to be null.*

The replica trick (29) can now be used, with the cumulant expansion of a Gaussian distribution as in (31)

$$\overline{Z^n} = \prod_{a=1}^{n} Tr_{s_a} \{ e^{-\sum_a S_a^0 - \overline{\sigma} \sum_a \int d^2x \epsilon_a(x) + \frac{1}{2} \sum_{a,b} \int\int d^2x d^2y \overline{(\sigma(x)\sigma(y) - \overline{\sigma}^2)} \epsilon_a(x) \epsilon_b(y)} \}$$

without any higher order terms, existing only two non-zero contributions for a Gaussian distribution. The label $a$ here takes into account the $n$ different replicas of the system.

Up till now, the temperature dependence has always been implicitly present in the action terms. In the study for critical systems, the linear term in the energy operator $\epsilon$, is proportional to $|T - T_c|$ and will give a null contribution at criticality. Moreover, density energy distribution in the same replica $\epsilon^a(x)\epsilon^{b=a}(x)$ will contribute trivially, with just a consequent shift in the critical temperature $T_c$. With the aim to obtain only information about universal properties, microscopic dependent quantity, like critical temperature, will not be taken into account. So the final from for the replicated partition function will be:

$$\overline{Z^n} = \prod_{a=1}^{n} Tr_{\{s_a\}} \{ e^{-\sum_a S_a^0 + g_{SR}^0 \sum_{a \neq b} \int \epsilon_a(x) \epsilon_b(x) d^2x} \} \tag{49}$$

In this form, in which the disorder has been integrated out, with only the spins degrees of freedom, the perturbation renormalization techniques presented in the section 1.3.2 will be used. In particular, the cumulant expansion can be performed with respect to the quantity:

$$g_{SR}^0 \sum_{a \neq b} \int_{|x|>1} \epsilon_a(x) \epsilon_b(x) d^2x$$

where in the integration boundaries, it has been considered a cut-off, reminiscent of the underlying discreet square lattice with unit pass $l = 1$.

## 2.1 Renormalization Group

### 2.1.1 0-loop order

We can divide the integration in such a way that the lower degrees of freedom can be disregarded, exploiting the conservation of the partition function at different scales of the system (as a consequence of the divergence of the correlation length) in an equivalent way of the procedure shown in 1.3.2 :

$$\sum_{a\neq b}\int_{|x|>1}\epsilon_a(x)\epsilon_b(x)d^2x =$$

$$= g^0_{SR}\sum_{a\neq b}\int_{1<|x|<r}\epsilon_a(x)\epsilon_b(x)d^2x + g^0_{SR}\sum_{a\neq b}\int_{|x|>r}\epsilon_a(x)\epsilon_b(x)d^2x$$

where r will represent the new cut-off of the fields. Therefore, the first term will not contribute to the renormalization equations in the new system's scale. while the second is the only one which will. To understand in which way, we need to rescale back following the changes below reported:

$$\begin{cases} x' = \frac{x}{r} \\ x' = \frac{d^2x}{r^2} \\ \epsilon'(x') = r^{h_\epsilon}\epsilon(x) \end{cases} . \tag{50}$$

where $h_\epsilon$ is the physical dimension of the density energy operator. Imposing the equivalency of the partition functions at different scales:

$$g^0_{SR}r^{2-2h_\epsilon}\sum_{a\neq b}\int_{|x'|>1}\epsilon'_a(x')\epsilon'_b(x')d^2x' = g_{SR,1}\sum_{a\neq b}\int_{|x'|>1}\epsilon'_a(x')\epsilon'_b(x')d^2x$$

we can obtain the first contribution for the renormalized short range perturbative parameter:

$$g_{SR,1} = g^0_{SR}r^{\epsilon_{SR}} \tag{51}$$

where it has been defined the parameter: $\epsilon_{SR} = 2 - 2h_\epsilon$ which plays the role of dimensional regularization. This quantity must be small for the perturbation method to be reasonable, and given its expression[29]

$$\epsilon_{SR} = \frac{4}{3}\left(\frac{Q-2}{\pi}\right) + \mathcal{O}((Q-2)^2)$$

this translates in considering $Q - 2 << 1$. Although for the fixed point we will analyzed the specif cases of $Q = \{1, 2, 3\}$, (not the general case in which Q is real) and since exact values of the dimensions of the energy operator, $h_\epsilon$, are known, specific values of $\epsilon_{SR}$ will be too and will be presented later.

### 2.1.2 1-loop order

At first order of the cumulant expansion, a new term must be considered, as the product of two perturbation expansion $\epsilon\epsilon$ and $\epsilon\epsilon$ which translates in:

$$\frac{(g^0_{SR})^2}{2}\int_{|x|>1} d^2x \int_{|x-y|>1} d^2y \sum_{a\neq b}\epsilon_a(x)\epsilon_b(x)\sum_{c\neq d}\epsilon_c(y)\epsilon_d(y)$$

Once again we would like to integrate out the small degrees of freedom. In this case although, due to the presence of a double integration one has to consider different contribution of the previous integral. The case in which both the integration of y and x are in the low degrees of freedom does not in the same way as the integrals on both higher degrees of freedom which will give a trivial constant contribution that can be neglected. The only fundamental term is related to an integration over the small degrees of freedom for one variable, and for high degrees of freedom for the other. This will lead to the term:

$$\frac{(g^0_{SR})^2}{2}\int_{|x|>r} d^2x \int_{1<|x-y|<r} d^2y \sum_{a\neq b}\epsilon_a(x)\epsilon_b(x)\sum_{c\neq d}\epsilon_c(y)\epsilon_b(y)$$

To reproduce a contribution to the $\epsilon\epsilon$ operator, the OPE (35) can be performed to contract two energy fields as follows:

$$\epsilon_a(x)\epsilon_a(y) = \mathcal{I}\langle\epsilon_a(x)\epsilon_a(y)\rangle = \frac{\mathcal{I}}{|x-y|^{2h_\epsilon}}$$

where $\mathcal{I}$ is the identity operator. All the possible contractions now must be counted. We fix two replicas to be equal, for instance the ones labelled by the indexes $b$ and $c$, this consists in choosing one of the $n$ possible replicas. Then we have 4 different ways of contraction for the other two indexes as shown in diagram below:

Having $n$ different replica choices, having fixed two terms, there can be $n-2$ choices for the remaining energy terms, such that the final combinatorial term will be given by $C_1 = 4(n-2)$. Now it can be inserted in the previous expression for the integrals computations:

$$\cancel{4}(n-2)\frac{(g^0_{SR})^2}{\cancel{2}}\int_{|x|>r} d^2x \sum_{a\neq d}\epsilon_a(x)\epsilon_d(y)\int_{1<|x-y|<r} d^2y\frac{\mathcal{I}}{|x-y|^{2h_\epsilon}}$$

Now we integrate over $y$ neglecting the contribution of replicas at different positions (since they give a null contribution).

$$2(n-2)(g^0_{SR})^2\int_{|x|>r} d^2x \sum_{a\neq d}\epsilon_a(x)\epsilon_d(x)\int^r d^2y\frac{1}{|x-y|^{2h_\epsilon}}$$

The integration now can be explicitly performed using polar coordinates:

$$2(n-2)(g^0_{SR})^2\int_{|x|>r}\sum_{a\neq d}\epsilon_a(x)\epsilon_d(x)d^2x\int^r d\rho 2\pi\frac{1}{|\rho|^{2h_\epsilon-1}} =$$

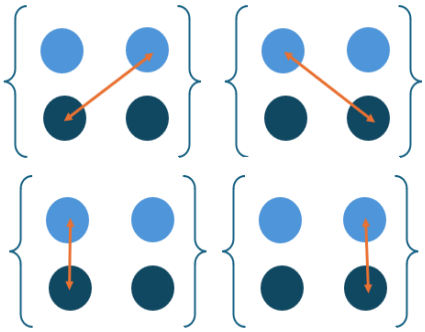

Figure 8: Diagrammatic counting for $\epsilon\epsilon$ contractions at 1-loop-order of the $g_{SR}$. Dots represent generic operators, in this case $\epsilon$. Dots with the same colour represent energy operators in the same position, for instance here light blue $x$ and dark blue $y$. The orange line represents the possible contraction between operators at different positions. Here the 4 different possible contractions are shown.

$$= 4\pi(n-2)(g^0_{SR})^2 \int_{|x|>r} \sum_{a\neq d} \epsilon_a(x)\epsilon_d(x) \frac{(r^{2-2h_\epsilon})}{2-2h_\epsilon} d^2x$$

As done for the 0-loop order, the system is rescaled following (50) and the equation is set equal to the partition function at a different scale, finding the identity:

$$4\pi(n-2)(g^0_{SR})^2 r^{2-2h_\epsilon} \int_{|x'|>1} \sum_{a\neq b} \epsilon'_a(x')\epsilon'_b(x')d^2x' \frac{r^{2-2h_\epsilon}}{2-2h_\epsilon} =$$

$$= g_{SR,2} \int_{|x'|>1} \sum_{a\neq b} \epsilon'_a(x')\epsilon'_b(x')d^2x'$$

entailing as a second order contribution:

$$g_{SR,2} = 4\pi(n-2) {g^0_{SR}}^2 \frac{r^{2\epsilon_{SR}}}{\epsilon_{SR}} \tag{52}$$

.

### 2.1.3 2-order loop

At the second order loop we have to take into account the term of the type:

$$\frac{{g^0_{SR}}^3}{3!} \int_{|x|>1} \sum_{a\neq b} \epsilon_a(x)\epsilon_b(x)d^2x \int_{|y|>1} \sum_{c\neq d} \epsilon_c(y)\epsilon_d(y)d^2y \int_{|z|>1} \sum_{e\neq f} \epsilon_e(z)\epsilon_f(z)d^2z$$

Now, performing the usual decomposition between small distances and higher distances, the only terms which we will be interested in, are integrals of the type:

$$\frac{{g^0_{SR}}^3}{3!}\int_{|x|>r}\sum_{a\neq b}\epsilon_a(x)\epsilon_b(x) =$$

$$=\int_{1<|x-y|<r}\int_{1<|x-z|<r}\sum_{c\neq d,e\neq f}\epsilon_c(y)\epsilon_d(y)\epsilon_e(z)\epsilon_f(z)d^2xd^2yd^2z$$

In this case, in order to have a term of the type $\epsilon\epsilon$, different contributions must be taken into account. Let's start by a double contraction. To consider all the possible double contractions among six different terms, and to generate a contribution through OPE of the type: $\langle\epsilon(x)\epsilon(y)\rangle_0\langle\epsilon(y)\epsilon(z)\rangle_0$ we must count the combinations that lead to this contribution.

In *Figure 9* there are given all the 24 possibilities. Since we can choose for instance $b=c, d=e, a\neq d, f\neq b, a\neq f$, given n replicas, the first contractions will contribute to $(n-2)$ possibilities, whilst the second one, to have another fixed replica index, will give the a contribution of $(n-3)$. So in total $C_{3,1}=24(n-2)(n-3)$. The contribution will so be of the type:

$$\frac{{g^0_{SR}}^3}{3!}24(n-2)(n-3)\int_{|x|>1}\sum_{a\neq f}\epsilon_a(x)\epsilon_f(x)d^2x\cdot$$

$$\cdot\int_{1<|x-y|<r}\int_{1<|x-z|<r}\langle\epsilon(x)\epsilon(y)\rangle_0\langle\epsilon(y)\epsilon(z)\rangle_0 d^2yd^2z =$$

$$={g^0_{SR}}^3 4(n-2)(n-3)\int_{|x|>1}\sum_{a\neq f}\epsilon_a(x)\epsilon_f(x)\cdot$$

$$\cdot\int_{1<|x-y|<r}\int_{1<|x-z|<r}\frac{1}{|x-y|^{2h_\epsilon}}\frac{1}{|y-z|^{2h_\epsilon}}d^2yd^2z$$

where, without loss of generality, the only term $\epsilon\epsilon$ remaining to contribute in the renormalization equation, must be evaluated in the same point of the space to give a non trivial contribution. We focus on the computation of the integral in $y$ and $x$:

$$I=\int_{1<|x-y|<r}\int_{1<|x-z|<r}\frac{1}{|x-y|^{2h_\epsilon}}\frac{1}{|y-z|^{2h_\epsilon}}d^2yd^2z$$

It will be now performed a change of variable of the type: $y'=y-x$ which gives:

$$I=\int_{1<|y'|<r}\int_{1<|x-z|<r}\frac{1}{|y'|^{2h_\epsilon}}\frac{1}{|y'+x-z|^{2h_\epsilon}}d^2y'd^2z =$$

$$=\int_{1<|y'|<r}\int_{1<|x-z|<r}\frac{1}{|y'|^{2h_\epsilon}}\frac{1}{|(z-x)-y'|^{2h_\epsilon}}d^2y'd^2z$$

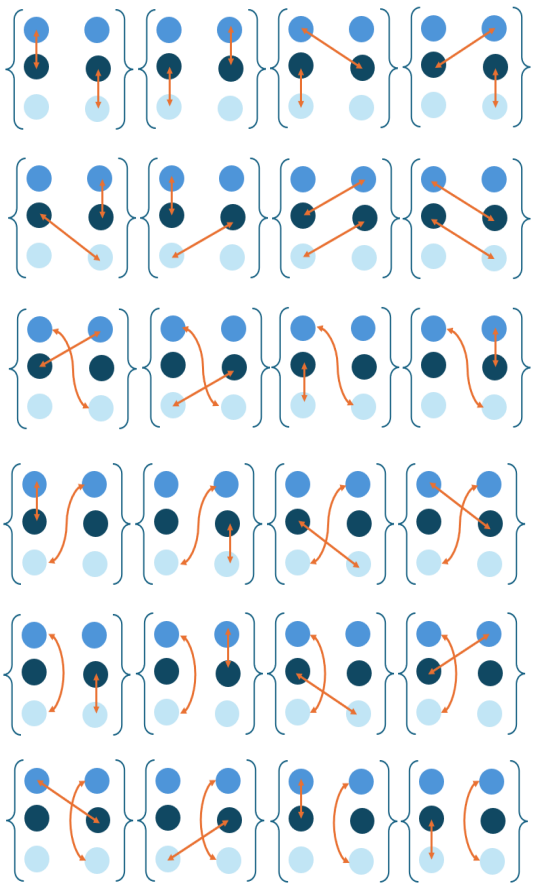

Figure 9: Diagrammatic counting for double contraction $\epsilon\epsilon$ $\epsilon\epsilon$ for $g_{SR}$. It gives 24 different possibilities

Now it can be defined $y' = \omega(z - x)$ and $d^2y' = |x - z|^2 d^2\omega$ as a new change of variable which gives:

$$I = \int_{1<|\omega|<r} \int_{1<|x-z|<r} \frac{|x-z|^2}{|x-z|^{2h_\epsilon}|\omega|^{2h_\epsilon}} \frac{1}{|(z-x)-\omega(z-x)|^{2h_\epsilon}} d^2\omega d^2z$$

where the extremes of integration have been taken only in the domain of interest, neglecting the possible contribution for distances smaller than 1 lattice size. Now the expression can be manipulated to get:

$$I = \int_{1<|\omega|<r} \int_{1<|x-z|<r} \frac{1}{|x-z|^{4h_\epsilon-2}|\omega|^{2h_\epsilon}} \frac{1}{|1-\omega|^{2h_\epsilon}} d^2\omega d^2z$$

With a final change of variable of the type $z' = z - x$:

$$I = \int_{1<|\omega|<r} \int_{1<|z'|<r} \frac{1}{|z'|^{4h_\epsilon-2}|\omega|^{2h_\epsilon}} \frac{1}{|1-\omega|^{2h_\epsilon}} d^2\omega d^2 z'$$

The integration can now be performed by factorization, for simplicity we will go back to the initial variables:

$$I = \int_{1<|y|<r} \frac{1}{|y^{4h_\epsilon-2}|} d^2y \int_{1<|z|<r} \frac{1}{|z|^{2h_\epsilon}|1-z|^{2h_\epsilon}} d^2z$$

We can solve the first integral with the same change used for the computation of (52) to go in polar coordinates:

$$I = 2\pi \frac{r^{4-4h_\epsilon}}{(4-4h_\epsilon)} \int_{1<|z|<r} \frac{1}{|z|^{2h_\epsilon}|1-z|^{2h_\epsilon}} d^2z =$$

$$= 2\pi \frac{r^{2\epsilon_{SR}}}{(2\epsilon_{SR})} \int_{1<|z|<r} \frac{1}{|z|^{2h_\epsilon}|1-z|^{2h_\epsilon}} d^2z = 2\pi \frac{r^{2\epsilon_{SR}}}{(2\epsilon_{SR})} \mathcal{I}_{3,1}$$

where we have denoted with $\mathcal{I}_{3,1}$ the last integration. All together, up till now, this gives a first contribution of the type:

$$g_{3,1} = {g^0_{SR}}^3 8\pi(n-2)(n-3) \frac{r^{2\epsilon_{SR}}}{(2\epsilon_{SR})} \mathcal{I}_{3,1} \int_{|x|>1} \sum_{a\neq f} \epsilon_a(x)\epsilon_f(x) \tag{53}$$

The second contribution comes from the contraction amongst three energy operators $\epsilon\epsilon\epsilon$ and two additional one $\epsilon\epsilon$. This will require the computation of correlation of the type: $\langle\epsilon(x)\epsilon(y)\epsilon(z)\rangle_0\langle\epsilon(y)\epsilon(z)\rangle_0$. The combinatory of the interactions is given by the diagram in *Figure 10* where degeneracy factors are considered. Once again this contribution gives a factor 24.

This time the only factor which takes into account the replica comes from a term $(n-2)$ such that $C_{3,2} = 4(n-2)$ the contraction of the three energy operators can give, projecting $\epsilon\epsilon\epsilon$ into $\epsilon$, a new $\epsilon$ contribution:

$$g^{SR,0}_{3,2} = 24(n-2) \frac{{g^0_{SR}}^3}{3!} \int_{|x|>r} \sum_{a\neq f} \epsilon_a(x)\epsilon_f(x) \cdot$$

$$\cdot \int_{1<|x-y|<r} \int_{1<|x-z|<r} \langle\epsilon(x)\epsilon(y)\epsilon(z)\epsilon(\infty)\rangle_0 \langle\epsilon(y)\epsilon(z)\rangle_0 d^2y d^2z$$

which requires the computation of a four point correlation function. This can be computed in terms of the Coulomb Gas formalism. Both the previous integral (53) and this one, can be carried out in this new representation which makes use of conformal field theory algebra and takes into account the presence of singularities [28]. The first term will be able to give a contribution of the type:

$$g^{SR,0}_{3,1} = 16\pi^2(n-2)(n-3) \frac{r^{2\epsilon_{SR}}}{\epsilon^2_{SR}} \int_{|x|>r} \sum_{a\neq f} \epsilon_a(x)\epsilon_f(x) \tag{54}$$

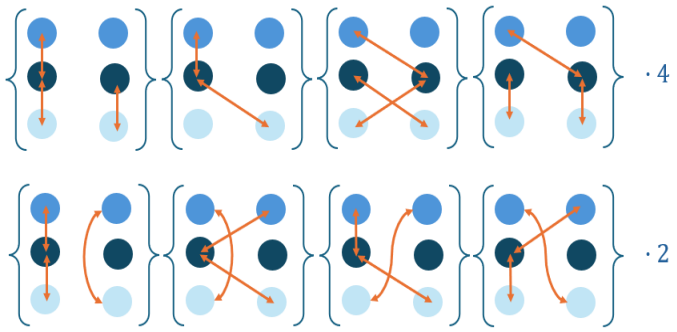


Figure 10: Diagrammatic counting for contractions with a triple contraction $\epsilon\epsilon\epsilon$ and a double one $\epsilon\epsilon$ for a 2-loop-order of $g_{SR}$. In the first row, a degeneracy of 4 has been considered for all the extreme dots at top right, left, and bottom right, left. The second row takes into account the degeneracy factor 2, for the two central dots. This can be done for simple symmetric reasons. All together the degeneracy will contribute to a factor 24

While this last integral, contributes in:

$$g_{3,2}^{SR,0} = -8\pi^2(n-2)\frac{r^{2\epsilon_{SR}}}{\epsilon_{SR}}\int_{|x|>r}\sum_{a\neq f}\epsilon_a(x)\epsilon_f(x) \tag{55}$$

and an additional contribution due to the presence of a singularity which gives:

$$g_{3,3}^{SR,0} = 8\pi^2(n-2)\frac{r^{2\epsilon_{SR}}}{\epsilon_{SR}^2}\int_{|x|>r}\sum_{a\neq f}\epsilon_a(x)\epsilon_f(x) \tag{56}$$

which can all be put together to give:

$$g_3^{SR,0} = g_{3,1}^{SR,0} + g_{3,2}^{SR,0} + g_{3,3}^{SR,0} =$$
$$= 8\pi^2\frac{n-2}{\epsilon_{SR}}{g_{SR}^0}^3 r^{2\epsilon_{SR}}\left(1+\frac{2(n-2)}{\epsilon_{SR}}\right)\int_{|x|>r}\sum_{a\neq f}\epsilon_a(x)\epsilon_f(x)$$

Then, with the usual scaling back of renormalization equations we get a term:

$$g_{SR,3} = 8\pi^2\frac{n-2}{\epsilon_{SR}}{g_{SR}^0}^3 r^{3\epsilon_{SR}}\left(1+\frac{2(n-2)}{\epsilon_{SR}}\right)\int_{|x'|>1}\sum_{a\neq b}\epsilon'_a(x')\epsilon'_b(x') \tag{57}$$

which can be added to the previous loop-orders (51), (52) to get the final equation:

$$g_{SR} = g_{SR,1} + g_{SR.2} + g_{SR,3} =$$
$$= g_{SR}^0 r^{\epsilon_{SR}} + 4\pi(n-2){g_{SR}^0}^2\frac{r^{2\epsilon_{SR}}}{\epsilon_{SR}} - 8\pi^2{g_{SR}^0}^3(n-2)\frac{r^{3\epsilon_{SR}}}{\epsilon_{SR}}\left(1-\frac{2(n-2)}{\epsilon_{SR}}\right)\Big) \tag{58}$$

### 2.1.4 Renormalization equation

Equation (58) can be written through a factorization:

$$g_{SR}(r) = g^0_{SR} r^{\epsilon_{SR}} \left( 1 + 4\pi(n-2) g^0_{SR} \frac{r^{\epsilon_{SR}}}{\epsilon_{SR}} - 8\pi^2 {g^0_{SR}}^2 (n-2) \frac{r^{2\epsilon_{SR}}}{\epsilon_{SR}} \left( 1 - \frac{2(n-2)}{\epsilon_{SR}} \right) \right)$$

At this point, the replica method used for the computation of the renormalized parameter can be removed, by setting the replica to zero, performing the limit of $n \to 0$:

$$g_{SR}(r) = g^0_{SR} r^{\epsilon_{SR}} \left( 1 - 8\pi g^0_{SR} \frac{r^{\epsilon_{SR}}}{\epsilon_{SR}} + 16\pi^2 {g^0_{SR}}^2 \frac{r^{2\epsilon_{SR}}}{\epsilon_{SR}} \left( 1 + \frac{4}{\epsilon_{SR}} \right) \right) \tag{59}$$

Our aim is to understand how variation with respect to the cut-off r, changes the parameter itself. To do this we will compute the so called *beta-function* which corresponds to the mathematical definition of the previous concept:

$$\beta = r \frac{dg(r)}{dr} \tag{60}$$

which allows to obtain a dynamical equation for the parameter of interest.

$$\beta = r \frac{d}{dr} \left[ g^0_{SR} r^{\epsilon_{SR}} \left( 1 - 8\pi g^0_{SR} \frac{r^{\epsilon_{SR}}}{\epsilon_{SR}} + 16\pi^2 {g^0_{SR}}^2 \frac{r^{2\epsilon_{SR}}}{\epsilon_{SR}} \left( 1 + \frac{4}{\epsilon_{SR}} \right) \right) \right]$$

Using Leibniz's rule for products derivatives:

$$\beta = \epsilon_{SR} g_{SR} + r g^0_{SR} r^{\epsilon_{SR}} \frac{d}{dr} \left[ 1 - 8\pi g^0_{SR} \frac{r^{\epsilon_{SR}}}{\epsilon_{SR}} + 16\pi^2 {g^0_{SR}}^2 \frac{r^{2\epsilon_{SR}}}{\epsilon_{SR}} \left( 1 + \frac{4}{\epsilon_{SR}} \right) \right]$$

By denoting:

$$Z_{\epsilon\epsilon} = 1 - 8\pi g^0_{SR} \frac{r^{\epsilon_{SR}}}{\epsilon_{SR}} + 16\pi^2 {g^0_{SR}}^2 \frac{r^{2\epsilon_{SR}}}{\epsilon_{SR}} \left( 1 + \frac{4}{\epsilon_{SR}} \right)$$

One can express the relation:

$$g_{SR} = g^0_{SR} r^{\epsilon_{SR}} Z_{\epsilon\epsilon} \tag{61}$$

From now on, the subscript $SR$ will be dropped, and $g_{SR}$ will be simply considered as $g$ to avoid heavy notation. All the coupling must be considered in the short-range sense in this section.

The previous two expressions can be used to rewrite the $\beta$ function as follows:

$$\beta = \epsilon g + g \frac{r}{Z_{\epsilon\epsilon}} \frac{dZ_{\epsilon\epsilon}}{dr} \tag{62}$$

A new quantity is introduced called *gamma-function* $\gamma_{\epsilon\epsilon}$:

$$\gamma_{\epsilon\epsilon} = \frac{r}{Z_{\epsilon\epsilon}} \frac{dZ_{\epsilon\epsilon}}{dr} \tag{63}$$

which allows to rewrite the beta-function as follows

$$\beta = g(\epsilon + \gamma_{\epsilon\epsilon})$$

A perturbative computation must be performed to obtain the gamma-function. First the following quantity is computed:

$$r\frac{dZ_{\epsilon\epsilon}}{dr} = r\frac{d}{dr}\left[1 - 8\pi g_0 \frac{r^\epsilon}{\epsilon} + 16\pi^2 {g_0}^2 \frac{r^{2\epsilon}}{\epsilon}\left(1 + \frac{4}{\epsilon}\right)\right] =$$

$$= -8\pi g_0 r^\epsilon + 32\pi^2 g_0^2 r^{2\epsilon}\left(1 + \frac{4}{\epsilon}\right)$$

Then a Taylor expansion in $g$ is performed:

$$\frac{1}{Z_{\epsilon\epsilon}} = \frac{1}{1 - 8\pi g_0 \frac{r^\epsilon}{\epsilon} + 16\pi^2 {g_0}^2 \frac{r^{2\epsilon}}{\epsilon}(1 + \frac{4}{\epsilon})} \simeq 1 + 8\pi g_0 \frac{r^\epsilon}{\epsilon} - 16\pi^2 {g_0}^2 \frac{r^{2\epsilon}}{\epsilon}\left(1 + \frac{4}{\epsilon}\right)$$

To maintain all this computation at second order, it will be sufficient to consider only:

$$\frac{1}{Z_{\epsilon\epsilon}} \simeq 1 + 8\pi g_0 \frac{r^\epsilon}{\epsilon}$$

Finally it can be computed:

$$\gamma_{\epsilon\epsilon} = \frac{1}{Z_{\epsilon\epsilon}} r\frac{dZ_{\epsilon\epsilon}}{dr} \simeq \left(1 + 8\pi g_0 \frac{r^\epsilon}{\epsilon}\right)\left(-8\pi g_0 r^\epsilon + 32\pi^2 g_0^2 r^\epsilon \left(1 + \frac{4}{\epsilon}\right)\right) =$$

$$= -8\pi g_0 r^\epsilon + 32\pi^2 g_0^2 r^\epsilon + \frac{128}{\epsilon}\pi^2 g_0^2 r^{2\epsilon} - 64\pi^2 g_0^2 \frac{r^{2\epsilon}}{\epsilon} + \mathcal{O}(g_0^3)$$

And using one last expansion to keep everything at second order starting from equation (62):

$$g \simeq g_0 r^\epsilon \left(1 - 8\pi g_0 \frac{r^\epsilon}{\epsilon}\right) \tag{64}$$

$$\gamma_{\epsilon\epsilon} \simeq -8\pi g\left(1 + 8\pi \frac{g}{\epsilon}\right) + 32\pi^2 g^2 + \frac{128}{\epsilon}\pi^2 g^2 - \frac{64}{\epsilon}\pi^2 g^2 + \mathcal{O}(g_0^3) =$$

$$= -8\pi g + 32\pi^2 g^2$$

Therefore:

$$\beta(g) = g(\epsilon - 8\pi g + 32\pi^2 g^2) \tag{65}$$

This represent the dynamical equation of our perturbative parameter. Although, to understand the behaviour at criticality, we must look for the possible fixed points of the system.

### 2.1.5 Fixed Points and stability

Fixed points can be computed looking for the values $g_c$ such that $\beta(g_c) = 0$. One first simple solutions of (65) comes from:

$$g_c^1 = 0 \tag{66}$$

this correspond to the well known criticality of the pure model, in fact the coupling constant being null simply brings back all the computation to the conformal critical action of the Pure Potts model. This is representative of the absence of the disorder in the model. Other two fixed points will be found solving the second order algebraic equation which turns out to give:

$$g_c^{2,3} = \frac{8\pi \pm \sqrt{(64\pi^2 - 128\pi^2\epsilon)}}{64\pi^2} = \frac{1}{8\pi} \pm \frac{\sqrt{1-2\epsilon}}{8\pi} \tag{67}$$

The stability study will be carried out through two approaches, the analytical one, and the graphical method[39]. We recall that a fixed point is said to be *stable* or *attractive* if the derivative of the dynamical equation computed at the fixed point has negative real part. Otherwise, it is said to be *repulsive* or *unstable* and finally *marginal* or *half-stable* in case the derivative is null. The derivative of the $\beta$ function reads:

$$\frac{d\beta(g)}{dg} = \epsilon - 16\pi g + 96\pi^2 g^2$$

Then for the pure point, it will simply give the dimensional contribution:

$$\left.\frac{d\beta(g)}{dg}\right|_{g=g_c^1} = \epsilon$$

Its stability is given by the following conditions:

$$\begin{cases} \epsilon > 0 & unstable \\ \epsilon < 0 & stable \end{cases} \tag{68}$$

One proceeds to study the second fixed point:

$$\left.\frac{d\beta(g)}{dg}\right|_{g=g_c^2} = \epsilon - 16\pi\left(\frac{1}{8\pi} + \frac{\sqrt{1-2\epsilon}}{8\pi}\right) + 96\pi^2\left(\frac{1}{8\pi} + \frac{\sqrt{1-2\epsilon}}{8\pi}\right)^2 =$$

$$= \epsilon - 2 - 2\sqrt{1-2\epsilon} + 96\pi^2\left(\frac{1}{64\pi^2} + \frac{1-2\epsilon}{64\pi^2} + \frac{\sqrt{1-2\epsilon}}{32\pi^2}\right) =$$

$$= -2\epsilon + 1 + \sqrt{1-2\epsilon}$$

Then:

$$\forall \epsilon < \frac{1}{2} : \left.\frac{d\beta(g)}{dg}\right|_{g=g_c^2} > 0$$

$$g_c^2 \; unstable \; \forall \epsilon \in \left( -\infty, \frac{1}{2} \right) \tag{69}$$

and due to the condition of g being real, this corresponds to the entire domain of existence of this new fixed point, except the marginal case of $\epsilon = \frac{1}{2}$.

Finally, repeating the same procedure for the last fixed point:

$$\left.\frac{d\beta(g)}{dg}\right|_{g=g^3} = \epsilon - 16\not{\pi}\left(\frac{1}{8\not{\pi}} - \frac{\sqrt{1-2\epsilon}}{8\not{\pi}}\right) + 96\pi^2\left(\frac{1}{8\pi} - \frac{\sqrt{1-2\epsilon}}{8\pi}\right)^2 =$$

$$= -2\epsilon + 1 - \sqrt{1-2\epsilon}$$

To study the stability it can be written:

$$-2\epsilon + 1 > \sqrt{1-2\epsilon}$$

$$4\epsilon^2 + 1 - 4\epsilon > 1 - 2\epsilon \rightarrow 2\epsilon(2\epsilon - 1) > 0$$

The above inequality gives, considering that this fixed point, for the same constraint on g being real, exist only for $\epsilon < \frac{1}{2}$, the following conditions:

$$\begin{cases} \epsilon < 0 & unstable \\ 0 < \epsilon < \frac{1}{2} & stable \end{cases} \tag{70}$$

All this analysis is revised through graphical means in *Figure* 11. The parameter $\epsilon$ has been considered in the five cases written below:

1. $\epsilon > \frac{1}{2}$

   there exist only a fixed point at $g_c^1 = 0$ shown with a red dot. To characterize the stability, the sign of beta function is analyzed. In panel (a), the function goes from being negative to positive which defines instability, in agreement with the analytical result

2. $\epsilon = \frac{1}{2}$

   there is the emerge of a new fixed point with a double degeneracy, which is marginal since the sign of the beta function does not change.

3. $0 < \epsilon < \frac{1}{2}$

   $g_c^1$ is left unchanged, the two new fixed points (green $g_c^2$ and blue $g_c^3$) get further at decreasing $\epsilon$, $g_c^2$ is unstable as the pure point, whilst $g_c^3$ is stable since the function $\beta$ passes from being positive to negative

4. $\epsilon = 0$

   the first and the third fixed point superimpose, their stability, in this case, is marginal due the constant sign of the beta-function

5. $\epsilon < 0$

   the stability of $g_c^3$ is exchanged with the one of $g_c^1$, while $g_c^2$ is left unchanged and still unstable.

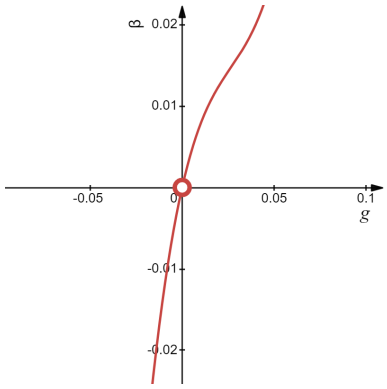


(a) $\epsilon > 0.5$:
One unstable fixed point: $g_c^1$

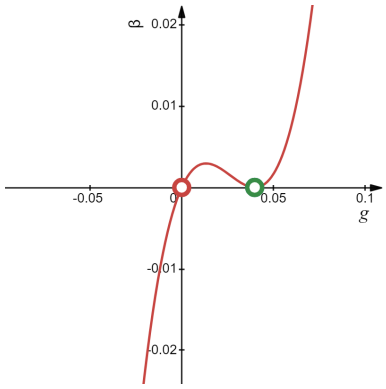


(b) $\epsilon = 0.5$:
Emergence of marginal $g_c^2 = g_c^3$

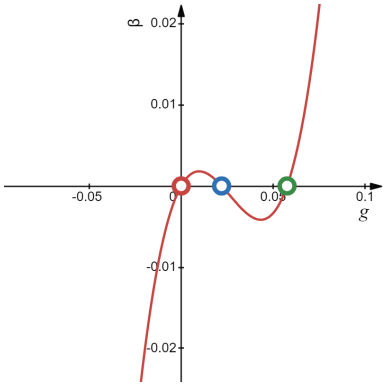


(c) $\epsilon = 0.4$
$g_c^1 \neq g_c^2 \neq g_c^3$ with stable $g_c^3$

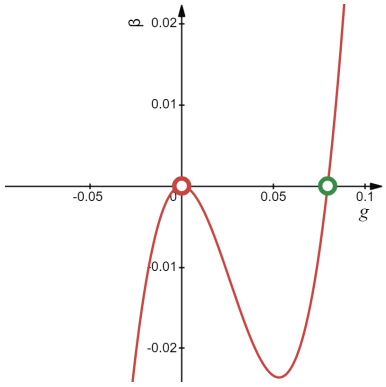


(d) $\epsilon = 0$
Marginal case for $g_c^1 = g_c^3 \neq g_c^2$

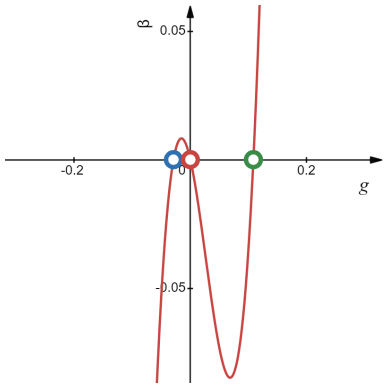


(e) $\epsilon = -1$
Once again $g_c^1 \neq g_c^2 \neq g_c^3$ with stable $g_c^1$

Figure 11: Fixed points' stability graphical analysis

The change in the stability of the fixed points, can be better visualized in the *bifurcation diagram*, a graph $g - \epsilon$ where only fixed point are drawn as a function of the parameter $\epsilon$. Whilst straight lines corresponds to stable fixed points, unstable are represented by dashed ones in *Figure* (12).

In this bifurcation diagram two important points have been highlighted: $(\frac{1}{2}, \frac{1}{8\pi})$ and $(0, 0)$, corresponding to cases (11b), (11d) of previous plots. The first one represents the point at which (considering decreasing values of the parameter), two new fixed point appear in the dynamical description, and represents a *saddle-node bifurcation*. The second one, is characterized by a change in stability between the first and the third fixed points. In literature, this type of fixed point is referred as *transcritical bifurcation*.

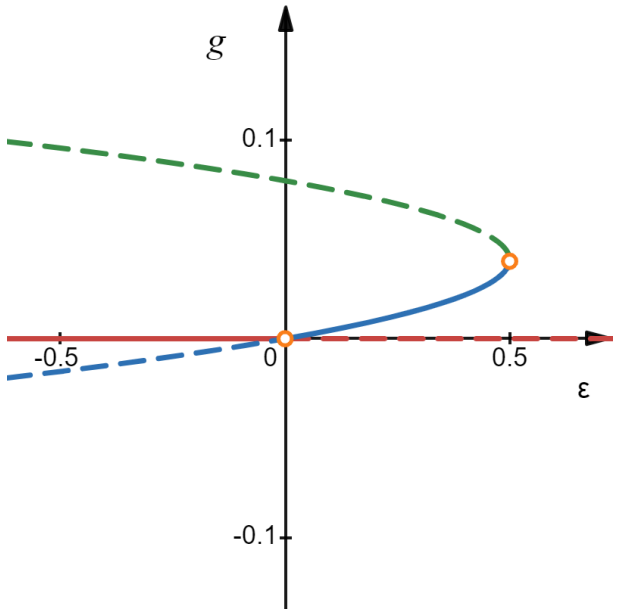


Figure 12: Bifurcation diagram

Up till now $\epsilon$ has been taken as a general parameter, but we would like to analyze more in depth what happens for a particular case. In fact, in the CFT theory the value of $\epsilon$ is representative of the dimension of the energy operator for a particular value $Q$ of the Potts model. In fact for instance it is known in the following cases:

$$\epsilon = \begin{cases} -0.5 & q = 1 \\ 0 & q = 2 \\ 0.4 & q = 3 \end{cases} \tag{71}$$

It will be therefore taken into account the case of the 3-state Potts model, which corresponds taking into account the fixed point at $\epsilon$ as in *Figure* 13. For this reason, being $g_3$ the only attractive fixed point, we will focus only on this

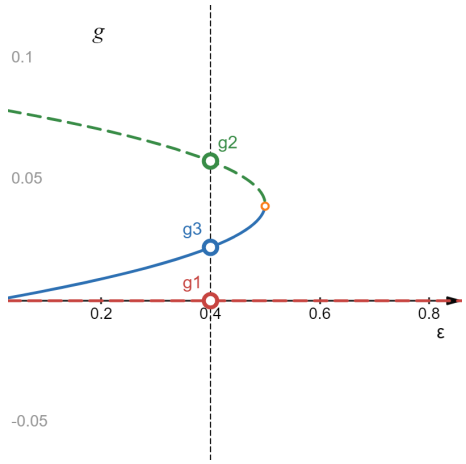


Figure 13: Fixed points of the bifurcation diagram for Q=2 Potts model

quantity for the computation of the disorder eigenvalue (consistent even with a perturbative approach where we assume $g$ to be small).

If finally fixed points are considered in the phase space of the disorder strength $r$ (16) and on the temperature $T$, the pure fixed point $g_c^1$ corresponds to $r = 1$, whilst $g_c^3$ represents a particular value of the parameter r, which must be $r > 1$ for the initial choice made. Since we're considering always models at criticality, the temperature axis will not be important in the description, the model will always be at $T = T_c$. Therefore if we want to describe a flow in this parameter space, it can be done in a 1-dimensional line in which the stability of the fixed point can be highlighted trough arrows. For the case of interest, the pure point is unstable, whilst the new fixed point, which will be the short range fixed point, will be stable. The result is presented in *Figure* 14.

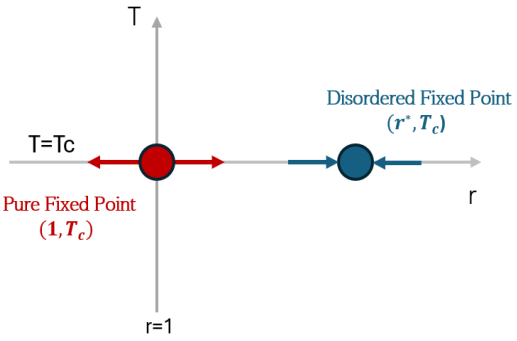


Figure 14: Flow in Phase Space r-T

### 2.1.6 Disorder Eigenvalue

The short-range disordered fixed point can be rewritten as follows:

$$g_c^3 = \frac{1}{8\pi} \pm \frac{1}{8\pi}(1-2\epsilon)^{\frac{1}{2}}$$

Then taking into account $\epsilon$ as a small perturbation parameter we can Taylor expand the expression as follows:

$$g_c^3 = \frac{1}{8\pi} - \frac{1}{8\pi}\left(1 - \epsilon - \frac{1}{2}\epsilon^2 - \frac{1}{2}\epsilon^3\right) = \frac{\epsilon}{8\pi} + \frac{\epsilon^2}{16\pi} + \mathcal{O}(\epsilon^3)$$

We are interested in the eigenvalue of the disorder at the pure and stable short range fixed points, in general this can be computed through the relation:

$$y_d = \left.\frac{d\beta(g)}{dg}\right|_{g_c}$$

$$\left.\frac{d\beta(g)}{dg}\right|_{g_c} = \epsilon - 16\pi g + 96\pi^2 g^2$$

At the pure point:

$$y_d^0 = \left.\frac{d\beta(g)}{dg}\right|_{g_c^1} = \epsilon \tag{72}$$

At the new random fixed point:

$$y_d' = \left.\frac{d\beta(g)}{dg}\right|_{g_c^3} = \epsilon - 2\epsilon - \epsilon^2 + \frac{96}{64}\epsilon^2 + o(\epsilon^3) = -\epsilon + \frac{\epsilon^2}{2} \tag{73}$$

where it is used the contract notation $y_d^0$ to denote the eigenvalue at the fixed point $g_c^0$ and $y'$ for $g_c^3$. This result for $Q = 3$ Potts model is an evidence of the existence of two different universality classes with their own set of critical exponents.

## 2.2 Energy Multifractality

In this section, it will be studied the dimension of the operator $\epsilon\epsilon$ in relation to the dimension of the energy operator $\epsilon$. In particular we will refer to $h$ as the generic physical dimension of an operator, as introduced in section 1.1.4 and $\Delta$ as the conformal dimension, which are linked through a simple factor: $h = 2\Delta$. In particular, at the pure point, the dimension between $\epsilon\epsilon$ and $\epsilon$ is given by:

$$\Delta_{\epsilon\epsilon} = 2\Delta_{\epsilon}$$

Now it is studied what happens for the dimension relationship at the new disordered fixed point. Having already computed the eigenvalue for the short-range fixed point, which is related to the energy energy term, with a simple dimensional expression it is possible to retrieve the corresponding conformal dimension:

$$y'_d = 2 - h'_{\epsilon\epsilon} = 2 - 2\Delta'_{\epsilon\epsilon}$$

It follows from the previous computation and equation (73):

$$2\Delta'_{\epsilon\epsilon} = 2 - y'_d = 2 + \epsilon - \frac{\epsilon^2}{2}$$

$$\Delta'_{\epsilon\epsilon} = 1 + \frac{\epsilon}{2} - \frac{\epsilon^2}{4}$$

This quantity must be compared with the conformal dimension of the energy operator $\epsilon$. For this end, one can artificially introduce in the perturbative action a new term which will be simply given by:

$$S = S^{Potts} + S^{Pert} + m_0 \int \sum_{a=1}^{n} \epsilon_a(x) d^2x$$

and we shall apply again the renormalization procedure to obtain a new dynamical equation for the parameter $m_0$.

### 2.2.1 0-loop order

The cumulant expansion in this case must be performed taking into account two perturbation terms. At the 0-loop order, only a term contributes to $m$. This is related to the additional energy field operator:

$$m_0 \sum_{a=1}^{n} \int_{1<|x|<r} \epsilon_a(x) d^2x + m_0 \sum_{a=1}^{n} \int_{|x|>r} \epsilon_a(x) d^2x$$

With the same rescale of the system (50), to integrate out small degrees of freedom one gets:

$$m_0 r^{2-h_\epsilon} \sum_{a=1}^{n} \int_{|x'|>1} \epsilon'_a(x') d^2x' = m' \sum_{a=1}^{n} \int_{|x'|>1} \epsilon'_a(x') d^2x' \tag{74}$$

which represents a simple dimensional change of the parameter corresponding to:

$$m_1 = m_0 r^{1+\frac{\epsilon_{SR}}{2}}$$

### 2.2.2 1-loop order

At first order a new additional term must be taken into account in the expansion, which is related to the double product between the $\epsilon\epsilon$ operator and the $\epsilon$ term (since the energy square term will not contribute to $m$). As before in the presence of a contraction, we have to count all the possible ones. This is done in *Figure 15* with 2 possibilities. Moreover choosing for instance $b = c$ there are $(n-1)$ possible replica for the last energy operator. All this together contributes to a combinatorial term of: $C_1 = 2(n-1)$. Therefore:

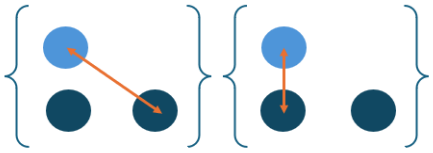

Figure 15: Combinatory diagram for $\epsilon\epsilon$ contraction at the 1-order-loop for m parameter giving only 2 possible diagrams

$$\cancel{2}\frac{g^0_{SR}}{\cancel{2}}\sum_{a\neq b}\int_{|x|>r}\epsilon_a(x)\epsilon_b(x)d^2x\ \cdot\left(\ m_0\int\sum_{c=1}^{n}\epsilon_c(y)d^2y\right)=$$

$$=2(n-1)g^0_{SR}m_0\int_{|x|>r}d^2x\sum_{a=1}^{n}\epsilon_a(x)\int_{1<|x-y|<r}d^2y\frac{\mathcal{I}}{|x-y|^{2h_\epsilon}}=$$

$$=4\pi(n-1)g^0_{SR}m_0\int_{|x|>r}\sum_{a=1}^{n}\epsilon_a(x)\frac{r^{\epsilon_{SR}}}{\epsilon_{SR}}d^2x=$$

$$=\frac{4\pi}{\epsilon_{SR}}(n-1)g^0_{SR}m_0r^{1+\frac{\epsilon_{SR}}{2}}\int_{|x'|>1}\sum_{a=1}^{n}\epsilon'_a(x')d^2x'$$

So we can consider as a second contribution to the renormalization of the parameter:

$$m_2=\frac{4\pi}{\epsilon_{SR}}(n-1)g^0_{SR}m_0r^{1+\frac{\epsilon_{SR}}{2}+\epsilon_{SR}} \tag{75}$$

### 2.2.3 2-loop order

The second order term must come from the product of two $\epsilon\epsilon$ with one single energy density operator $\epsilon$ giving the general form:

$$\cancel{3}\frac{g_{SR}}{\cancel{3}!^2}m_0\int_{|x|>1}d^2x\sum_{a\neq b}\epsilon_a(x)\epsilon_b(x)\ \cdot$$

$$\cdot\int_{1<|x-y|<r}\sum_{c\neq d}\epsilon_c(y)\epsilon_d(y)d^2y\int_{1<|x-z|<r}\sum_{e}\epsilon_e(z)d^2z$$

In the equation above it has already taken into account the correct integration ranges which will contribute in the renormalization group, following the arguments in previous section 2.1.3. The first term to take into account is a double contractions of energy operators at different positions. The diagrammatic combinatory of this case is simpler with respect to the previous 2-loop-order one. In *Figure 16* the 8 possibilities are shown

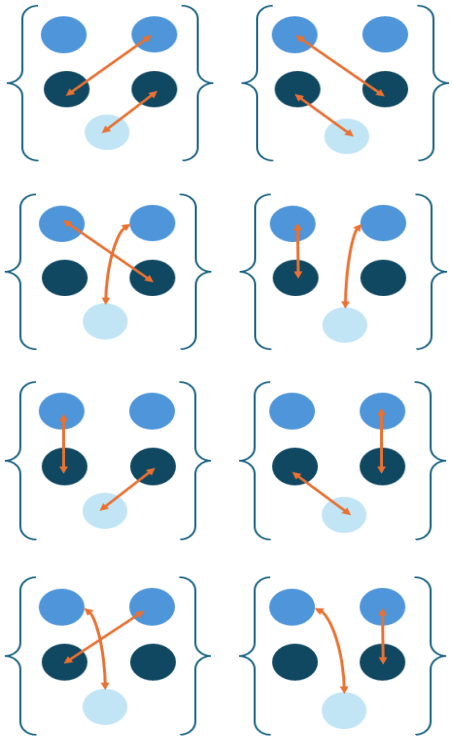

Figure 16: Combinatory diagram for 2-order-loop contribution in the parameter m. Here two contractions $\epsilon\epsilon$ are considered, giving 8 possibilities

This time, when we choose the first contraction for instance $b = c$ and the second $d = e$, the replica degeneracy will account for a term of the type: $(n-1)(n-2)$ giving a general contribution of $C_N = 8(n-1)(n-2)$ which will give as a first contribution:

$$m^0_{3,1} = \frac{g^2_{SR}}{2} m_0 8(n-1)(n-2) \int_{|x|>r} \sum_a \epsilon_a(x) d^2x \cdot$$

$$\cdot \int_{1<|x-y|<r} \frac{1}{|x-y|^{2h_\epsilon}} d^2y \int_{1<|x-z|<r} \frac{1}{|y-z|^{2h_\epsilon}} d^2z$$

The second contribution instead will take into account the contraction of three energy operators $\epsilon\epsilon\epsilon$ and the other two $\epsilon\epsilon$ that, due to the presence of the

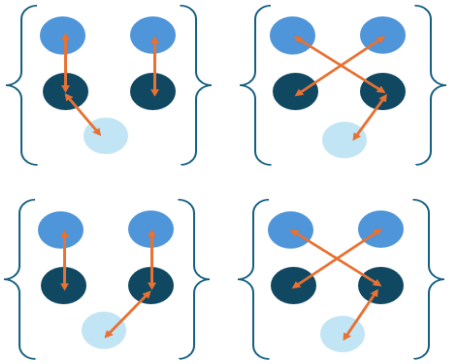

Figure 17: Combinatory diagram at 2-order-loop for m with a contraction $\epsilon\epsilon\epsilon$ and $\epsilon\epsilon$. Only 4 contributions are present

projection into $\epsilon$, will contribute with a new density operator. In *Figure 17* the diagram is presented with its only 4 contributions and with a replica degeneracy factor of $(n-1)$ which will contribute to the final $C_{3,2} = 4(n-1)$ This will give a term:

$$m^0_{3,2} = \frac{g^2_{SR}}{2} m_0 4(n-1) \int_{|x|>1} \sum_a \epsilon_a(x) d^2x \cdot$$

$$\cdot \int_{1<|x-y|<r} d^2y \int_{1<|x-z|<r} d^2z \langle \epsilon(x)\epsilon(y)\epsilon(z)\epsilon(\infty)\rangle_0 \langle \epsilon(y)\epsilon(z)\rangle_0$$

From this term as the computation of section 2.1.3, it gives two additional contribution of the renormalization group equations, and these integrals are solved through the Coulomb Gas formalism already mentioned. The three contributions will therefore be[29]:

$$m^0_{3,1} = 16\pi^2 g^2_{SR} m_0 (n-1)(n-2) \left(\frac{r^{2\epsilon_{SR}}}{\epsilon^2_{SR}}\right) \int_{|x|>r} \sum_a \epsilon_a(x) d^2x \tag{76}$$

$$m^0_{3,2} = -4\pi^2 g^2_{SR} m_0 (n-1) \left(\frac{r^{2\epsilon_{SR}}}{\epsilon_{SR}}\right) \int_{|x|>r} \sum_a \epsilon_a(x) d^2x \tag{77}$$

$$m^0_{3,3} = 8\pi^2 g^2_{SR} m_0 (n-1) \left(\frac{r^{2\epsilon_{SR}}}{\epsilon^2_{SR}}\right) \int_{|x|>r} \sum_a \epsilon_a(x) d^2x \tag{78}$$

If one sums up these three terms it gets a contribution:

$$m^0_3 = m_{3,1} + m_{3,2} + m_{3,3} =$$

$$= \left[ -4\pi^2 g^2_{SR} m_0 (n-1) \left(\frac{r^{2\epsilon_{SR}}}{\epsilon_{SR}}\right) \left(1 - \frac{4n-6}{\epsilon_{SR}}\right)\right] \int_{|x|>r} \sum_a \epsilon'_a(x') d^2x'$$

And rescaling following equations (50):

$$m_3 = \left[ -4\pi^2 g_{SR}^2 m_0 (n-1) \left( \frac{r^{2\epsilon_{SR}}}{\epsilon_{SR}} \right) \left( 1 - \frac{4n-6}{\epsilon_{SR}} \right) \right] r^{1+\frac{\epsilon_{SR}}{2}} \int_{|x'|>r} \sum_a \epsilon'_a(x') d^2x'$$

So putting all terms together with (74) and (75), the rescaled parameter will be:

$$m = m_1 + m_2 + m_3 = m_0 r^{1+\frac{\epsilon_{SR}}{2}} + m_0 r^{1+\frac{\epsilon_{SR}}{2}} \frac{4\pi}{\epsilon_{SR}} (n-1) g_{SR}^0 r^{\epsilon_{SR}} +$$

$$-4\pi^2 \frac{n-1}{\epsilon_{SR}} {g_{SR}^0}^2 r^{2\epsilon_{SR}} m_0 r^{1+\frac{\epsilon_{SR}}{2}} \left( 1 - \frac{4n-6}{\epsilon_{SR}} \right) \tag{79}$$

### 2.2.4 Dimension's computation

From previous expression one could reorganize terms as:

$$m = m_0 r^{1+\frac{\epsilon_{SR}}{2}} \left[ 1 + \frac{4\pi}{\epsilon_{SR}} (n-1) g_{SR}^0 r^{\epsilon_{SR}} + \right.$$

$$\left. -4\pi^2 \frac{n-1}{\epsilon_{SR}} {g_{SR}^0}^2 r^{2\epsilon_{SR}} \left( 1 - \frac{4n-6}{\epsilon_{SR}} \right) \right] \tag{80}$$

And by rewriting

$$m = Z_\epsilon m_0 r^{1+\frac{\epsilon_{SR}}{2}} \tag{81}$$

it can be obtained the adimensional quantity:

$$Z_\epsilon = 1 + 4\pi(n-1) g_{SR}^0 r^{\epsilon_{SR}} - 4\pi^2 \frac{n-1}{\epsilon_{SR}} {g_{SR}^0}^2 r^{2\epsilon_{SR}} \left( 1 + \frac{4n-6}{\epsilon_{SR}} \right)$$

and in the limit of the replicas going to zero ($n \to 0$), it simply gives

$$Z_\epsilon = 1 - 4\pi g_{SR}^0 r^{\epsilon_{SR}} + \frac{4\pi^2}{\epsilon_{SR}} {g_{SR}^0}^2 r^{2\epsilon_{SR}} \left( 1 + \frac{6}{\epsilon_{SR}} \right) \tag{82}$$

From now on, as in previous related computation in section 2.1.4, the index for short range will be neglected for simplicity. It can be compute the associated beta function:

$$\beta_\epsilon = r \frac{dm}{dr} = m \left( \left( 1 + \frac{\epsilon}{2} \right) + \gamma_\epsilon \right) \tag{83}$$

being

$$\gamma_\epsilon = \frac{r}{Z_\epsilon} \frac{dZ_\epsilon}{dr}$$

We first we compute

$$r \frac{dZ_\epsilon}{dr} = r \frac{d}{dr} \left( 1 - 4\pi g_0 r^\epsilon + \frac{4\pi^2}{\epsilon} {g_0}^2 r^{2\epsilon} \left( 1 + \frac{6}{\epsilon} \right) \right) =$$

$$= -4\pi g_0 r^\epsilon + 8\pi^2 {g_0}^2 \left(1 + \frac{6}{\epsilon}\right)$$

No we can compute the inverse up to the first order in $g_0$:

$$\frac{1}{Z_\epsilon} \simeq \frac{1}{1 - \frac{4\pi}{\epsilon} g_0 r^\epsilon} = 1 + \frac{4\pi}{\epsilon} g_0 r^\epsilon$$

Therefore one can compute

$$\left(1 + \frac{4\pi}{\epsilon} g_0 r^\epsilon\right)\left( - 4\pi g_0 r^\epsilon + 8\pi^2 {g^0}^2 \left(1 + \frac{6}{\epsilon}\right)\right) =$$

$$= -4\pi g_0 r^\epsilon + 8\pi^2 {g_0}^2 r^{2\epsilon} + \frac{48}{\epsilon} {g_0}^2 r^{2\epsilon} - \frac{16}{\epsilon} {g_0}^2 r^{2\epsilon} + \mathcal{O}({g_0}^3)$$

And with the previous expression (64):

$$g \simeq g_0 r^\epsilon \left(1 - 8\pi g_0 \frac{r^\epsilon}{\epsilon}\right)$$

$$\gamma_\epsilon = -4\pi g - 3\not{2}\frac{g}{\epsilon} + 8\pi g^2 + 3\not{2}\frac{g}{\epsilon} = -4\pi g + 8\pi g^2$$

To compute the energy dimension this time, we can make use of the Callan-Symanzik relation [40]:

$$2\Delta'_\epsilon = 2\Delta_\epsilon - 2\gamma_\epsilon(g_c) \tag{84}$$

In particular, in this case this reads:

$$2\Delta'_\epsilon = \Delta_{\epsilon\epsilon} + 8\pi g - 16\pi g^2$$

$$g_c = \frac{\epsilon}{8\pi} + \frac{\epsilon^2}{16\pi^2} + o(\epsilon^3)$$

$$2\Delta'_\epsilon = \Delta_{\epsilon\epsilon} + \epsilon + \frac{\epsilon^2}{2} - \frac{\epsilon^2}{4} = \Delta_{\epsilon\epsilon} + \epsilon + \frac{\epsilon^2}{4}$$

We recall that:

$$\Delta_{\epsilon\epsilon} = 1 - \frac{y_d}{2}$$

and at the pure point this corresponds to:

$$\Delta_{\epsilon\epsilon} = 1 - \frac{\epsilon}{2}$$

So finally we can substitute to obtain twice the conformal dimension at the new fixed point:

$$2\Delta'_\epsilon = 1 + \frac{\epsilon}{2} + \frac{\epsilon^2}{4}$$

But then, if this is compared with the the conformal dimension of the energy-energy operator, we find out that since:

$$\Delta'_{\epsilon\epsilon} = 1 + \frac{\epsilon}{2} - \frac{\epsilon^2}{4}$$

$$\Delta'_{\epsilon\epsilon} \neq 2\Delta'_\epsilon$$

coming from a second order correction in the perturbative parameter $\epsilon$. This embodies the property of multifractality for the energy operator.

## 2.3 Numerical simulations

In this section, the first numerical results obtained trough Monte Carlo techniques developped in *Fortran* will be shown in order to confirm the presence of the short-range class of universality. This will be done in the case of the $Q = 3$ disordered Potts model explaining, through a pseudo code, the way in which the quantities of interest have been obtained. Some of the techniques introduced in section 1.4 will be revised. The numerical analysis will be divided in two parts. The first one will be focused on the computation of the magnetization and the related critical exponents. Since there is a one-to-one correspondence between classes of universality and sets of critical exponents, it will be studied what happens at different values of disorder. Finally it will be computed the disorder eigenvalue through a perturbative numerical technique at the the pure fixed point (72).

### 2.3.1 SR-Potts model implementation and pseudo-code

To implement a Potts model, we have to consider again the discreet Hamiltonian version from equation (14). The spins, as mentioned above, will be taken to have only values: $s_i = \{1, 2, 3\}$ where $i = 1, ..., L^2$, being $L$ the linear size of the lattice. The square lattice will be constructed considering spins over a matrix as in *Figure 18*, in which nearest neighbours will be in general given, for a spin $s_i$ that does not being to the contour domain, by: $(i-1, i+1, i+L, i-L)$. A special care is given for the case of boundary spins, in which additional constraints are added. For clarity it will be brought an example: if $i = 1$ then the nearest neighbours will be the position of the spins at $(L, 2, 1+L, L(L-1)+1)$ due to periodic boundary conditions considered.

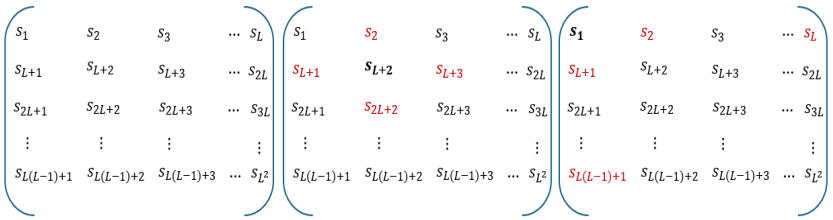

Figure 18: Spins as elements of a square matrix to mimic a lattice in the left panel. In the central panel an example of nearest neighbours is given for an internal spin while on the right the special case for the boundary spin $s_1$ is presented

The coupling $\langle J_{ij} \rangle$ which will take two possible values $\{J_1, J_2\}$ will be taken for each spin at a lattice site equivalent for the spin below and on the right for convenience. These will be identified as: $J^B_{\langle ij \rangle}$, $J^R_{\langle ij \rangle}$, and their value will be chosen through the additional random generator among two values, following

the relation:

$$J^B_{\langle ij\rangle} = \ J^R_{\langle ij\rangle} = \frac{J_1 + J_2}{2} + \sigma_i \frac{J_1 - J_2}{2}$$

In this way $\sigma$ can be a lattice variable instead of an edge one, as in equation (14), for the sake of simplicity.

This constraint for the bottom and right interactions is a microscopic detail for the implementation of disorder. We can affirm that it does not change the first and the second cumulant of the disorder probability that will be specified below. Two equation are needed to fix the parameters to work at critical points. The first one will be the duality condition [22] which determines the location of the critical point:

$$(e^{J_1} - 1)(e^{J_2} - 1) = Q \tag{85}$$

where $Q = 3$ here. The second equation comes form the definition of the parameter already introduced, the disorder strength:

$$r = \frac{J_1}{J_2}$$

The random variable $\sigma_i$ is taken to choose its values with equal probability. This actually consist in fixing $P(\{\sigma\})$ in such a way that $\overline{\sigma} = 0$ and each site is independent to each other: $\overline{\sigma_i \sigma_j} = 0$ if $i \neq j$. With first and second cumulant to be fixed, this is equivalent to a Gaussian disorder as explained at the beginning of section 2, therefore this represents an effective short range implementation. The parameter $r$ will be chosen freely in its domain while the implicit equation (85) will be solved through bisection method with an error of the order $\sim 10^{-12}$.

The actual parameters used will be listed afterword; despite their actual values, the simulations used share common codes and it will be presented here. After a first initialization of spins to be $s_i = 1 \ \forall \ i$ a first Montecarlo is performed for the system to thermalize. For a given size of the lattice $L$ there will be a total number of iterations given by $n_{Therm} \cdot \tau_L$ where $\tau_L$ is a lattice dependent parameter that takes into account how larger lattices need more time to reach uncorrelated measures. For each iteration the FK cluster will be created using the Swendsen-Wang Algorithm presented at section 1.4.5 with probability for the formation of a bond between nearest neighbours given by:

$$p_1 = 1 - e^{J_1}, \ p_2 = 1 - e^{J_2}$$

After thermalization the magnetization will be computed. This quantity in the cluster model is related to the size of the largest FK constructed, denoted by $A$. At the end of each simulation, the magnetization will simply be given by the average over the number of iterations:

$$\tilde{m} = \left\langle \frac{A}{L^2} \right\rangle \tag{86}$$

For each disorder value (therefore for each set of $J_1$ and $J_2$), the average over the disorder is taken simulating in an equivalent way $n_{samples}$ such that at the

end of each of them we can get the final quantity:

$$m = \frac{\tilde{m}}{n_{samples}} \tag{87}$$

### 2.3.2 Effective critical exponent simulations

In sections 1.1.1, 1.1.2 it has been shown the behaviour of some observable at criticality. The magnetization behaves for instance

$$m \simeq \left( \frac{T - T_c}{T_c} \right)^{\beta}$$

while the correlation length scales:

$$\xi \simeq \left| \frac{T - T_c}{T_c} \right|^{-\nu}$$

From theoretical results, it is known that the system will show a second order phase transition, which corresponds to the divergence of the correlation length. In a numerical simulation this phenomena cannot be observed, the divergence will be possible only with an infinite lattice size. Then, what happens, is due to finite sized effects that $\xi$ becomes comparable to the system size, therefore in general $\xi \simeq L$. If one performs some substitution it is possible to obtain that:

$$\left| \frac{T - T_c}{T_c} \right| \simeq L^{-\frac{1}{\nu}}$$

which entails

$$m \simeq L^{-\frac{\beta}{\nu}} \tag{88}$$

This allows to better understand the computation of the magnetization through the FK cluster fractal dimension. It is known in percolation model that:

$$A_{FK} \sim L^{D_f}$$

where this new variable is the so-called *fractal dimension* of the cluster linked to the critical exponent through the relation[41]:

$$D_f = 2 - \frac{\beta}{\nu}$$

Normalizing over $L^2$ as done in (86), exactly gives the same fraction of critical exponents, therefore this quantity is proportional to the magnetization $m$ and represents an improved estimator of it. From now, one, we will refer to the fraction of these two critical exponents as *effective magnetic exponent*:

$$\Delta(L) = \frac{\beta}{\nu} \tag{89}$$

The dependence on lattice size is crucial, since in theoretical comparisons with analytical calculations, the subleading correction due to the finite size of the lattice strongly affect the values. A possible comparison could be only done in theory in the limit:

$$\Delta = \lim_{L\to\infty} \Delta(L) \tag{90}$$

Numerically the effective critical exponent will be computed as follows. Taking for instance the magnetization at $L$ and at its double size $2L$, their ratio

$$\frac{m(2L)}{m(L)} = \frac{(2L)^{-\Delta}}{L^{-\Delta}}$$

can be manipulated to extract the critical exponent:

$$\Delta = -\frac{1}{log(2)} log\left(\frac{m(2L)}{m(L)}\right)$$

In this section the disorder strength has been chosen to be $r \in \{1, 6, 100, 1000\}$. The number of samples for $r \neq 1$ will be $n_{Samples} = 10^6$ (since in the pure case there will be no disorder implementation or disorder averages to be taken into account, for this particular case the magnetization computed will simply be $\tilde{m}$). The number of iteration for the thermalization have been set $n_{Therm} = 10^3$. The number of iteration, corresponding to the number of step for the average $\tilde{m}$ is $n_{iter} = 10^4$. The simulations have been run for: $L = \{8, 16, 32, 64, 128\}$.

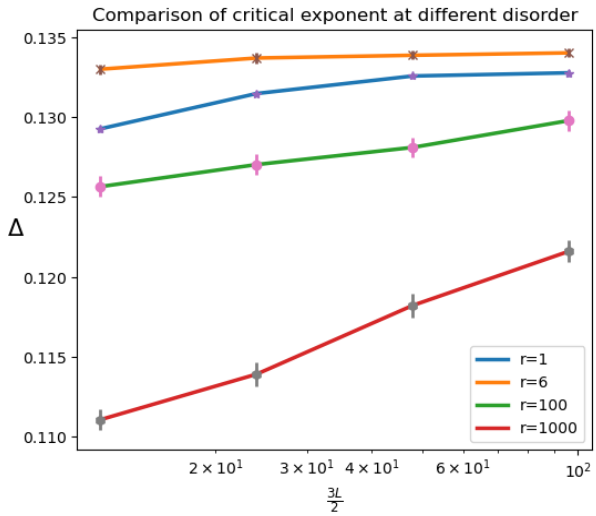


Figure 19: Effective critical exponent at increasing lattice size $L$ for different disorder strengths $r$

The result of the simulation for the *effective critical exponent* are shown in *Figure 19*. We will analyze curve by curve to understand the physics behind

the behaviour observed. At $r = 1$, which corresponds to the pure model, we see the presence of an increasing $\Delta$ which seems to have an asymptotic behaviour for larger lattice size, it seems to have a quite fast asymptotic behaviour to a specific value following the general idea behind equation (90). The same seems to happen even for $r = 6$, but by simple visual inspection, it can already been stated that the asymptotic behaviour is different with respect to the previous case, in fact, the curve seems to be shifted. For the curves at $r = 100$ and $r = 1000$, both show a monotonic behaviour, although there is no possibility to distinguish the pattern of the two previous curves.

We might explain what is happening by taking into account the stability analysis of section 2.1.5, with a particular focus on the phase diagram of *Figure* (14). In the numerical simulation we are taking the condition of working at criticality, so $T = T_c$, we are considering only a 1 dimensional system for the parameter space. The behaviour of the curve can be examined in two ways, either by keeping the lattice size or the disorder value fixed. Let's start by the latter. As we have said, the presence of a finite size of the systems leads to correction to the critical exponent, increasing the lattice size, this correction becomes less and less dominant. This can be seen in an equivalent way as a *numerical renormalization*, in which the system is rescaling its size (changing the linear parameter $L$) till it reaches a fixed point, in which the critical exponent will no longer change (related to the presence of the asymptotic behaviour). We can focus on characterizing better the differences of $r = 1$ and $r = 6$ fitting the curves following a parametric form of a typical power low behaviour at criticality:

$$m\left(\frac{3L}{2}\right) = a + b\left(\frac{3L}{2}\right)^{-c}$$

The numerical fits are shown in *Figure* 20.

This allows to extract the parameter a, which corresponds to the critical value in the limit $L \to \infty$ for both curves. A visual representation of the result is given in *Figure* (21) with the corresponding theoretical predictions.

The agreement that can be seen allows us to state that the two critical exponents are indeed different, and this is sufficient to affirm that the numerical calculation gives proof of the existence of a different class of universality. In this case, it corresponds to the prediction for the existence of the short-range random fixed point. The results will be summed up in *Table* 2, in which the errors have been computed from diagonalization of the covariance matrix for the fitting parameters.

What happens, although, for the other two curves? Since all quantities have to converge to a relevant fixed point, then all curves have an asymptotic behavior. We can assume that these curves, at higher disorder values, will simply require a longer convergence that cannot be captured at the simulated length scale of the lattices considered. There are then two aspects to be considered, if all curves must converge to a value how can we distinguish critical quantities? Moreover, what causes curves to have a slower convergence? The answer to both is actually given by a single concept, *other than the subleading correction*

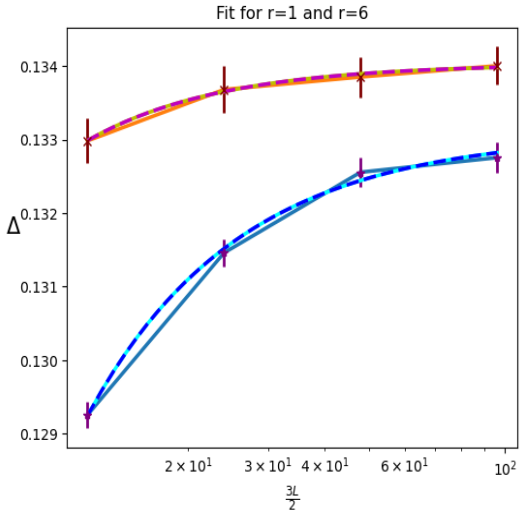


Figure 20: Fit of for r=1 and r=6

*due to the lattice size, there are additional correction due to the distance form the criticality of the disorder strength* $r_c$. But this means that models far from criticality show a double correction to scaling, which may affect in a great way the values of critical exponents and significantly slow down the asymptotic behaviour. This explains the trend for $r = 100, 1000$. But still it does not explain how to distinguish critical $r$ values. Well this is still an open question, in fact it is not easy to distinguish precisely for instance $r_c = 6$ from $r_c = 6.1$, if simulated, at the moment. One last question would be, in fact, related to what the curves for $r = 100, 1000$ will converge to. Theoretical results would lead us to claim that they will tend to the SR value of the critical exponent, being the only stable fixed point, since the pure point is unstable. But to claim this numerically, a perturbative approach will be developped and will be presented in the following section.

| $\Delta^{num}$ | $\Delta^{the}$ |
|---|---|
| $a_1 = 0.13308 \pm 0.00034$ | 0.13333 |
| $a_6 = 0.13403 \pm 0.00046$ | 0.13446 |

Table 2: Fitted parameters $a$, given by $L \to \infty$, corresponding to the critical exponent $\Delta$ for r=1 and r=6

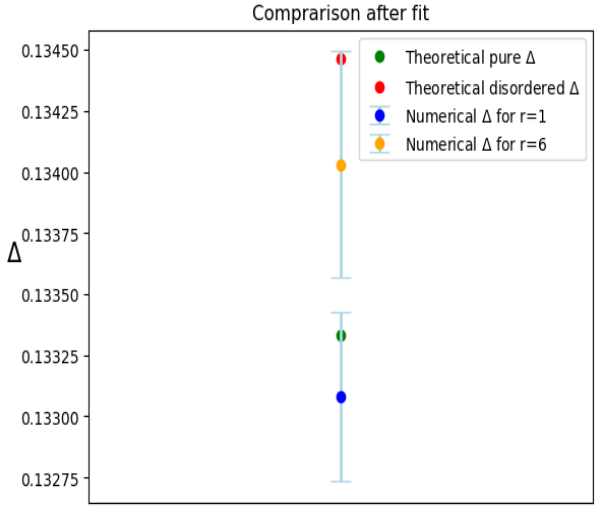


Figure 21: Asymptotic behaviour and comparison with theoretical results

### 2.3.3 Numerical disorder operator eigenvalue

The *renormalization flow* previously seen is only related to the finite size effects of the systems but does not provide the stability of the two classes of universality. In fact we would like better to understand, what is the actual behaviour at fixed lattice size $L$, but varying the disorder. This kind of approach is more similar to the one developped for the computation of the fixed points through the procedure of 2 and in the same way, the behaviour will be characterized considering small perturbation with respect to a known critical model. For the simulation this will entail to consider small values of the disorder with respect to the pure one, so values of $r \sim 1$.

In the theoretical framework of renormalization group, perturbation due to the introduction of the disorder allows to establish a relation with the average magnetization in the absence of randomness by means of a scaling function:

$$m(\mu^2; L) = m(0; L) f((\mu^2 - \mu_c^2) L^{y_d}) \tag{91}$$

where $\mu$ is simply linked to the disorder strength:

$$\mu = \frac{\Delta J}{2}$$

characterized by the following condition: $\mu_c = 0$ at the pure point. Rewriting the previous equation it can be expressed the final form:

$$\frac{m(\mu^2; L)}{m(0; L)} = f(\mu^2 L^{y_d}) \tag{92}$$

The variation of the disorder corresponds to actual change in $\mu$ which is linked to the variance of the disorder distribution ($\mathcal{P}\{\sigma\}$). This justify the possibility of plotting the fraction of the average magnetization computed as a function of what it will be called the *scaling variable* $\mu^2 L^{y_d}$.

Recalling that we work near a critical point, the functional dependence of $f$ must be unique, so considering different curves there must exist one value of $y_d$ in such a way that all the curves at different $L$ collapse onto a single one. The value which allows this, will correspond to the numerical prediction of the renormalization group eigenvalue at the pure point.

In *Figure* 22b, it is shown the result of the collapse using the value numerical value $y_d = 0.40$ with an uncertainty of $\sim 10^{-2}$. More details for the actual procedure implemented to extract the values and the error will be given in section 3.3. The result is in agreement with the theoretical prediction of (72)

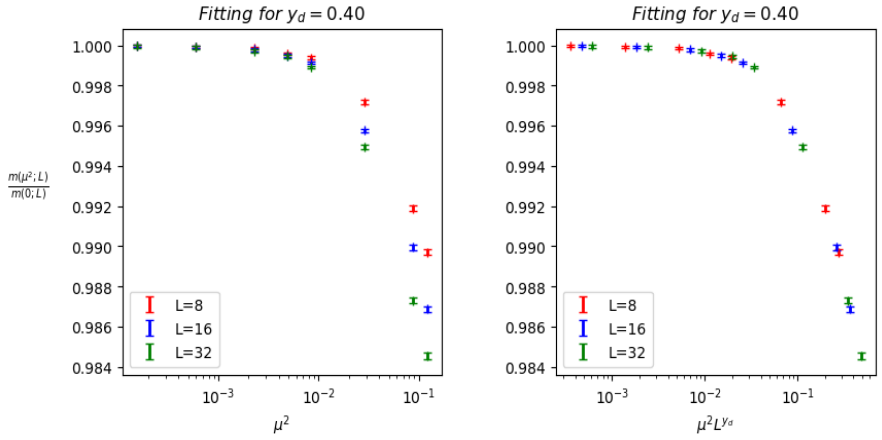


(a) (b)

Figure 22: Normalized magnetization computed at small values of disorder strength $r$. This procedure, equivalent to a perturbation technique to the pure point, show in the left panel how all the curves at fixed $L$ have a similar behaviour. In the right panel it is shown how, using an appropriate scaling variable, all functions can be collapsed into a single curve, giving the numerical form of the universal scaling function for the magnetization

when $\epsilon$ is set for $Q = 3$. In particular, since the value of the renormalization eigenvalue is positive, this confirms that the pure point is repulsive, together with the previous claim that curves at $r = 100, 1000$ will converge to the value of the short-range critical exponents. Finally this is better seen in the *Figure* 22a where, all the curves at fixed L go away from the pure value of the magnetization, and at increasing lattice size this flow is more enhanced, confirming the repulsiveness of the pure fixed point.

# 3 Long-range disordered Potts model

In this section it will be analysed the disordered Potts model with long-range correlation. This corresponds to the case in which the correlation exponent of equation (17) is taken as $a < 2$. For this section, due to an higher complexity, given by the presence of two perturbative parameters, the renormalization computation will be carried out only up to the 1-loop order. For the long range Potts model the probability distribution cannot be expressed in the same way as it has been done in section 2, in general, higher order cumulants starts to be relevant and cannot be neglected anymore. The Gaussian integration of (31) cannot be any longer performed as well as in numerical simulations, the Gaussian implementation is no longer appropriate. Firstly we would study analytically through renormalization group procedures how the dynamical equations modify, following a built-in critical action[29], if new fixed points are found along with their stability conditions and their universality class. Finally, moved by the possibility to characterize the renormalization group eigenvalue numerically, following the results of section 2.3, we will repeat the procedure for different values of $Q$ highlighting the main differences with the previous case.

## 3.1 Renormalization Group

The general idea, since we would like to generalize the short-range disorder, is to consider a probability distribution whose integration could bring two different terms, the short range part which we would like to prove to be relevant for $a \geq 2$ and a long range one, which should dominate for $a < 2$. This is in general consist in modifying directly equation (47), building manually a possible action who could be used to describe the physics. Namely this will be done by considering:

$$S = S^0 + S_{pert} + S^{LR}$$

being $S_{pert}$ the previous $\epsilon\epsilon$ operator contribution, while the new perturbation term will be related to:

$$S^{LR} = g^0_{LR} \int \epsilon(x)\sigma(x)d^2x$$

It consists on a direct interaction between the energy density operator and the disorder one. This is equivalent to having taken the replicated partition function directly as:

$$\overline{Z^n} = \prod_{a=1}^{n} Tr_{\{s_a\}} e^{-\sum_a S^0_a - g^0_{LR}\sum_a \int \epsilon_a(x)\sigma(x)d^2x - g^0_{SR}\sum_{a\neq b}\int \epsilon_a(x)\epsilon_b(x)d^2x} \tag{93}$$

And the usual expansion of the exponential can be performed considering the new perturbation term:

$$\tilde{S}_{pert} = g^0_{LR}\sum_a \int \epsilon_a(x)\sigma(x)d^2x + g^0_{SR}\sum_{a\neq b}\int \epsilon_a(x)\epsilon_b(x)d^2x$$

Having already studied the contribution of the first term, up to second order, in section 2.1.3, now it will be taken into account only the contributions coming from the second new term and its interaction with the first one. The general expansion will be given by:

$$e^{S_{pert}} = 1 + g^0_{LR}\sum_a \int \epsilon_a(x)\sigma(x)d^2x + g^0_{SR}\sum_{a\neq b}\int \epsilon_a(x)\epsilon_b(x)d^2x+$$
$$+\frac{{g^0_{LR}}^2}{2}\sum_{a,b}\int\int \epsilon_a(x)\sigma(x)\epsilon_b(y)\sigma(b)d^2xd^2y+$$
$$+\frac{{g^0_{SR}}^2}{2}\sum_{a\neq b}\sum_{c\neq d}\int\int \epsilon_a(x)\epsilon_b(x)\epsilon_c(y)\epsilon_d(y)d^2xd^2y+$$
$$+\frac{g_{SR}g_{LR}}{2}\sum_{a,b\neq c}\int\int \epsilon_a(x)\sigma(x)d^2x\epsilon_b(y)\epsilon_c(y)d^2xd^2y \tag{94}$$

### 3.1.1 0-loop order

One applies the same procedure of integrating out the smaller degrees of freedom to the term:

$$g^0_{LR}\sum_a \int_{1<|x|<r} \epsilon_a(x)\sigma(x)d^2x + g^0_{LR}\sum_a\int_{|x|>r}\epsilon_a(x)\sigma(x)d^2x$$

Performing the rescaling with the usual change in lattice size taking into account the disorder operator:

$$\begin{cases} x' = \frac{x}{r} \\ x' = \frac{d^2x}{r^2} \\ \epsilon'(x') = r^{h_\epsilon}\epsilon(x) \\ \sigma'(x') = r^{h_\sigma}\sigma(x) \end{cases} . \tag{95}$$

and imposing the equivalency of partition function at different scales:

$$g^0_{LR}r^{2-(h_\epsilon+h_\sigma)}\sum_a\int_{|x'|>1}\epsilon'_a(x')\sigma'(x')d^2x = g_{LR,1}\sum_a\int_{|x'|>1}\epsilon'_a(x')\sigma'(x')d^2x$$

which entails the first contribution to the renormalization of the random parameter to be:

$$g_{LR,1} = g^0_{LR}r^{\epsilon_{LR}} \tag{96}$$

where it has been set the new regularization term $\epsilon_{LR} = 2-(h_\epsilon+h_\sigma)$. The computation will be characterized by considering this as a new perturbative quantity. The dimension of the disorder operator is strictly related to the correlation parameter $a$ (17) by:

$$h_\sigma = \frac{a}{2}$$

and substituting the energy operator dimension as a function of $\epsilon_{SR}$ we get:

$$\epsilon_{LR} = 1 - \frac{a}{2} + \frac{\epsilon_{SR}}{2} \tag{97}$$

### 3.1.2 1-loop order

It is now possible to carry on with the contribution to the first order. This is equivalent to consider terms from (94) like $O(g_{SR}^2)$ that gives a contribution to the second order for the short range renormalization equations shown in (52). Although, this time, there are two additional terms which must be taken into account.

The first which will be considered is the one that will contribute at second order to the short-range perturbative parameter $g_{SR}$ given by $\mathcal{O}(\epsilon\sigma \cdot \epsilon\sigma)$. One proceeds integrating out the lower degrees of freedom as in all previous computations. This time the OPE must be performed between the disorder operators, which follow the equation below:

$$\sigma(x)\sigma(y) = \mathcal{I}\langle\sigma(x)\sigma(y)\rangle_0 = \frac{\mathcal{I}}{|x-y|^{2h_\sigma}}$$

In fact, if one contracts the $\epsilon\epsilon$ operator, we will remain with an operator of the type $\sigma\sigma$. This will not contribute for irrelevancy arguments. Therefore the final relevant term will be:

$$\frac{{g_{LR}^0}^2}{2}\sum_{a,b}\int_{|x|>r}\epsilon_a(x)\epsilon_b(y)\int_{1<|x-y|<r}\langle\sigma(x)\sigma(y)\rangle_o$$

therefore one obtains:

$$\frac{{g_{LR}^0}^2}{2}\sum_{a,b}\int_{|x|>r}\epsilon_a(x)\epsilon_b(y)\int_{1<|x-y|<r}\frac{\mathcal{I}}{|x-y|^{2h_\sigma}}$$

Considering only the contribution to the renormalization which will give an effective change:

$$\frac{{g_{LR}^0}^2}{2}\sum_{a\neq b}\int_{|x|>1}\epsilon_a(x)\epsilon_b(x)\int_{1<|x-y|<r}\frac{1}{|x-y|^{2h_\sigma}}$$

Performing now the integration in polar coordinate as to get (52) we finally get:

$$\frac{{g_{LR}^0}^2}{2}\sum_{a\neq b}\int_{|x|>r}\epsilon_a(x)\epsilon_b(x)2\pi\frac{r^{2-2h_\sigma}}{2-2h_\sigma}$$

and re-scaling with (95)

$$\frac{{g_{LR}^0}^2}{\not{2}}\sum_{a\neq b}\int_{|x'|>1}\epsilon'_a(x')\epsilon'_b(x')\not{2}\pi\frac{r^{2-2h_\sigma+2-2h_\epsilon}}{2-2h_\sigma} = g_{SR,2}\sum_{a\neq b}\int_{|x'|>1}\epsilon'_a(x')\epsilon'_b(x')d^2x'$$

From equations (97) it is possible to obtain the relations: $2h_\sigma = 2-2\epsilon_{LR}+\epsilon_{SR}$ such that the second order contribution coming from the long range perturbation gives:

$$g_{SR,2} = \pi {g_{LR}^0}^2\frac{r^{2\epsilon_{LR}}}{2\epsilon_{LR}-\epsilon_{SR}} \tag{98}$$

The second contributions instead, comes from the interaction of the type $\mathcal{O}(\sigma\epsilon\cdot\epsilon\epsilon)$ in which the only possible OPE comes from the energy field operators from a contraction of two indexes among three possible fields. This will modify the quantity $g_{LR}$. The arguments from all possible integration having divided the low and high degrees of freedom give always a single relevant contribution in which one variable is integrated over low distances and the second over high ones.

The contraction in this case is exactly equivalent with the one of *Figure* 15, giving a contribution (taking into account in the same way the degeneracy due to the replicas) of $C_{2,2} = 2(n-1)$. One gets therefore:

$$\frac{g_{SR}g_{LR}}{2}\sum_{a,b\neq c}\int\int \epsilon_a(x)\sigma(x)\epsilon_b(y)\epsilon_c(y)d^2xd^2y =$$

$$= C_{2,2}\frac{g_{SR}g_{LR}}{2}\sum_c\int_{|x|>r}\int_{1<|x-y|<r}\epsilon_a(x)\sigma(x)\epsilon_a(y)\epsilon_c(y)d^2xd^2y$$

Following the usual OPE for the density energy operators:

$$C_{2,2} = \frac{g_{SR}g_{LR}}{2}\sum_c\int_{|x|>r}\epsilon_c(x)\sigma(x)d^2x\int_{1<|x-y|<r}\frac{\mathcal{I}}{|x-y|^{2h_\epsilon}}d^2y$$

which through integration, neglecting the lower bound gives:

$$2(n-1)r^{\epsilon_{SR}}\frac{g_{SR}g_{LR}}{2\epsilon_{SR}}\sum_c\int_{|x|>r}\epsilon_c(x)\sigma(x)d^2x$$

and finally scaling back with equations (95), and setting it equal to the rescaled quantity:

$$(n-1)\frac{r^{\epsilon_{SR}+\epsilon_{LR}}}{\epsilon_{SR}}g^0_{SR}g^0_{LR}\sum_a\int_{|x'|>1}\epsilon_a(x')\sigma'(x')d^2x' =$$

$$= g_{LR,2}\sum_a\int_{|x'|>1}\epsilon_a(x')\sigma'(x')d^2x'$$

which gives to the perturbative long-range term the following contribution

$$g_{LR,2} = (n-1)\frac{r^{\epsilon_{SR}+\epsilon_{LR}}}{\epsilon_{SR}}g^0_{SR}g^0_{LR} \tag{99}$$

All the above computation, (51, 52, 96, 98, 99), gives as a final result:

$$\begin{cases} g_{SR} = g^0_{SR}r^{\epsilon_{SR}} + 4\pi(n-2){g^0_{SR}}^2\frac{r^{2\epsilon_{SR}}}{\epsilon_{SR}} + \pi{g^0_{LR}}^2\frac{r^{2\epsilon_{LR}}}{2\epsilon_{LR}-\epsilon_{SR}} \\ g_{LR} = g^0_{LR}r^{\epsilon_{LR}} + 4\pi(n-1)g^0_{SR}g^0_{LR}\frac{r^{\epsilon_{SR}+\epsilon_{LR}}}{\epsilon_{SR}} \end{cases}$$

And in the limit of zero replicas of the system, $n \to 0$:

$$\begin{cases} g_{SR} = g^0_{SR}r^{\epsilon_{SR}} - 8\pi{g^0_{SR}}^2\frac{r^{2\epsilon_{SR}}}{\epsilon_{SR}} + \pi{g^0_{LR}}^2\frac{r^{2\epsilon_{LR}}}{2\epsilon_{LR}-\epsilon_{SR}} \\ g_{LR} = g^0_{LR}r^{\epsilon_{LR}} - 4\pi g^0_{SR}g^0_{LR}\frac{r^{\epsilon_{SR}+\epsilon_{LR}}}{\epsilon_{SR}} \end{cases} \tag{100}$$

These equations represent the renormalized parameters at 1-loop-order. As it can be seen they are not independent from each other, the short-range one depends on the long-range and vice-versa, this will lead to a more complex treatment.

### 3.1.3 Fixed Points

For the computation of the fixed point we need to rewrite the two previous expression using the beta functions. While in the previous short-range case the dynamical equation was represented by a 1-dimensional system, the presence of two coupled differential equation will lead to the study of a 2-dimensional phase space and a system of non-linear dynamical equations. Let's start by rewriting everything in terms of the beta functions, below defined:

$$\begin{cases} \beta_{SR} = r\frac{dg_{SR}}{dr} \\ \beta_{LR} = r\frac{dg_{LR}}{dr} \end{cases}$$

Equations (100) can the be written as:

$$\begin{cases} g_{SR} = g^0_{SR} r^{\epsilon_{SR}} \left(1 - 8\pi g^0_{SR} \frac{r^{2\epsilon_{SR}}}{\epsilon_{SR}} + \pi \frac{{g^0_{LR}}^2}{g^0_{SR}} \frac{r^{2\epsilon_{LR}-\epsilon_{SR}}}{2\epsilon_{LR}-\epsilon_{SR}}\right) \\ g_{LR} = g^0_{LR} r^{\epsilon_{LR}} \left(1 - 4\pi g^0_{SR} \frac{r^{\epsilon_{SR}+\epsilon_{LR}}}{\epsilon_{SR}}\right) \end{cases}$$

$$\begin{cases} g_{SR} = g^0_{SR} r^{\epsilon_{SR}} Z_{SR} \\ g'_{LR} = g^0_{LR} r^{\epsilon_{LR}} Z_{LR} \end{cases} . \tag{101}$$

where the new quantities defined are:

$$\begin{cases} Z_{SR} = 1 - 8\pi g^0_{SR} \frac{r^{\epsilon_{SR}}}{\epsilon_{SR}} + \pi \frac{{g^0_{LR}}^2}{g^0_{SR}} \frac{r^{2\epsilon_{LR}-\epsilon_{SR}}}{2\epsilon_{LR}-\epsilon_{SR}} \\ Z_{LR} = 1 - 4\pi g^0_{SR} \frac{r^{\epsilon_{SR}}}{\epsilon_{SR}} \end{cases} . \tag{102}$$

and the two additional quantities can be introduced:

$$\begin{cases} \gamma_{SR} = r\frac{g_{SR}}{Z_{SR}}\frac{dZ_{SR}}{dr} \\ \gamma_{LR} = r\frac{g_{LR}}{Z_{LR}}\frac{dZ_{LR}}{dr} \end{cases} \tag{103}$$

$$\begin{cases} \beta_{SR} = g_{SR}\epsilon_{SR} + \gamma_{SR} \\ \beta_{LR} = g_{LR}\epsilon_{LR} + \gamma_{LR} \end{cases} . \tag{104}$$

We can focus on the computation of one first, starting with the short-range case.

$$r\frac{dZ_{SR}}{dr} = \frac{d}{dr}\left(1 - 8\pi g^0_{SR}\frac{r^{\epsilon_{SR}}}{\epsilon_{SR}} + \pi\frac{{g^0_{LR}}^2}{g^0_{SR}}\frac{r^{2\epsilon_{LR}-\epsilon_{SR}}}{2\epsilon_{LR}-\epsilon_{SR}}\right) =$$

$$= -8\pi g^0_{SR} r^{\epsilon_{SR}} + \pi\frac{{g^0_{LR}}^2}{g^0_{SR}} r^{2\epsilon_{LR}-\epsilon_{SR}}$$

$$\frac{1}{Z_{SR}} = 1 + 8\pi g^0_{SR}\frac{r^{\epsilon_{SR}}}{\epsilon_{SR}} - \pi\frac{{g^0_{LR}}^2}{g^0_{SR}}\frac{r^{2\epsilon_{LR}-\epsilon_{SR}}}{2\epsilon_{LR}-\epsilon_{SR}}$$

Since we have computed RG equations at 1-loop order, we have to stop at expansions which are most quadratic like

$$\mathcal{O}(g^2_{SR}, g^2_{LR}, g_{SR}g_{LR})$$

So following the same order for the computation of gamma:

$$\gamma_{SR} = \left(-8\pi g^0_{SR}r^{\epsilon_{SR}} + \pi\frac{{g^0_{LR}}^2}{g^0_{SR}}r^{2\epsilon_{LR}-\epsilon_{SR}}\right)\left(1 + 8\pi g^0_{SR}\frac{r^{\epsilon_{SR}}}{\epsilon_{SR}} - \pi\frac{{g^0_{LR}}^2}{g^0_{SR}}\frac{r^{2\epsilon_{LR}-\epsilon_{SR}}}{2\epsilon_{LR}-\epsilon_{SR}}\right) =$$

$$= -8\pi g^0_{SR}r^{\epsilon_{SR}} + \pi\frac{{g^0_{LR}}^2}{g^0_{SR}}r^{2\epsilon_{LR}-\epsilon_{SR}} + o(g^3)$$

It can be computed the beta-function:

$$\beta_{SR} = \epsilon_{SR}g_{SR} + g_{SR}\left(-8\pi g^0_{SR}r^{\epsilon_{SR}} + \pi\frac{{g^0_{LR}}^2}{g^0_{SR}}r^{2\epsilon_{LR}-\epsilon_{SR}}\right) + o(g^3)$$

And considering now, at first order:

$$\begin{cases} g_{LR} = g^0_{LR}r^{\epsilon_{LR}} + o(g^2) \\ g_{SR} = g^0_{SR}r^{\epsilon_{SR}} + o(g^2) \end{cases}$$

we can write the final expression:

$$\beta_{SR} = \epsilon_{SR}g_{SR} - 8\pi g^2_{SR} + \pi g^2_{LR} \tag{105}$$

The same computation can be applied to obtain the long-range beta-function:

$$r\frac{dZ_{LR}}{dr} = r\frac{d}{dr}\left(1 - 4\pi g^0_{SR}\frac{r^{\epsilon_{SR}}}{\epsilon_{SR}}\right) = -4\pi g^0_{SR}\frac{r^{\epsilon_{SR}}}{\epsilon_{SR}}$$

$$\frac{1}{Z_{LR}} = 1 + 4\pi g^0_{SR}\frac{r^{\epsilon_{SR}}}{\epsilon_{SR}}$$

Therefore the gamma function:

$$\gamma_{LR} = \left(-4\pi g^0_{SR}\frac{r^{\epsilon_{SR}}}{\epsilon_{SR}}\right)\left(1 + 4\pi g^0_{SR}\frac{r^{\epsilon_{SR}}}{\epsilon_{SR}}\right) = -4\pi g^0_{SR}r^{\epsilon_{SR}} + o(g)$$

and taking into account the first order change in the parameter:

$$\beta_{LR} = \epsilon_{LR}g_{LR} - 4\pi g_{SR}g_{LR} \tag{106}$$

Fixed points can be found imposing the system of equations (105), (106) to be null. We will consider for this aim three different cases:

1. $g_{SR} = g_{LR} = 0$ :

   This corresponds exactly to the pure fixed point, in which disorder is not present at criticality. The fixed point will be denoted

   $$\vec{g_P} = (0, 0) \tag{107}$$

2. $g_{LR} = 0, g_{SR} \neq 0$:

   This is equivalent to say that the disorder implemented does not have the long-range character but only the short range one.

   Necessarily $\epsilon_{SR} - 8\pi g_{SR} = 0$, which gives

   $$\vec{g_{SR}} = \left(\frac{\epsilon_{SR}}{8\pi}, 0\right) \tag{108}$$

   and this is in agreement, up to the first order, to equation (67), confirming how the action built is able to include the previous SR result and to generalize it.

3. $g_{SR}, g_{LR} \neq 0$:

   This final case will be referred to as long-range case, due to the presence of a non-null-term for the long-range parameter.

   It will imply: $\epsilon_{LR} - 4\pi g_{SR} = 0 \rightarrow g_{SR} = \frac{\epsilon_{LR}}{4\pi}$ which can be substituted in the first equation: $\epsilon_{SR}\frac{\epsilon_{LR}}{4\pi} - 8\pi(\frac{\epsilon_{LR}}{4\pi})^2 + \pi g_{LR}^2 = 0$. This gives as a result:

   $$\vec{g_{LR}}^{1,2} = \left(\frac{\epsilon_{LR}}{4\pi}, \pm\frac{\epsilon_{LR}}{2\pi}\sqrt{2 - \frac{\epsilon_{SR}}{\epsilon_{LR}}}\right) \tag{109}$$

### 3.1.4 Stability of Fixed Points and RG eigenvalues

Being the system of differential equations (the beta-functions expressions) non linear, to study the stability of the fixed points it must be linearized. This corresponds to the computation of the Jacobian matrix, defined as follows:

$$J = \begin{pmatrix} \frac{d\beta_{SR}}{dg_{SR}} & \frac{d\beta_{SR}}{dg_{LR}} \\ \frac{d\beta_{lR}}{dg_{SR}} & \frac{d\beta_{LR}}{dg_{LR}} \end{pmatrix}$$

Performing the derivatives this corresponds to:

$$J = \begin{pmatrix} \epsilon_{SR} - 16\pi g_{SR} & 2\pi g_{LR} \\ -4\pi g_{LR} & \epsilon_{LR} - 4\pi g_{SR} \end{pmatrix} \tag{110}$$

Then the stability will be given by the eigenvalues of the Jacobian matrix computed at each fixed point[42]. To make the discussion about stability more simpler, the values of $\epsilon_{SR}$ will be taken from the beginning as the ones of interest. In fact focusing on a particular case of the spin values (Q=1,2,3), the dimension of the energy operator is known, as well as the regularization parameter $\epsilon_{SR}$ which depend on.

**Q=1** The Potts, model will corresponds to a long-range percolation model in which $\epsilon_{SR} = -0.5$. We can start the analysis of the fixed point from the pure one:

$$J|_{\vec{g}=g\vec{P}} = \begin{pmatrix} -\frac{1}{2} & 0 \\ 0 & \epsilon_{LR} \end{pmatrix}$$

The matrix is diagonal, the eigenvalues simply corresponds to:

$$\begin{cases} \lambda^1 = -\frac{1}{2} \\ \lambda^2 = \epsilon_{LR} \end{cases} \tag{111}$$

Moreover we have fixed $\lambda^1 < 0$. We can distinguish three different cases:

- $\epsilon_{LR>0}$:
  *Saddle point node*, it is attractive along one direction and repulsive along the other
- $\epsilon_{LR} = 0$:
  Node with an attractive direction and a marginal one: *Stable degenerative point*
- $\epsilon_{LR} < 0$:
  *Stable node*, the pure point is an attractive fixed point

At the short-range fixed point:

$$J|_{\vec{g}=g\vec{S}_R} = \begin{pmatrix} \frac{1}{2} & 0 \\ 0 & \epsilon_{LR} + \frac{1}{4} \end{pmatrix}$$

Even in this case, being the jacobian diagonal, it is possible to determine the eigenvalues by simply looking at the diagonal elements:

$$\begin{cases} \lambda^1 = \frac{1}{2} \\ \lambda^2 = \epsilon_{LR} + \frac{1}{4} \end{cases} \tag{112}$$

Once again we can distinguish three different case:

- $\epsilon_{LR} > -\frac{1}{4}$:
  *Unstable node* since both eigenvalues are positive
- $\epsilon_{LR} = -\frac{1}{4}$:
  *Unstable degenerate node*, one negative and one null
- $\epsilon_{LR} < -\frac{1}{4}$:
  *Saddle point node*, one stable and one unstable direction

Finally, we study the Jacobian for the long range fixed point:

$$J|_{\vec{g}=g\vec{S}_R} = \begin{pmatrix} -\frac{1}{2} - 4\epsilon_{LR} & \pm\epsilon_{LR}\sqrt{2 + \frac{1}{2\epsilon_{LR}}} \\ \mp 2\epsilon_{LR}\sqrt{2 + \frac{1}{2\epsilon_{LR}}} & 0 \end{pmatrix}$$

For symmetric reasons, which are all related to taking one of the two bond strength greater than the other, the two fixed point will behave in the exact same way, therefore it will be analysed just the case of $\vec{g} = \vec{g_{LR}}^1$

$$J|_{\vec{g}=\vec{g_{LR}}^1} = \begin{pmatrix} -\frac{1}{2} - 4\epsilon_{LR} & +\epsilon_{LR}\sqrt{2+\frac{1}{2\epsilon_{LR}}} \\ -2\epsilon_{LR}\sqrt{2+\frac{1}{2\epsilon_{LR}}} & 0 \end{pmatrix}$$

We can compute the trace:

$$Tr(J) = -\frac{1}{2} - 4\epsilon_{LR}$$

And the determinant:

$$det(J) = 2\epsilon_{LR}^2\left(2+\frac{1}{2\epsilon_{LR}}\right) = 4\epsilon_{LR}^2 + \epsilon_{LR}$$

we are in this case more interested in the stability rather then the actual eigenvalues. The first information about the stability of the fixed point is given by the trace of the jacobian. In this case:

$$Tr(J) > 0 \iff \epsilon_{LR} < -\frac{1}{8}$$

but together with the conditions of existence : $(-\infty, -\frac{1}{4}], \cup [0, +\infty)$ we get that the fixed points could be attractive or repulsive if:

$$\begin{cases} \epsilon_{LR} \leq -\frac{1}{2} & unstable \\ \epsilon_{LR} \geq 0 & stable \end{cases} . \tag{113}$$

Moreover, the classification of the fixed point is fully given by $Tr^2(J)$ and $4det(J)$ In this case it is always true that: $Tr^2(J) > 4det(J)$ so we can summarize the type of fixed point in the following:

- $\epsilon_{LR} < -\frac{1}{4}$:
  *unstable node*
- $\epsilon_{LR} > 0$:
  *stable node*

The case $\epsilon_{SR} = -\frac{1}{4}, 0$, they become degenerate nodes, respectively unstable and stable. The general stability for all possible different values of $\epsilon_{LR}$ and the type of fixed point is given in *Figure* 23. Moreover in *Figure* 24 it can be found the numerical representation of the phase space whose directions for stability are in agreement with the theoretical analysis[2].

[2]The numerical representation of the phase space has been obtained using an already existing code for 2-dimensional non linear phase plots[43]

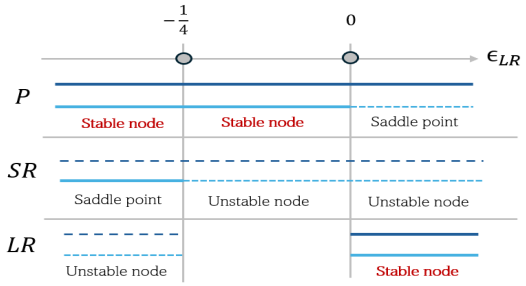


Figure 23: Summary of the stability of fixed points Q=1

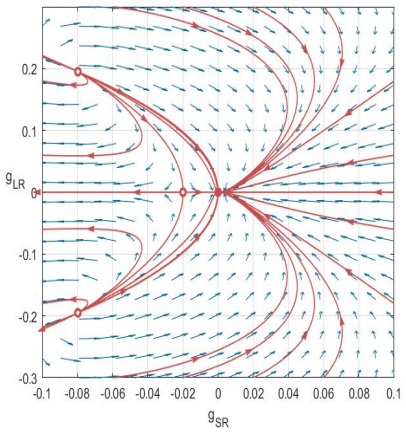


(a) $\epsilon_{LR} < -0.25$:

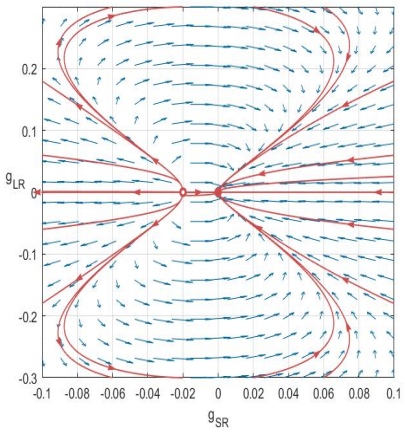


(b) $-0.25 < \epsilon_{LR} < 0$:

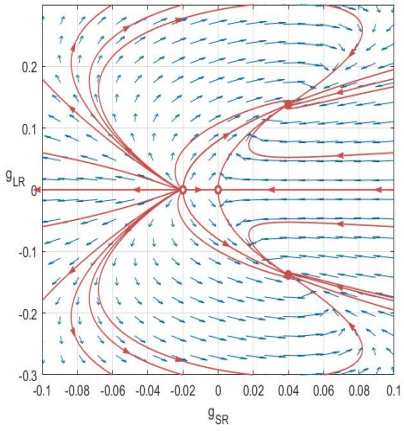


(c) $\epsilon_{LR} > 0$

Figure 24: Phase diagram and stability analysis for q=1

**Q=2** In this case, corresponding to $\epsilon_{SR} = 0$, the short-range fixed point (108) collapses into the pure point (107), therefore it is sufficient to analyze just one of them and one of the long-range fixed point to have a complete picture. For the pure/short-range point the eigenvalues will simply be:

$$\begin{cases} \lambda^1 = 0 \\ \lambda^2 = \epsilon_{LR} \end{cases}$$

So we can distinguish two cases:

- $\epsilon_{LR} > 0$:
  *unstable degenerate fixed point*
- $\epsilon_{LR} < 0$:
  *stable degenerate fixed point*

Whilst for the long range jacobian, we can simplify it in the form:

$$J|_{\vec{g}=g\vec{L}R^1} = \begin{pmatrix} -4\epsilon_{LR} & +\epsilon_{LR}\sqrt{2} \\ -2\epsilon_{LR}\sqrt{2} & 0 \end{pmatrix}$$

Once again, in this case we focus more on the characterization of the fixed points rather than the specif value:

$$Tr(J) = -4\epsilon_{LR}, \ det = 4(J)\epsilon_{LR}^2$$

and in this case, due to the condition $Tr^2(J) = 4det(J)$ entailing:

- $\epsilon_{LR} < 0$:
  unstable star node
- $\epsilon_{LR} > 0$:
  stable star node

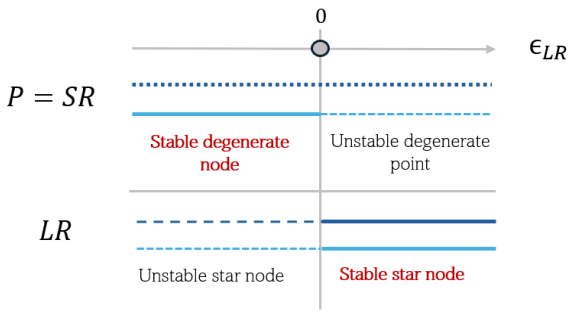


Figure 25: Summary of the stability of fixed points Q=2

In *Figure* 25 the stability conditions will be summarized. Finally, the corresponding numerical phase plot will be shown in *Figure* 26.

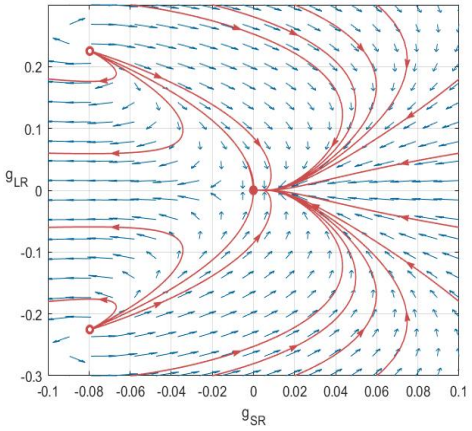


(a) $\epsilon_{LR} < 0$:

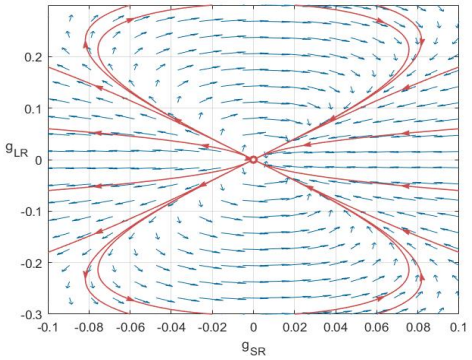


(b) $\epsilon_{LR} = 0$

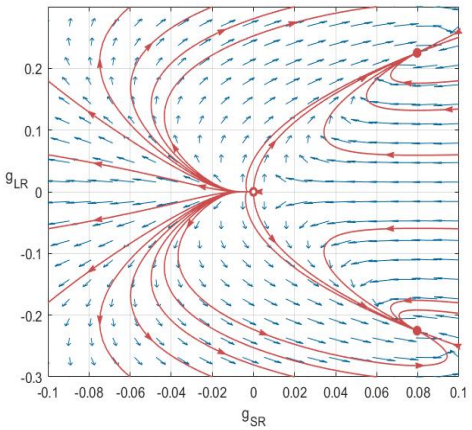


(c) $\epsilon_{LR} > 0$

Figure 26: Phase diagram and stability analysis for Q=2

**Q=3** In this case, we have to take into account the study for all the three fixed points with $\epsilon_{SR} = 0.4$. Staring from the pure one, the matrix becomes:

$$J|_{\vec{g}=\vec{gP}} = \begin{pmatrix} \frac{2}{5} & 0 \\ 0 & \epsilon_{LR} \end{pmatrix}$$

Therefore

$$\begin{cases} \lambda^1 = \frac{2}{5} \\ \lambda^2 = \epsilon_{LR} \end{cases}$$

- $\epsilon_{LR} > 0$:
  unstable node
- $\epsilon_{LR} = 0$:
  degenerate unstable node
- $\epsilon_{LR} < 0$:
  saddle point

For the short-range fixed-point:

$$J|_{\vec{g}=g\vec{S}R} = \begin{pmatrix} -\frac{2}{5} & 0 \\ 0 & \epsilon_{LR} - \frac{1}{5} \end{pmatrix}$$

Once again, being the matrix diagonal it is possible to compute

$$\begin{cases} \lambda^1 = -\frac{2}{5} \\ \lambda^2 = \epsilon_{LR} - \frac{1}{5} \end{cases}$$

This corresponds to the following cases:

- $\epsilon_{LR} < \frac{1}{5}$:
  stable node
- $\epsilon_{LR} = \frac{1}{5}$:
  stable degenerate node
- $\epsilon_{LR} > \frac{1}{5}$:
  saddle point

Finally we analyzed the case of the LR-fixed point: $\vec{g} = \vec{gLR}^1$

$$J|_{\vec{g}=g\vec{LR}^1} = \begin{pmatrix} \frac{2}{5} - 4\epsilon_{LR} & +\epsilon_{LR}\sqrt{2 - \frac{2}{5\epsilon_{LR}}} \\ -2\epsilon_{LR}\sqrt{2 - \frac{2}{5\epsilon_{LR}}} & 0 \end{pmatrix}$$

whose trace is computed below:

$$Tr(J) = \frac{2}{5} - 4\epsilon_{LR}$$

It gives:

$$\begin{cases} Tr(J) > 0 & \epsilon_{LR} < \frac{1}{10} \\ Tr(J) < 0 & \epsilon_{LR} > \frac{1}{10} \end{cases} . \tag{114}$$

Whilst the determinant:

$$det(J) = 4\epsilon_{LR}^2 - \frac{4\epsilon_{LR}}{5}$$

even in this case, as for $Q = 1$

$$Tr^2(J) > 4det(J) \ \forall \epsilon_{LR}$$

So we can summarize, taking into account the domain of existence (due to the presence of the square root) the ranges:

$$\epsilon_{LR} < 0 \ || \ \epsilon_{LR} > 0.2$$

- $\epsilon_{LR} < 0$:
  unstable node
- $\epsilon_{LR} > 0.2$:
  stable node

And they will become degenerate, respectively unstable and stable for $\epsilon_{LR} = 0, 0.2$. Everything will be summarized in the *Figure* 27.

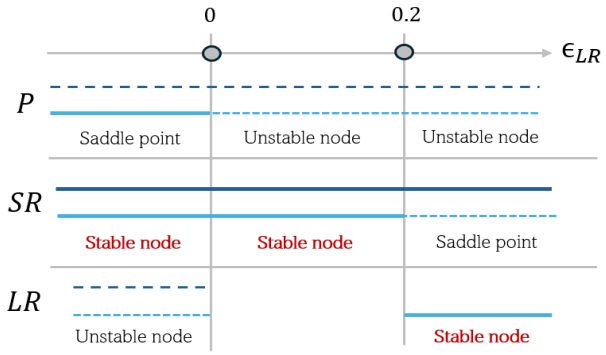


Figure 27: Summary of the stability of fixed points Q=3

In *Figure* 28 it is represented the corresponding phase space computed numerically, the stability of the fixed points once again show an agreement with the theoretical computation.

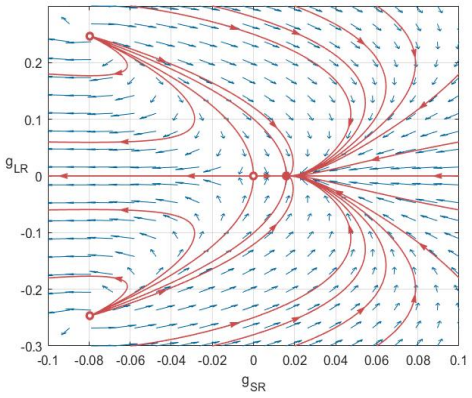


(a) $\epsilon_{LR} < 0$:

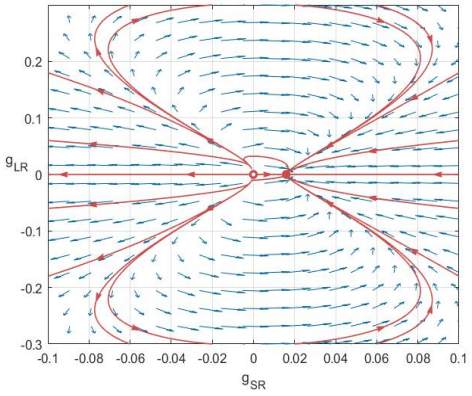


(b) $0 < \epsilon_{LR} < 0.2$

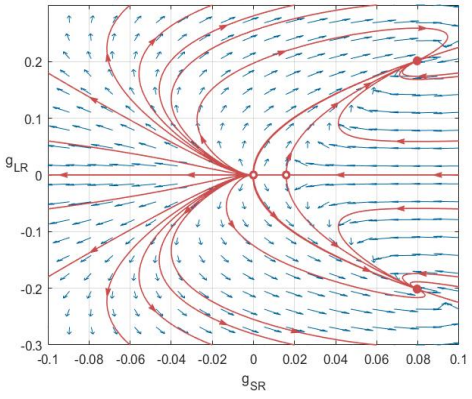


(c) $\epsilon_{LR} > 0.2$

Figure 28: Phase diagram and stability analysis for Q=3

## 3.2 Operators renormalization

It is wanted at this point to understand the way both the energy $\epsilon$ operator and the disorder one $\sigma$ renormalize. The first step is to add into the action two new quantities, following the same procedure of 2.2:

$$S = S^0_{Potts} + S_{Pert} + S_\epsilon + S_\sigma$$

$$S = S^0_{Potts} + g_{LR}\sum_a \int d^2x \sigma(x)\epsilon^a(x) + g_{SR}\sum_{a\neq b}\int d^2x \epsilon^a(x)\epsilon^b(x) +$$

$$+ m_0 \sum_a \int d^2x \epsilon^a(x) + h_0 \int d^2x \sigma(x)$$

As we have seen from the previous renormalization, there exists a mixing between long-range and short-range parameters. The same will happen even for the additional quantities $m$ and $h$. Therefore the following system must be considered for the renormalization of these two quantities:

$$\begin{pmatrix} m \\ h \end{pmatrix} = \begin{pmatrix} Z_\epsilon & Z_{\epsilon\sigma} \\ Z_{\sigma\epsilon} & Z_\sigma \end{pmatrix} \begin{pmatrix} m_0\ r^{2-h_\epsilon} \\ h_0\ r^{2-h_\sigma} \end{pmatrix}$$

Even in this part, it will be chosen to perform renormalization up to 1-order loop.

### 3.2.1 Energy operator

Let's start with the energy term at 0-order loop. This contribution gives a simple dimensional quantity. In fact:

$$m_0 \sum_a \int_{|x|>r} d^2x \epsilon^a(x) \to m_0 \sum_a r^{2-h_\epsilon} \int_{|x|>r} d^2x \epsilon^a(x)$$

performing the rescaling (95). This allows to write:

$$m_1 = m_0 r^{2-h_\epsilon}$$

An additional contribution is given by the 1-loop-term that comes from the product of energy energy operator $\epsilon\epsilon$ and the energy $\epsilon$ one: We have already seen this expression at (75), the main steps are repeated:

$$C_2 g^0_{SR} m_0 \sum_a \int_{|x|>r} d^2x \epsilon^a(x) \int_{1<|x-y|<r} \frac{1}{|x-y|^{2h_\epsilon}} d^2y$$

Using again the polar coordinates:

$$2(n-1) g^0_{SR} m_0 2\pi \frac{r^{2-2h_\epsilon}}{2-2h_\epsilon} \sum_a \int_{|x|>r} d^2x \epsilon^a(x)$$

and rescaling back one finds the second contribution for the energy operator:

$$m_2 = 4(n-1)g^0_{SR}m_0\frac{r^{2-2h_\epsilon}}{2-2h_\epsilon}r^{2-h_\epsilon}$$

Up till now, the previous expression in the short-range section has been obtained, although in this case there is another contribution that must be taken into account. This comes from the disorder-energy $\sigma\epsilon$ operator which couples with the disorder $\sigma$:

$$h_0\int d^2x\sigma(x)\cdot\left(g^0_{LR}\sum_a\int d^2y\sigma(y)\epsilon^a(y)\right)$$

and following the OPE of $\langle\sigma(x)\sigma(y)\rangle_0 = \frac{\mathcal{I}}{|x-y|^{2h_\sigma}}$ one simply obtains the additional contribution:

$$m_3 = h_0 g^0_{LR}\frac{r^{2-2h_\sigma}}{2-2h_\sigma}r^{2-h_\epsilon} \tag{115}$$

Finally obtaining the complete expression:

$$m = m_1 + m_2 + m_3 =$$

$$= m_0 r^{2-h_\epsilon} + 4(n-1)g^0_{SR}m_0\frac{r^{2-2h_\epsilon}}{2-2h_\epsilon}r^{2-h_\epsilon} + h_0 g^0_{LR}\frac{r^{2-2h_\sigma}}{2-2h_\sigma}r^{2-h_\epsilon}$$

$$m = m_0 r^{2-h_\epsilon}\left(1 + 4(n-1)g^0_{SR}\frac{r^{2-2h_\epsilon}}{2-2h_\epsilon}\right) + h_0 r^{2-h_\sigma}\left(g^0_{LR}\frac{r^{2-h_\sigma-h_\epsilon}}{2-2h_\sigma}\right) \tag{116}$$

So in the Z matrix representation one can write:

$$Z_\epsilon = 1 + 4(n-1)g^0_{SR}\frac{r^{\epsilon_{SR}}}{\epsilon_{SR}} \tag{117}$$

and in the same way:

$$Z_{\epsilon\sigma} = g^0_{LR}\frac{r^{\epsilon_{LR}}}{2\epsilon_{LR}-\epsilon_{SR}} \tag{118}$$

### 3.2.2 Disorder operator

Now it is possible to compute the renormalization of the disorder field operator. For the zero-loop-order the renormalized term always corresponds to a dimensional change:

$$h_0\int_{|x|>r} d^2x\sigma(x) \to h_0 r^{2-h_\sigma}\int_{|x'|>1} d^2x'\sigma'(x')$$

with a first contribution given by:

$$h_1 = h_0 r^{2-h_\sigma} \tag{119}$$

Meanwhile at the 1-loop order we have one contribution that comes from $\epsilon\sigma$ and $\epsilon$:

$$m_0 \sum_a \int d^2x \epsilon^a(x) \cdot \left( g^0_{LR} \sum_b \int d^2y \sigma(y) \epsilon^b(y) \right)$$

From which one gets the contribution with the OPE of the $\epsilon\epsilon$ (which has a combinatorial of a simple factor $n$):

$$h_2 = g^0_{LR} m_0 n 2\pi \frac{r^{2-2h_\epsilon}}{2-2h_\epsilon} r^{2-h_\sigma} \tag{120}$$

and combining all together:

$$h = h_1 + h_2 = h_0 r^{2-h_\sigma} + g^0_{LR} m_0 n 2\pi \frac{r^{2-2h_\epsilon}}{2-2h_\epsilon} r^{2-h_\sigma}$$

such that the Z matrix elements will be

$$Z_\sigma = 1 \tag{121}$$

$$Z_{\sigma\epsilon} = n g^0_{LR} 2\pi \frac{r^{2-h_\sigma-h_\epsilon}}{\epsilon_{SR}} \tag{122}$$

### 3.2.3 Operators dimension

Putting all pieces together (117, 118, 121, 122), one obtains:

$$Z = \begin{pmatrix} 1 + 4(n-1) g^0_{SR} \frac{r^{\epsilon_{SR}}}{\epsilon_{SR}} & g^0_{LR} \frac{r^{\epsilon_{LR}}}{2\epsilon_{LR}-\epsilon_{SR}} \\ n g^0_{LR} 2\pi \frac{r^{\epsilon_{LR}}}{\epsilon_{SR}} & 1 \end{pmatrix}$$

and in the limit of $n \to 0$ one finally obtains:

$$Z = \begin{pmatrix} 1 - 4 g^0_{SR} \frac{r^{\epsilon_{SR}}}{\epsilon_{SR}} & g^0_{LR} \frac{r^{\epsilon_{LR}}}{2\epsilon_{LR}-\epsilon_{SR}} \\ 0 & 1 \end{pmatrix} \tag{123}$$

The mixing of operators phenomenon is evident in the Z matrix representation, in fact in this long-range case it is non diagonal. For the computation of the dimension operators the matrix must be diagonalized. Being $Z$ tridiagonal this can be done easily, since the diagonal matrix simply corresponds to the one with only diagonal elements:

$$Z' = \begin{pmatrix} 1 - 4\pi g^0_{SR} \frac{r^{\epsilon_{SR}}}{\epsilon_{SR}} & 0 \\ 0 & 1 \end{pmatrix} \tag{124}$$

In particular, at first-order, this corresponds to the absence of the dynamics for the disorder implemented, up till this point, it does not renormalize. This will be better understood at the end of this section.

Given $Z'$, we can compute $\gamma_\epsilon$:

$$r\frac{dZ_\epsilon}{dr} = 4\pi g^0_{SR} r^\epsilon_{SR}$$

$$\gamma_\epsilon = \frac{r}{Z_\epsilon}\frac{dZ_\epsilon}{dr} = 4\pi g^0_{SR} r^\epsilon_{SR}(1 - 4\pi g^0_{SR} r^{\epsilon_{SR}}) = 4\pi g^0_{SR} r^{\epsilon_{SR}} - 16\pi^2 (g^0_{SR})^2 r^{\epsilon_{SR}}$$

Considering the first order (3.1.3) we get

$$\gamma_\epsilon = 4\pi g_{SR} - 16\pi^2 g^2_{SR} \tag{125}$$

So finally using the already mentioned Callan-Symanzik equations:

$$2\Delta'_\epsilon = 2\Delta_\epsilon - 2\gamma(g_c) = \Delta_{\epsilon\epsilon} - 8\pi g_{SR} + 32\pi^2 g^2_{SR}$$

Computed at the pure point:

$$2\Delta'^P_\epsilon = 2\Delta_\epsilon$$

as expected. Computed at the short range point:

$$2\Delta'^{SR}_\epsilon = \Delta_{\epsilon\epsilon} - \epsilon + \frac{\epsilon^2}{2}$$

At the long range instead:

$$2\Delta'^{LR}_\epsilon = \Delta_{\epsilon\epsilon} - 2\epsilon + 2\epsilon^2$$

confirming the difference between the physics of the short-range and the long-range fixed points. Whilst for the disorder operator, being $Z_\sigma = 1$ despite the fixed point considered, it will always be true that $\gamma_\sigma = 0$, this will entails:

$$2\Delta'_\sigma = 2\Delta_\sigma$$

So that the disorder dimension does not change.

## 3.3 Numerical results

In the long-range Potts model, the numerical implementation of the disorder must be taken with some care. Up to know in fact, in the numerical part, the correlation between spins it has been simply chosen to be the uncorrelated one, equivalent to the Gaussian case, but now it is needed to build the power law decay (17). For this, the property of the Ising model at criticality and its characteristic power-law decay for spins is used:

$$\langle \sigma_i \sigma_j \rangle = |i-j|^{-1/4}$$

This yet does not represent what we need, since we would like to work with an algebraic parameter that is able to vary. The idea is to consider *n-Ising models*, which can all be simulated at criticality, building for each n-model an auxiliary variable as follows:

$$\tilde{\sigma_i} = \prod_{j=1}^{n} \sigma_i^j \tag{126}$$

We can build the correlations between these new spins by simple multiplicative property:

$$\langle \tilde{\sigma_i} \tilde{\sigma_j} \rangle = |i-j|^{-n/4} \tag{127}$$

and we can now set our correlation exponent

$$a = \frac{n}{4} \tag{128}$$

which can be varied by changing the number of simulations of the Ising model. This gives the power-law behaviour expected for long-range disorder. However, $a$ can only vary discretely between a certain set of values, since $n$ must be necessarily integer. It is important to note that all the simulations will always be made at criticality. We will study in the following the three Potts models corresponding to the values of $Q = 1, 2, 3$ [3]. In particular for Q=1 there will be simulated 8 Ising copies meanwhile for the cases of $Q = 2, 3$ they will be 10. As shown in section 2.3 a general pseudo-code will be presented below, and later specific values of parameters will be taken into account. The first step will be to simulate n-Ising models. This will be done considering a square lattice of length $L$ with periodic boundary conditions. All spins are initialized and all the systems are thermalized with a first set of Monte Carlo sweeps. The type of update for the spins will be once again done through a non-local algorithm using the construction of the FK cluster, in particular this time it will be used the Wolff algorithm. A random cluster of spins will be constructed taking into account, between spins of the same values, a probability, to create the stochastic cluster, of

$$p = 1 - e^{-2J}$$

[3] The numerical results of this section will be part of a paper to be published, representing results that confirm the validity of the action built and which are in great agreement with the theoretical renormalization group eigenvalue predictions at the pure point [44]

with

$$J = log(1 + \sqrt{Q})$$

where for Ising $Q = 2$. At the end of this construction, all spins will be reversed. This will be repeated for all the steps of the thermalization. In particular they will be chosen $n_{therm} = 1000$ steps, and an additional quantity which takes into account the autocorrelation time at a given lattice size (the larger the more the time needed to thermalize):

$$n_L = \begin{cases} 4 & if\ L = 8 \\ 4 & if\ L = 16 \\ 4 & if\ L = 32 \\ 5 & if\ L = 64 \\ 6 & if\ L = 128 \end{cases}$$

such that the final thermalization is given by: $N_{Therm} = n_{therm} \cdot n_L$. At the end of this the variables for the lattices will be created following equation (126). For each simulation of these critical models, there will be considered different $dn = 1000$ samples; they will be needed to perform disorder averages. At this point one has to distinguish from what it is implemented for the case of Q=1, Q=2 and Q=3. In the first case, since the spins can be taken only as single valued, there is, actually, no dynamics in the systems, so the simulations are much faster, and they will not require thermalization steps, nor updates. It simply will be constructed the corresponding FK cluster, using now two different probabilities

$$p_0 = 1 - e^{J_1}$$

and

$$p_1 = 1 - e^{J_2}$$

to take into account the randomness of the model. In fact everything will be equivalent to what has been chosen for the bonds values in 2.3 . The magnetization will be computed in the equivalent way using (86) and (87).

In the case of Q=2, and Q=3 thermalization will be needed to study the system at thermodynamical equilibrium as well as sweeps to get uncorrelated observables. To do this, two MonteCarlo functions will be used, following the Wolff update of the previous case. Although for the case of $Q = 3$ we must define better what reversing a cluster of spins actually means when there are three different values. In this case, if for instance the cluster is of spins of value 2, it will be extracted a random number to choose amongst the two remaining $Q$ quantities, $\{1, 3\}$, and all the cluster' spins will be set to that value. Finally, the disordered averages for the magnetization will be computed. In this second section of numerical analysis, we will be more interested on the computation of the renormalization group eigenvalues through numerical perturbation in an equivalent way to 2.3.3. This will be done with respect to the pure point, therefore it will tell us the stability or instability of those fixed points. Although, through theoretical prediction of the renormalization group eigenvalues we could

get, if the pure point is unstable, which of the two other possible fixed points, SR or LR, will be the actual stable one. In comparison with theoretical values, we must consider the two following remarks. The first one is related to the fact that in the theoretical computation we have considered two disordered eigenvalues while in the numeric we will still consider a scaling function depending only on one as in (92). We recall although that the action has been constructed adding a term. Since $\lambda_1$ and $\lambda_2$ are related to be the short-range and long-range distributions, we expect at a given fixed point to have just one of them, depending on the dominating character of the disorder distributions. The second remark is strictly linked to the action for the perturbation of the long-range case:

$$\tilde{S}_{pert} = \sum_a S_a^0 + g_{LR} \sum_a \int d^2x \sigma(x) \epsilon^a(x) + g_{SR} \sum_{a \neq b} \int d^2x \epsilon^a(x) \epsilon^b(x)$$

that we recall, it has been constructed adding directly the term $\mathcal{O}(\epsilon\sigma)$. In fact, while the term $\mathcal{O}(\epsilon\epsilon)$ comes from a Gaussian integration that makes $g_{SR}$ proportional to the variance of the disorder variable, so $\mu^2$, the other term, since no integration is performed, will be simply proportional to the disorder operator, so its implicit dependence will be $\propto \mu$. This is quite important since in the collapse, following the universal scaling function, the scaling variable $\mu^2 L^{y_d}$ should be considered actually as $\mu^2 L^{2y_d}$, with an addition factor 2. A way to avoid this is to plot everything in such a way that the scaling function and the magnetization are function of just $\mu$. But to better see numerically the presence of this effect, the first path will be chosen. Therefore, since we are computing the eigenvalues at the pure point, which will simply corresponds to dimensional quantities

$$y_d = 2 - h_d$$

being $y_d$ the disorder eigenvalue and $h_d$ the operator physical dimensionality we specify that the actual comparison will be made as follows:

$$\begin{cases} y_d^{SR} = \epsilon_{SR} = 2 - h_{\epsilon\epsilon} \\ y_d^{LR} = 2\epsilon_{LR} = 2(2 - h_{\sigma\epsilon}) \end{cases} \tag{129}$$

This simply means that the numerical eigenvalue computed will be twice the actual theoretical quantity in case the long-range behaviour is the relevant one. This scheme will be analyzed in depth in the following section.

### 3.3.1 Q=1

The computation of $y_d$ for $Q = 1$ has been performed for the following values of $a$ at different lattice size $L$:

$$a \in \{0.25, 0.5, 0.75, 1, 1.25, 1.5, 1.75, 2\}$$

$$L \in \{8, 16, 32, 64, 128, 256\}.$$

The magnetizations at various disorder strengths $r$, has been taken in the range [1, 4], and they have been obtained computing disordered averages over $N = 10^7$ samples. Here the numerical method implemented will be shown for the particular case of $a = 0.75$. The same technique will be applied for all other values of $a$.

The magnetization for a given disorder value ($r \neq 1,\ \mu \neq 0$) normalized with the magnetization of the pure case ($r = 1, \mu^2 = 0$) is computed at fixed lattice size. The ratio has been plotted as a function of the disorder strength parameter $\mu^2$.

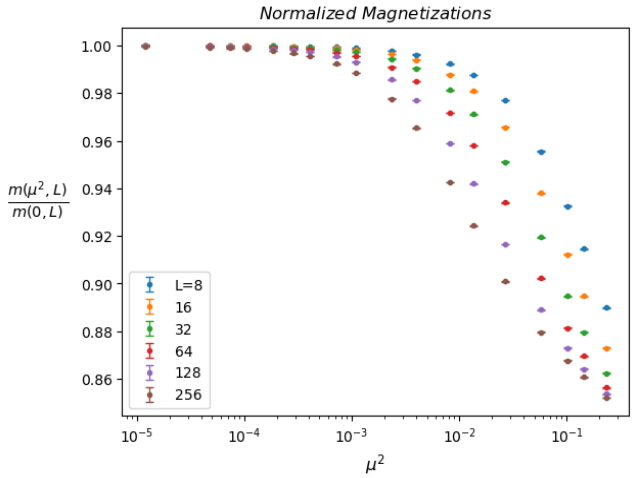


Figure 29: Fraction of magnetization at a given disorder over the magnetization of the pure model (r=1) at different lattice sizes plotted against the scaling variable $\mu^2 L^{y_d}$ for $a = 0.75$

In *Figure* 29 the different curves show a similar behaviour although they seem shifted one with respect to the other. Due to the uniqueness of the scaling function $f$, it can be introduced the dependence to the lattice size through the renormalization group exponent: $\mu^2 L^{y_d}$. Re-plotting the curves with this new scaling variable, there must exist a value of $y_d$ for which all data points collapse into a single curve. Although this procedure was already introduced in 2.3, in this case more details will be given. With this aim, an initial guess of the exponent $\tilde{y_d} = 0.68$ has been chosen through visual inspection first. This unique

functional form holds for disorder values sufficiently close to the pure fixed point. As it can be seen in the plot, for higher values of disorder strength the collapse is lost. This is in agreement with theoretical argument statements that the unique functional form is preserved only in the vicinity of critical points and at higher disorder values the perturbation is lost.

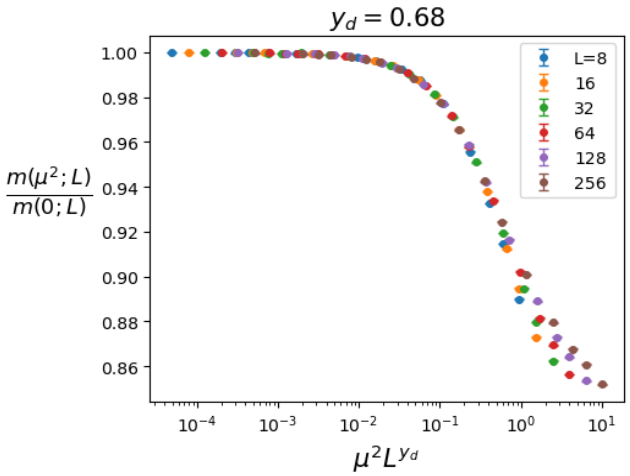


Figure 30: Fraction of magnetization at a given disorder over the magnetization of the pure model at different lattice sizes plotted against the scaling variable $\mu^2 L^{y_d}$ for $a = 0.75$

To avoid these effects, to extract a more precise value of the critical exponent $y_d$, one can focus on a smaller domain of the scaling variable. In addition, for a better representation for the collapse, it will be considered a slightly different form of the data:

$$1 - \frac{m(\mu^2, L)}{m(0, L)} = 1 - f(\mu^2 L^{y_d})$$

In order to understand better how the value of $y_d$ is affected by the lattice size $L$, the collapse has been performed, not as previously, amongst curves at all $L$, but taking pairs only. The critical exponent variable $y_d$ has been varied upon a range centered at the initial guess $\tilde{y_d}$ which in this case corresponds to $\tilde{y_d} = 0.68$. For each value of the exponent two curves at subsequent lattice size (for instance $L = 16$ and $L = 32$, or $L = 64$ and $L = 128$) have been interpolated and their y-distance (in absolute value) has been computed. The numerical $y_d$ is chosen as the one which minimize the curves' distance, $y_d^{opt}$. Four different pairs of curves with the corresponding numerical renormalization exponent are shown in *Figure* 31 in double logarithmic scale. The computation is in agreement with a precise collapse as it can be seen.

A numerical uncertainty to each result has been computed considering the quantity $\overline{y_d}$ taken as the exponent which causes a deviation of 20% with respect

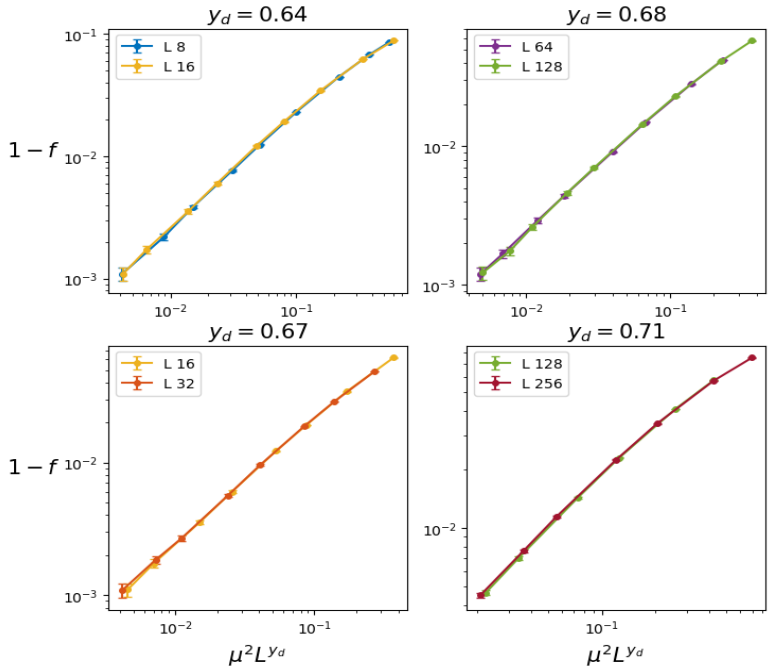


Figure 31: Collapse of the function for couples of curves at different subsequen lattice sizes

to the minimum distance between curves. This is supported by visual inspection, taking into account the variances of each data point in the collapse representation, neglected till this point. The corresponding error has been computed as the difference between the two quantities: $|\overline{y_d} - y_d^{opt}|$. Form the previous figure one can observe a variation of the critical exponent at increasing lattice size. This can be explained in terms of additional finite size effects which has not been considered up to this point. This justifies taking into account as a final exponent, $y_d$ from the largest couple of $L$, leading to an improvement of the accuracy of the result from the simple initial guess, going from $\tilde{y_d} = 0.68$ to $y_d^{num} = 0.71$. This method has been applied for all the values of $a$, and the initial guesses have been plotted below in *Figures* 32 in this case.

The final values of the correlation exponents have been summed up in the *Table* 3 below and compared with the theoretical results. In *Figure* 33 a graphical representation of the numerical results is presented for clarity. The sign of the numerical values of $y_d$ defines the relevancy of the disorder. A positive value describes a flow from the pure fixed point towards a critical disordered fixed point whilst a negative value is an evidence of the absence of this flow and an irrelevancy of the disorder. Finally when $y_d$ corresponds to marginal case, it is more complex to describe what happens due to possible logarithmic correction. The numerical result in particular show how the disorder is relevant

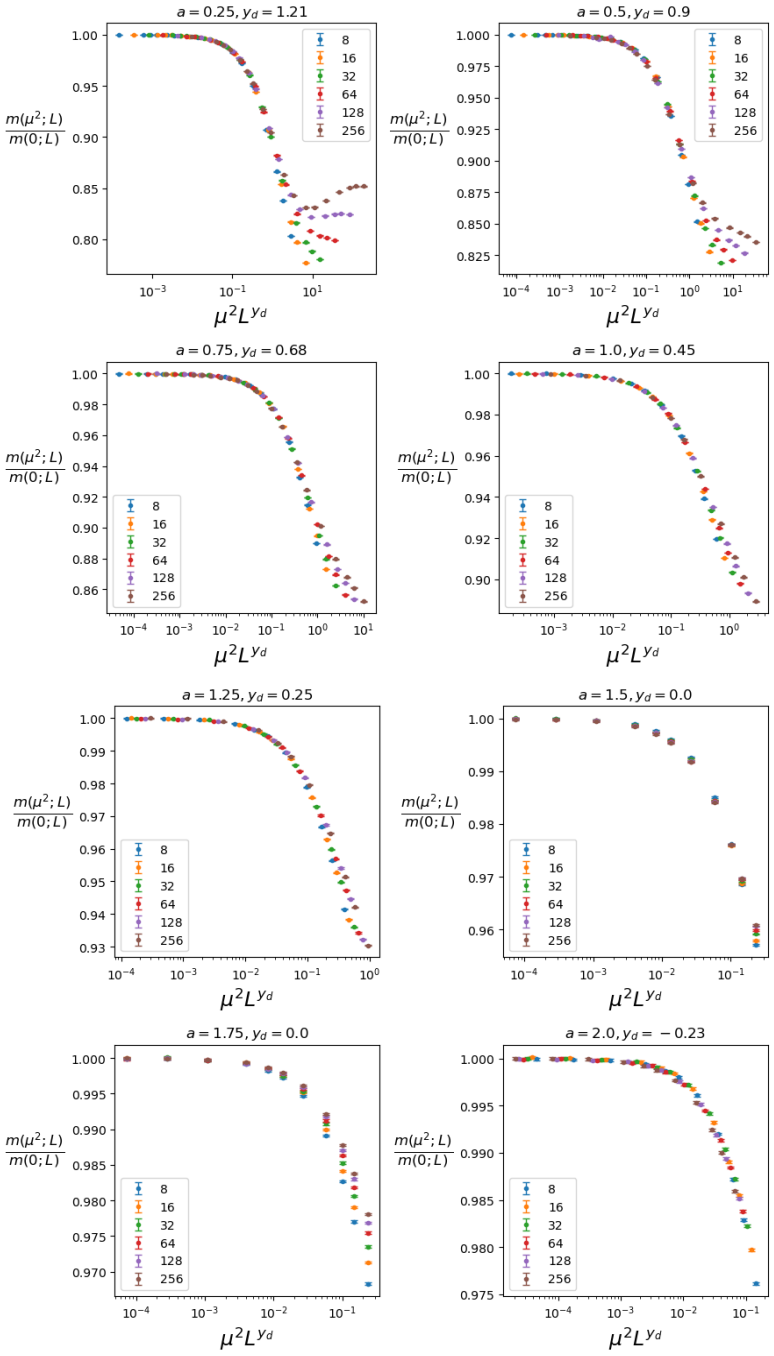


Figure 32: Collapse and initial guess of $y_d$ through visual inspection for the correlation exponent $a \in \{0.25, 2\}$

| a | $y_d^{num}$ | $2\epsilon_{LR}$ | $\epsilon_{SR}$ |
|---|---|---|---|
| 0.25 | 1.25 ± 0.02 | 1.25 | -0.5 |
| 0.5 | 0.97 ± 0.02 | 1 | -0.5 |
| 0.75 | 0.71 ± 0.02 | 0.75 | -0.5 |
| 1 | 0.45 ± 0.03 | 0.5 | -0.5 |
| 1.25 | 0.17 ± 0.03 | 0.25 | -0.5 |
| 1.5 | 0.01± 0.03 | 0 | -0.5 |
| 1.75 | -0.1 ± 0.02 | -0.25 | -0.5 |
| 2 | -0.12 ± 0.03 | -0.5 | -0.5 |

Table 3: Comparison between numerical results and theoretical ones for Q=1

for $a \leq 1.5$ and moreover, the flow which can be seen is in agreement with the values of the long-range fixed point. This is perfectly equivalent to the stability analysis made in 2.1.5, in fact the result of Q=1 shown in *Figure* 24, rewriting the condition for which the long-range fixed point is stable, corresponds to:

$$\epsilon_{LR} > 0 \rightarrow 1 - \frac{a}{2} + \frac{\epsilon_{SR}}{2} > 0 \rightarrow a < \frac{3}{2} \; where \; \epsilon_{SR} = -\frac{1}{2}$$

which is exactly what is seen numerically. Although the pure fixed point results stable for $a > 1.5$ the results must be taken with greater care since, in this case logarithmic corrections could influence a lot what happens after the change in the stability, being the disorder irrelevant.

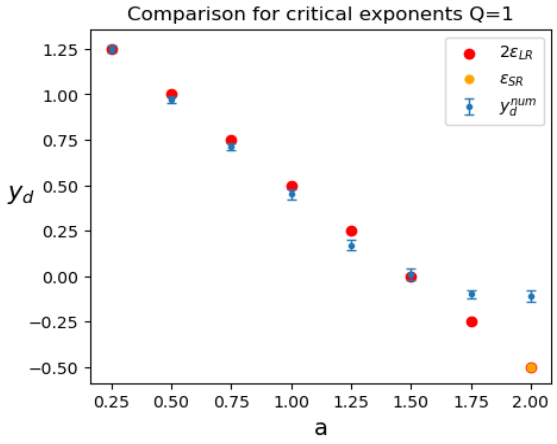


Figure 33: Comparison between the theoretical eigenvalue and the numerical results for L=128-256 taking into account the factor 2 for the long-range theoretical result

### 3.3.2 Q=2

For $Q = 2$, due to the presence of a dynamics, some parameters have been modified. The number of samples has been reduced to $N = 10^6$ due to a higher computational complexity, while the range for the disorder strength r=[1,4] has been left unchanged. The lattice size considered have been $L \in \{64, 128\}$ for a trade-off between the accuracy argument presented before and the increased running time of simulations. Finally two additional values of $a$ are considered with respect to the previous ones: $\{2.25, 2.5\}$. The technique shown before has been applied for each correlation exponent and the initial guesses are shown in *Figures* 34 and 35.

The final results for $y_d$ values are shown in the *Table* 4 below with the corresponding graphical representation in *Figure* 36.

The disorder critical exponent is relevant for $a < 2$ and marginal for $a \geq 2$. When these values are compared with the theoretical prediction, the first important remark is related to the effective change of the disorder type, between the short-range and the long-range one, captured by numerical results. In this case there is a good comparison with all values of a, in particular this is in agreement with *Figure* 25, in fact the long-range fixed point is stable for:

$$\epsilon_{SR} > 0 \rightarrow 1 - \frac{a}{2} > 0 \rightarrow a < 2$$

The marginality for $a > 0$ is well confirmed and observed in the plot below.

| a | $y_d^{num}$ | $2\epsilon_{LR}$ | $\epsilon_{SR}$ |
|---|---|---|---|
| 0.25 | 1.72 ± 0.02 | 1.75 | 0 |
| 0.5 | 1.48 ± 0.02 | 1.5 | 0 |
| 0.75 | 1.20 ± 0.01 | 1.25 | 0 |
| 1 | 1.00 ± 0.02 | 1 | 0 |
| 1.25 | 0.73 ± 0.01 | 0.75 | 0 |
| 1.5 | 0.44 ± 0.01 | 0.5 | 0 |
| 1.75 | 0.17 ± 0.02 | 0.25 | 0 |
| 2 | 0.02 ± 0.02 | 0 | 0 |
| 2.25 | -0.02 ± 0.03 | -0.25 | 0 |
| 2.5 | -0.03 ± 0.02 | -0.5 | 0 |

Table 4: Comparison between numerical results and theoretical ones for Q=2

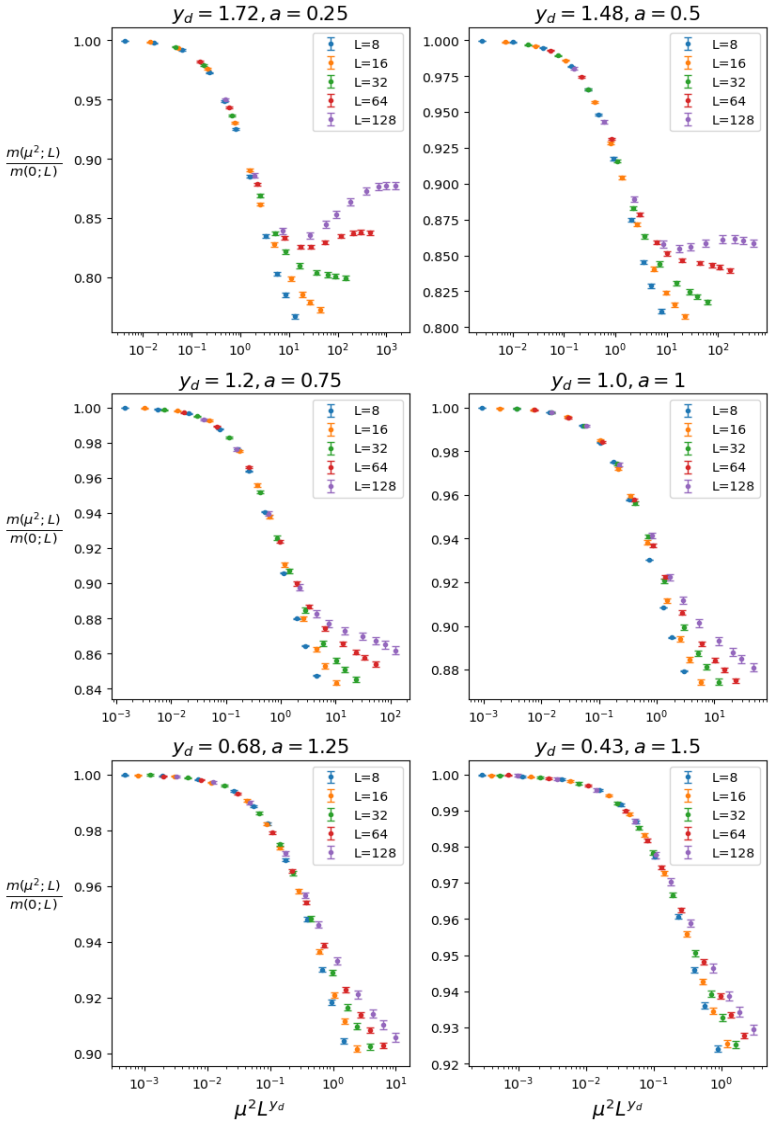


Figure 34: Comparison between the theoretical eigenvalue and the numerical result for L=64-128 for Q=2 at $a \in \{0.25, 1.5\}$

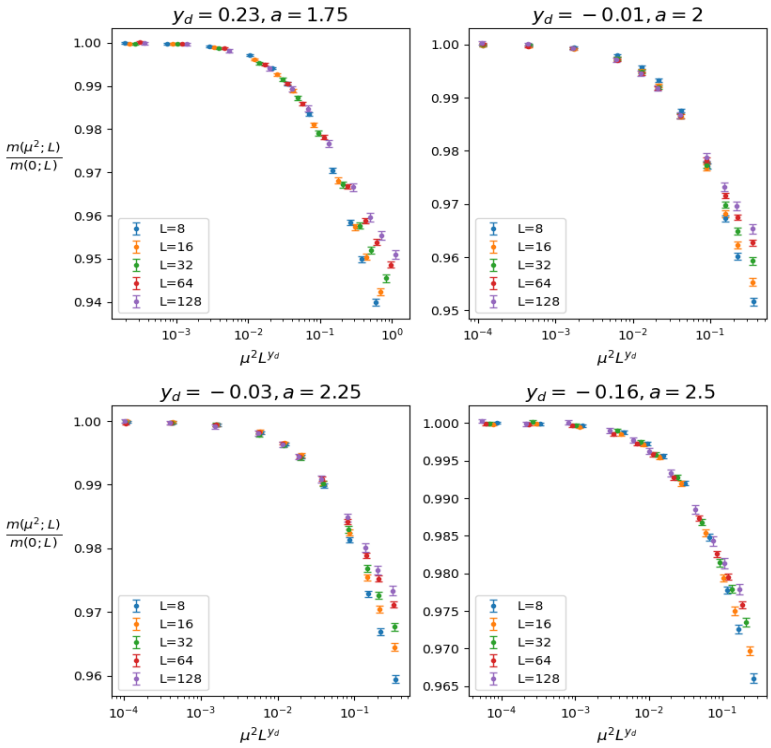


Figure 35: Comparison between the theoretical eigenvalue and the numerical result for L=64-128 for Q=2 $a \in \{1.75, 2.5\}$

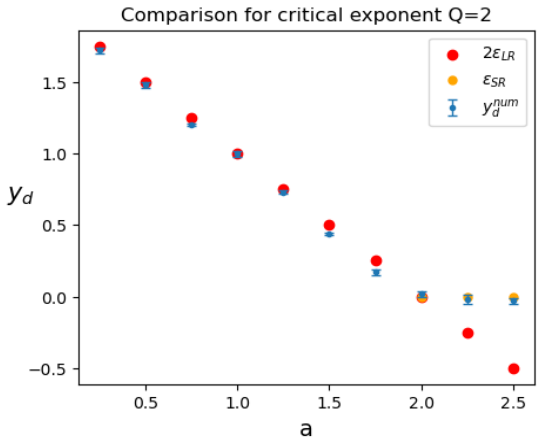


Figure 36: Comparison between the theoretical eigenvalue and the numerical result for L=128-256

### 3.3.3 Q=3

Finally, the results for $Q = 3$ are reported, using the same parameters for the $Q = 2$ case. The initial guess are represented in *Figure* 37, 38 and there will follow the *Table* 5 to compare the final results.

| a | $y_d^{num}$ | $2\epsilon_{LR}$ | $\epsilon_{SR}$ |
|---|---|---|---|
| 0.25 | 2.05 ± 0.02 | 2.15 | 0.4 |
| 0.5 | 1.91 ± 0.02 | 1.9 | 0.4 |
| 0.75 | 1.63 ± 0.01 | 1.65 | 0.4 |
| 1 | 1.43 ± 0.02 | 1.4 | 0.4 |
| 1.25 | 1.12 ± 0.03 | 1.15 | 0.4 |
| 1.5 | 0.89 ± 0.02 | 0.9 | 0.4 |
| 1.75 | 0.60 ± 0.02 | 0.65 | 0.4 |
| 2 | 0.52 ± 0.03 | 0.4 | 0.4 |
| 2.25 | 0.35 ± 0.02 | -0.25 | 0.4 |
| 2.5 | 0.35 ± 0.02 | -0.5 | 0.4 |

Table 5: Eigenvalue at the pure point for Q=3

In this case, it is confirmed the good agreement with theoretical predictions which are able to capture the effective change from the long-range disorder to the short-range case at $a = 2$. In fact, the eigenvalue remains relevant at all values of $a$, although it cannot longer be compared with the long-range value, but with its short-range one. If we consider in fact *Figure* 27 we can see that the long-range is relevant for:

$$\epsilon_{LR} > \frac{1}{5} \to 1 - \frac{a}{2} + \frac{0.4}{2} > \frac{1}{5}$$

$$a < 2$$

Moreover, for $a \geq 2$, from theoretical computation we know that the only stable model is the short-ranged one and this can be seen with the comparison with the short range value. The system does not flow in any case towards the pure fixed point being $y_d$ always positive. The whole critical behaviour is described by the two disordered fixed points and once again at $a = 2$ it is seen the effective change between the long-range disorder into the short-range version. The final result is shown in *Figure* 39.

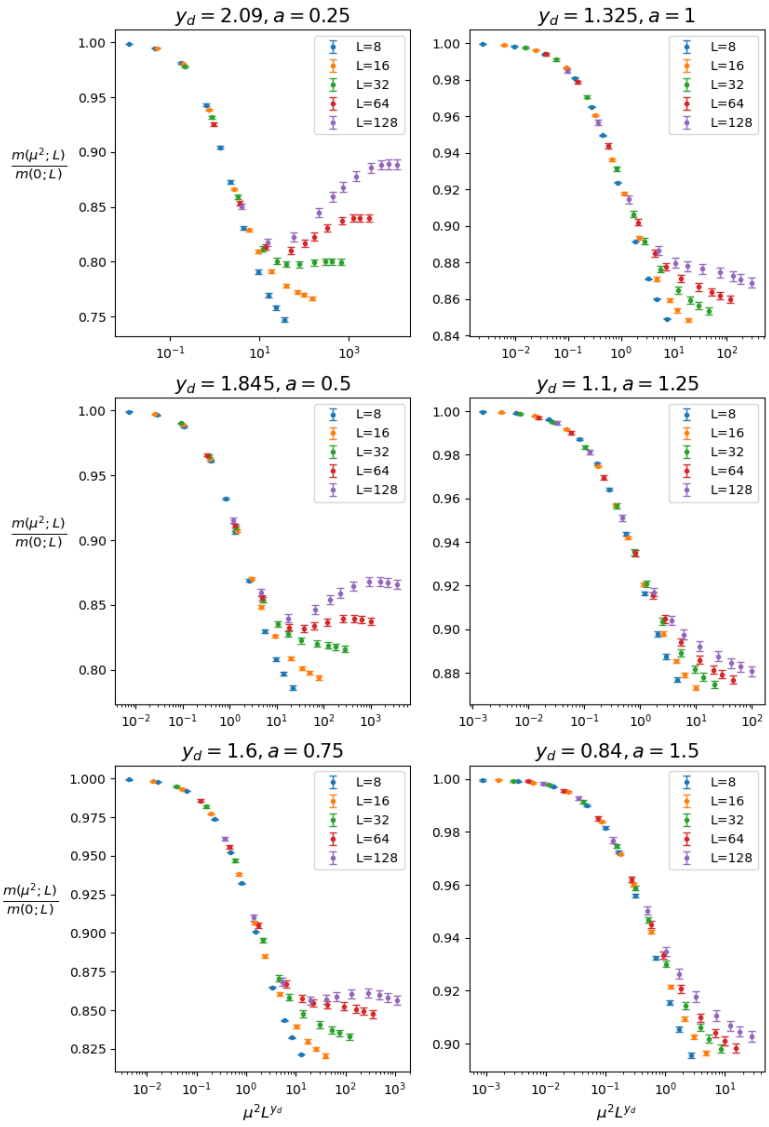


Figure 37: Initial guess for $y_d$ at Q=3: $a \in \{0.25, 1.5\}$

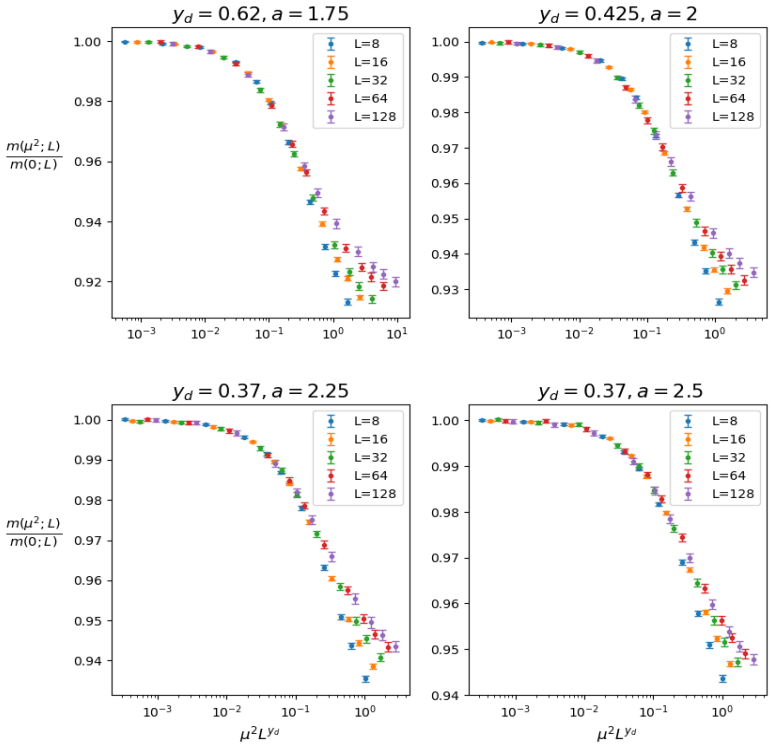


Figure 38: Initial guess for $y_d$ at Q=3: $a \in \{1.75, 2.5\}$

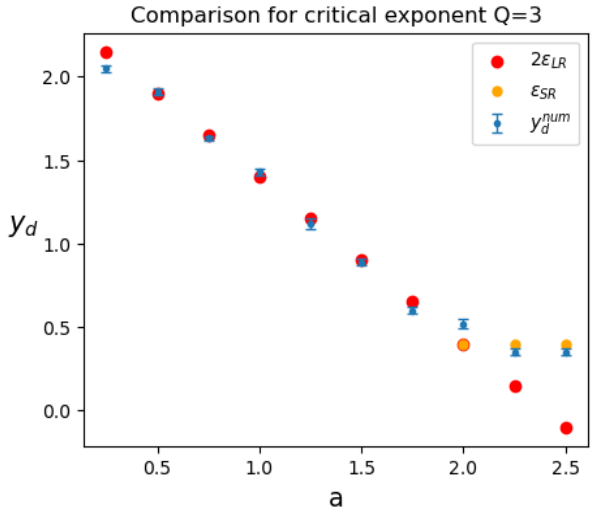


Figure 39: Comparison with theoretical results for Q=3

# Conclusions

In this thesis we have investigated how the presence of disorder, in well-known statistical models, affects the critical behaviour of second-order phase transitions. Focusing on the Q-states Potts model, we have generalized the classical expression of its Hamiltonian taking into account interactions between spins as random bimodal variables: $J_{\langle ij \rangle} \in \{J_1, J_2\}$. We have characterized the correlation between bonds by taking an algebraic decay expression $\propto |i-j|^{-a}$ and by distinguishing two main cases based on the value of $a$: short-range and long-range disorder.

After a general introduction to theoretical methods and numerical techniques, such as the replica trick for disorder's treatment, RG, the connection between conformal invariance and critical points and MonteCarlo methods, we focused on the short-range case, corresponding to $a \geq 2$. We applied the perturbative renormalization group idea in real space, using the conformal field theory formalism, up to second-loop-order following an analogous study carried out by Picco, Dotsenko and Pujol[28]. We obtained a dynamical equation whose solution gives a disordered fixed point with a different universality class from the classical, pure, one. We analyzed in detail the domain of its stability for $Q = 1, 2, 3$ making use of both theoretical and graphical methods of non-linear equations. We later focused more on the $Q = 3$ case to compute the renormalization group eigenvalue; this led to a more extensive analysis for the dimension of the energy operator. In fact, while the operator dimensions for $\epsilon \cdot \epsilon$ and $\epsilon$ are linked by a simple factor 2 at the pure point we were able to prove the multifractality property of the energy operator since at the short range fixed point this relation does not hold any longer $\Delta'_{\epsilon\epsilon} \neq 2\Delta'_{\epsilon}$.

The same methods have been applied for the long-range study, $a < 2$, motivated by a recent work of Chippari, Picco, Santachiara[29], by performing RG at first-loop-order. A system of two dynamical equations has been computed and it has provided us with three different fixed points, one of which belonging to a different universality class from both the pure and the short-range ones found at previous computations. Its stability has been studied in details providing theoretically the domain of stability and numerical phase space plots which confirmed the analytical results looking at the direction of trajectories, describing the renormalization flow, close to fixed points. The dimensions of both the energy and the disorder operators have been computed, proving how the latter does not change through renormalization procedures.

Numerical simulations through non-local Monte Carlo methods for the computation of the magnetization were used to show, in the short-range case, the presence of two distinct classes of universality, in agreement with theoretical predictions. The difference between the pure and short-range universality has been confirmed by comparing the values of the effective magnetic critical exponent by fitting techniques.

The most relevant result of the thesis comes from the implementation of a numerical method for the computation of the disorder renormalization group

eigenvalue. Exploiting a perturbative approach around the known critical pure model, Potts models with weak disorder implementations have been simulated. Exploiting scaling arguments and universality properties we have been able to quantify the disorder eigenvalues allowing to characterize the stability of the pure point numerically. Moreover by comparing with theoretical predictions it has been proved which of the fixed points was relevant, moreover we showed the expected effective change of the disorder from long-range to short range at $a = 2$ for $Q = 2$ and $Q = 3$. This is one of the reasons for the importance of this numerical method developped, that is considered as the main outcome of the thesis.

This developped method poses the basis for a possible implementation for numerical computations of the renormalization group eigenvalue at the new long or short-range fixed points. In fact, up till now the numerical perturbation technique has been developped from the known pure model and the next step would be to generalize this, by perturbing with respect to the disordered critical ones, which are described by two different conformal actions. The main difficulty here relies on the need to localize precisely the new disorder strength critical values $r_c$, since perturbation techniques require them for the success of the computation. In fact, collapses of curves make sense only close to critical models. If the disorder strength were to be known, this numerical method would provide an additional understanding of the relevancy of the disorder and a direct comparison with theoretical result. In particular, focusing on the long-range case and recalling the Halperin-Weinrib conjecture with their argument on the correlation exponent $\nu = \frac{2}{a}$, it could be given a first numerical relation between these two critical exponents for a non-Gaussian distribution implementation.

Finally, for the analytic part, it would be interesting to better understand what happens at second-order-loop, in the long-range case, for the computation of the disorder dimension through the Z matrix . In particular it would be of great importance to study more in depth the mixing of short-range and long-range characters in the renormalization equations, to gain a better perspective for a possible renormalization of the disorder operator at higher orders.

# List of Figures

# List of Tables

# References


[1] Jarosław Kwapień and Stanisław Drożdż. Physical approach to complex systems. *Physics Reports*, 515(3):115–226, 2012. Physical approach to complex systems.

[2] National Research Council. *Physics in a New Era: An Overview*. The National Academies Press, Washington, DC, 2001.

[3] Shraddha Gupta, Nikolaos Mastrantonas, Cristina Masoller, and Jürgen Kurths. Perspectives on the importance of complex systems in understanding our climate and climate change—The Nobel Prize in Physics 2021. *Chaos: An Interdisciplinary Journal of Nonlinear Science*, 32(5):052102, 05 2022.

[4] Debashish Chowdhury, Ludger Santen, and Andreas Schadschneider. Statistical physics of vehicular traffic and some related systems. *Physics Reports*, 329(4):199–329, 2000.

[5] Meinard Kuhlmann. Explaining financial markets in terms of complex systems. *Philosophy of Science*, 81(5):1117–1130, 2014.

[6] Dragutin Mihailovic, Darko Kapor, Sinisa Crvenkovic, and Anja Mihailović. Physics of complex systems: Discovery in age of goedel, 06 2022.

[7] Richard Foote. Mathematics and complex systems. *Science*, 318(5849):410–412, 2007.

[8] James P. Sethna. Abrupt phase transitions. In *Statistical Mechanics: Entropy, Order Parameters, and Complexity*. Oxford University Press, 01 2021.

[9] Amikam Aharoni. *Introduction to the Theory of Ferromagnetism*, volume 109. Clarendon Press, 2000.

[10] Frederick E. Wang. Iv - superconductivity. In Frederick E. Wang, editor, *Bonding Theory for Metals and Alloys*, pages 65–108. Elsevier, Amsterdam, 2005.

[11] Andreas Schmitt. Introduction to superfluidity. *Lect. Notes Phys*, 888(1), 2015.

[12] Gregg Jaeger. The ehrenfest classification of phase transitions: introduction and evolution. *Archive for history of exact sciences*, 53:51–81, 1998.

[13] Dean Rickles, Penelope Hawe, and Alan Shiell. A simple guide to chaos and complexity. *Journal of epidemiology and community health*, 61:933–7, 12 2007.

[14] James P. Sethna. Order parameters, broken symmetry, and topology, 2009.

[15] Barry Cipra. An introduction to the ising model. *The American Mathematical Monthly*, 94(10):937–959, 1987.

[16] M. Kardar. Phase Transitions. Lectures, Statistical Mechanics I, Chapter I.C. `https://web.mit.edu/8.334/www/lectures/lec2.pdf`.

[17] Ryo Tamura, Shu Tanaka, and Naoki Kawashima. A method to control order of phase transition: Invisible states in discrete spin models, 2012.

[18] Mehran Kardar. *Statistical physics of fields*. Cambridge University Press, 2007.

[19] Ming Li, Run-Ran Liu, Linyuan Lü, Mao-Bin Hu, Shuqi Xu, and Yi-Cheng Zhang. Percolation on complex networks: Theory and application. *Physics Reports*, 907:1–68, 2021. Percolation on complex networks: Theory and application.

[20] Riccardo Ben Alì Zinati and Alessandro Codello. Functional rg approach to the potts model. *Journal of Statistical Mechanics: Theory and Experiment*, 2018(1):013206, January 2018.

[21] FY Wu. The potts model. *Reviews of Modem Physics*, 54(1), 1982.

[22] Wolfgang Kinzel and Eytan Domany. Critical properties of random potts models. *Phys. Rev. B*, 23:3421–3434, Apr 1981.

[23] Abel Weinrib and B. I. Halperin. Critical phenomena in systems with long-range-correlated quenched disorder. *Phys. Rev. B*, 27:413–427, Jan 1983.

[24] Francesco Chippari, Marco Picco, and Raoul Santachiara. Long-range quenched bond disorder in the bidimensional potts model. *Journal of Statistical Mechanics: Theory and Experiment*, 2023(4):043301, April 2023.

[25] Wolfhard Janke and Martin Weigel. Harris-luck criterion for random lattices. *Physical Review B*, 69(14), April 2004.

[26] Leticia F. Cugliandolo. Advanced statistical physics: Quenched disordered systems, lecture notes in sadvanced statistical physics, November 2017.

[27] Tommaso Castellani and Andrea Cavagna. Spin-glass theory for pedestrians. *Journal of Statistical Mechanics: Theory and Experiment*, 2005(05):P05012, May 2005.

[28] Vladimir Dotsenko, Marco Picco, and Pierre Pujol. Renormalisation-group calculation of correlation functions for the 2d random bond ising and potts models. *Nuclear Physics B*, 455(3):701–723, September 1995.

[29] Francesco Chippari, Marco Picco, and Raoul Santachiara. Two-dimensional ising and potts model with long-range bond disorder: A renormalization group approach. *SciPost Physics*, 15(4), October 2023.

[30] John Cardy. *Scaling and Renormalization in Statistical Physics*. Cambridge Lecture Notes in Physics. Cambridge University Press, 1996.

[31] Joshua Qualls. Lectures on conformal field theory. 11 2015.

[32] Barry M. McCoy. The connection between statistical mechanics and quantum field theory, 1994.

[33] Pagnani Andrea. Introduction to probabilities, unpublished lecture notes in stochastics simulations in physics, October 2022.

[34] Wolfhard Janke. *Monte Carlo Methods in Classical Statistical Physics*, pages 79–140. Springer Berlin Heidelberg, Berlin, Heidelberg, 2008.

[35] Christophe Chatelain. Random and out-of-equilibrium potts models. 12 2012.

[36] MP Nightingale and HWJ Blöte. Monte carlo computation of correlation times of independent relaxation modes at criticality. *Physical Review B*, 62(2):1089, 2000.

[37] Robert H. Swendsen and Jian-Sheng Wang. Nonuniversal critical dynamics in monte carlo simulations. *Phys. Rev. Lett.*, 58:86–88, Jan 1987.

[38] Ulli Wolff. Comparison between cluster monte carlo algorithms in the ising model. *Physics Letters B*, 228(3):379–382, 1989.

[39] Armin Fuchs. *Nonlinear dynamics in complex systems*. Springer, 2014.

[40] E. Fradkin. *Quantum Field Theory: An Integrated Approach*. Princeton University Press, 2021.

[41] Dietrich Stauffer and Amnon Aharony. *Introduction To Percolation Theory: Second Edition*. Taylor & Francis, 2nd edition, 1992.

[42] Steven H Strogatz. *Nonlinear dynamics and chaos: with applications to physics, biology, chemistry, and engineering*. CRC press, 2018.

[43] Yu Zhang. Phase portrait plotter on 2d phase plane, 2024. Retrieved July 11, 2024.

[44] Santachiara Raoul Lecce Ivan, Picco Marco. Magnetic exponent for the long-range bond disordered potts model. *To be published*.